# UNIVERSITÀ DEGLI STUDI DI PADOVA

Dipartimento di Fisica e Astronomia “Galileo Galilei”

Master Degree in Astrophysics and Cosmology

Final Dissertation

## Milky Way thin and thick disk kinematics with GAIA data

Thesis supervisor

Prof./Dr. Giovanni Carraro

Candidate

Artem Lutsenko

Academic Year 2022/23

# Abstract

The evolution of galaxies has been studied for many years, but there is still no uniform scenario to describe our Galaxy and galaxies in the neighborhood as well as high-redshift galaxies.

The work describes the basic ideas about the thick and thin disk of the Milky Way galaxy. A detailed analysis of the kinematics of the Milky Way disk in the vicinity of the Sun was performed using the GAIA catalogs EDR3 and Gaia DR3. To determine the local kinematics of the stellar disks of the Milky Way galaxy, we used a complete sample of red giant branch stars distributed in a cylinder centered on the Sun with a radius of 1 kpc and a height of 1 kpc. The kinematic properties of this sample were determined separately for each hemisphere of the Galaxy in search of possible asymmetries. The kinematical properties show the existence of two kinematically different components: a thin disk with average velocities $V_R$ , $V_\Phi$ , $V_Z$ about -1, -239.0 km/s, respectively, and velocity dispersions $\sigma_R$ , $\sigma_\Phi$ , $\sigma_Z$ at 31 , 20 and 11 km/s, as well as a thick disk with average velocity components of about +1, -225, 0 km/s and velocity dispersions of 49, 35, and 22 km/s. It was found that within the height of 500 pc above/below the galactic plane the stars of the thick disk constitute about half of the disk stars. So many stars of the red giant branch with thick disk kinematics could indicates the secular evolution scenario origin for the thick disk of the Milky Way galaxy.

Then we explored the vertical structure of the Galactic disk by using a complete sample of main sequence stars distributed in cones within solid angle |b|<75 and up to distance of 2.5 kpc. In order to extend the sample of stars with measured velocities we made an assumption that the proper motion is aligned with the Galactic disk. The number density distribution along the vertical Z axis was build.

We showed how rotational velocity $V_\Phi$ changes with the distance from the disk plane. We constructed dependence of contributions of the thin and thick disk components on the distance from the Galactic plane. According to our calculations the thick disk is more numerous than it is usually considered to be.

# Contents

# Listing of figures

# Listing of tables

# Listing of acronyms

**RHB** . . . . . Red Horizontal Branch

**CAT** . . . . . Coude Auxiliary Telescope

**ESO** . . . . . European Southern Observatory

**CES** . . . . . Coude Echelle Spectrometer

**SEM** . . . . . Stochastic-Estimation-Maximization

**MDA** . . . . . Multivariate discriminant analisys

**CADIS** . . . . . Calar Alto Deep Imaging Survey

**NOT** . . . . . Nordic Optical Telescope

**SNIa** . . . . . Super nova Ia

**SDSS DR5** . . . . . Sloan Digital Sky Survey Data Release 5

**UVES** . . . . . Ultraviolet and Visual Echelle Spectrograph

**VLT** . . . . . Very Large Telescope

**HVTD** . . . . . High-velocity thick disk

**MRSH** . . . . . Metal-rich stellar halo

**EDR3** . . . . . Gaia Early Data Release 3

**RC** . . . . . Red clump stars

**CDF** . . . . . Cumulative distribution function

**RAVE DR5** . . . . Radial Velocity Experiment Data release 5

**APOGEE** . . . . . Apache Point Observatory Galactic Evolution Experiment

**MS** . . . . . Main sequence stars

**KDE** . . . . . Kernel density estimation

**RMSD** . . . . . Root mean square deviation

**EDR3** . . . . . Early Data Release 3

**mag** . . . . . Magnitude

**CCD** . . . . . Charge-coupled device

**BP** . . . . . Blue photometer

**RP** . . . . . Red photometer

**RVS** . . . . . Radial-velocity spectrometer

**L2** . . . . . Second Lagrange (L2) point

# 1 Introduction

The galactic formation is one of the hot topics of astrophysics. Generally there are two ways to improve our understanding of galactic evolution. The first one is to observe different stages of galactic formation by external and high-redshift galaxies. The second one is to study our Galaxy in details trying to reproduce the history of Milky Way. These two ways require different observational techniques and different instruments.

In this work we focus on the second approach. The understanding of our Galaxy has been improved significantly since Gaia data arrived. This unique mission of European Space Agency provides a tremendous number of galactic sources with precisely measured positions and proper motions.

In this work we aim to study the solar neighborhood. The disk density distribution and the disk kinematical characteristics are the main interests, since the different scenarios of galactic formation and different mechanisms of galactic evolution predict different current shape of the disk. The chemical information, such as metallicity indicator and chemical elemental abundances, is also a key ingredient of the reconstruction of history of the Galaxy.

However, here we mainly analyse the kinematical properties, leaving the chemical analysis for future works. First we review the literature related to the galactic disk studies in chapter 2, then we analyse the local red giant stars kinematics in chapter 3, we extended our volume of sample to reveal the thin and the thick scale heights of the vertical density distribution function of the disk using main sequence stars in chapter 4. The main conclusions are presented in chapter 5.

# 2

# Considerations of the thick disk of Milky Way and external galaxies

## 2.1 First observations

Allen et al. [3] presented observations of the radio continuum emission of the edge-on disk galaxy NGC 891. The observation was made by Westerbork Synthesis Radio Telescope at wavelengths 49.2, 21.2 and 6.0 cm. After the processing and cleaning procedures the authors compared the three maps of observations. They noted that the observed distribution along z axis was not well described by a single exponent, but a superposition of two exponent was suitable. The author showed that the radiation is definitely detected up to 6 kpc of z value. They also compared their results with the Galaxy and pointed there is also an indication of a separation into two components for the Galaxy.

David Burstein [4] studied five edge-on So type galaxies NGC 4111, NGC 4350, NGC 4474, NGC 4570 and NGC 4762 by analysing surface photometry of these galaxies. He showed that the brightest part of the perpendicular luminosity profile can be fitted by the thin disk and bulge components. However, in order to fit the fainter part, it required assumption on existing the third component, which was named thick disk. Moreover, the author concluded the main properties of the thick disk as being with intermediate flattening between a bulge and a thin disk, more diffuse than the thin disk, with an exponential luminosity gradient. But at the time

of this work it was not clear is a thick disk a peculiarity of lenticular galaxies or it is applicable for the spiral galaxies as well.

Another work of Tsikoudi [5] about the structure of lenticular So galaxy NGC 3115 was published in the same with the previous paper 1979 year. Tsikoudi analysed the surface photometry of edge-on lenticular galaxy and tried to fit its luminosity profile. He fitted the luminosity profile by sum of Gaussian and exponential functions identifying Gaussian function, which was noticeable up to 270 pc from the midplane, for the galactic disk and the exponential one, which was more extended and was noticeable up to 3.8 kpc, for "surrounding envelope".

Hummel et al. [6] observed three edge-on spiral galaxies NGC 4244, NGC 4565 and NGC 5907 with the Westerbork Synthesis Radio Telescope at 610 and 1410 MHz frequencies. After the cleaning procedure, they integrated the full resolution maps for the frequency of 1410MHz in narrow strips parallel to the major axis. They found that the observed distribution are more extended in z-direction for NGC 4565 and NGC 5907. They showed that for both of these galaxies the observed z-distribution point to the tail, which is due to the thick disk component.

Observations of external galaxies is a very important key to study our Milky Way. Since we are inside the Galaxy we can not directly reproduce such quantities as brightness and density profile. Thus, one of the ways is to study external galaxies and try to apply the same for our own. After these few works above, there was a logical question: does our Galaxy have a thick disk? But it was not so easy to answer this question. Data collection and further analysis for the big enough samples to preform statistical estimations were very time-consuming task, since there were no powerful computers. Despite all the difficulties, Gilmore and Reid [7] published their work. They analysed the sample of 12500 stars brighter than 18 magnitude in infrared Jonson band in about 18 degree square towards the South Galactic Pole. They derived absolute magnitudes using the distance measurement from photometric parallaxes. The authors were assuming the stars being Main Sequence stars only. They derived stellar luminosity function in absolute magnitudes, the mass of stars in the solar neighborhood and then the mass-to-light ration. But the most important results for us, they derived the density law with the distance from the Galactic plane. They fitted the vertical density profile by two exponential functions: the first one is with scale height of about 300 pc and the second one with the scale height of about 1450 pc. Gilmore and Reid identified the first component as old disk and the second one with scale height of about 1450 as thick disk. They also computed that the Galactic disk contains about 2% of the thick disk in the solar neighborhood.

A bit later Sandage and Fouts [8] presented their estimated normalization for the two disk components and for the halo in the solar neighborhood. For this work, they used only radial ve-

locity information from the spectrograph of the Mount Wilson 100 in. Hooker reflector and Shectman's Reticon detector. They chose three Galactic cardinal directions: $l = 180°, b = 0°; l = 90°, b = 0°; l = 0°, b = 90°$ to get U, V and W velocities directly from radial velocities. The radial velocity data was collected for 430 stars in the $l = 180°, b = 0°$ direction, for 445 stars in the $l = 90°, b = 0°$ direction and for 420 stars in $l = 0°, b = 90°$ direction. They observed more thick disk and halo stars than it was expected from the paper of Gilmore and Reid. Thus, they suggested new normalisation for the disk components and halo in the Solar neighborhood. These values are about 90%, 10% and 0.5% for the thin disk, thick disk and halo respectively. The author measured the velocity dispersion for thin and thick disks. The values $\sigma_U = 28, \sigma_V = 17, \sigma_W = 17 km/s$ for the thin disk and $\sigma_U = 50, \sigma_V = 40, \sigma_W = 42 km/s$ for the thick one. They also checked their results on the subsample of the Yale Trigonometric Catalog with calculated U, V and W velocities. As they showed, there was no significant difference with the values derived from their approach. Continuing the analysis, Sandage [9] calculated the scale heights for the components. He used the data from the previous work [8]. Assuming the Gaussian distribution function for the vertical velocity, he computed the run of density with the height for the thin, thick disks and halo. For the thin and thick disk he took the values of velocity dispersion from the previous paper [8] and for the halo component the value of 90 km/s was applied. Scale height of the thin disk component was derived as about 270pc, scale height of the thick disk component was derived as about 940pc and finally about 3.2kpc for the halo component. He also estimated the mass of halo stars, which was 2% of total mass of the Galaxy.

## 2.2 Further observations for external galaxies

With a growth of observational data, a thick disk existence for external galaxies found more and more confirmations. Van Dokkum et al. [10] studied edge-on spiral galaxy NGC 6504. Using observation performed in seven photometric bands, they tried to fit the light profile at the seven positions along the major axis of the galaxy. The inner parts of the disk profile were well approximated by the exponential function, while the at larger distances from the center it was fitted better by the square sech function. The author confirmed the constant scale height for the components and estimated that the thick disk scale height is about 4 times bigger than the thin disk one. The central surface brightness of the thick disk was computed as 1% of the brightness of the thin disk.

Tikhonov and Galazutdinova[11] studied NGC 2366 galaxy by the data from Hubble Space

Telescope. They, analysing the obtained photometry of the galaxy, estimated the distance of $3.13 \pm 0.25$ Mpc. They also showed that the visible distribution of stars followed separation into three subsystems: thin disk, thick disk and halo. The estimated sizes of disk components in Z direction of this galaxy were 4 and 8 kpc for thin and thick disk respectively.

Comerón et al[12] analysed the data of NGC 4244, which is the only nearby late-type spiral edge-on galaxy for which thick disk was not confirmed. Using the data from Spitzer Survey of Stellar Structure in Galaxies the authors found the sings of the two-component structure of the disk of NGC 4244. They noted as well that the galaxy is not perfectly edge on. They assumed that the weak thick disk of the galaxy can be a consequence of a limited secular evolution or of a high amount of gaseous accretion after the galactic formation.

Lehnert et al.[13] compared the star formation history and dynamics of the Galaxy with the distant disk galaxies. According to their analysis the Milky Way formed stars with a high star formation intensity and generated outflows and high turbulence in the interstellar medium. This phase took place during around first 4 Gyr and concerned to the thick disk. Around half of the mass of the galaxy formed at this stage. This analysis came from the Milky Way's progenitor galaxies chosen by abundance matching.

## 2.3 Evolution of observational results for the Milky Way

Rose [14] obtained the density profile of red horizontal-branch (RHB) stars. The data were observed at three-dimentional spectral-classification system based on photographic image-tube spectra. The spectra were covered the wavelengths 340-450 nm with resolution of 0.25 nm. The aim of this article was to look at the metal-rich RHB stars to compute their density distribution and kinematics. They calculated the scale height of these stars and the dispersion of the vertical velocity component. The scale height is in a range from 500pc to 1kpc and z-velocity dispersion is around 40 km/s. According to these numbers, the author assumed that RHB belong to the thick disk component, rather than to the thin disk or to the halo component.

Another analysis of spectroscopic and photometric data from Lick Observatory was done by Friel[15]. Observation was done in two field, the first one was SA 94 ($l = 175°$, $b = 51°$) and the second one is in Serpens ($l = 36°$, $b = 51°$). He tried to fit the resulting data with the two components Galactic model, but the enormous number density value were required. Also, he noted the intermediate group of stars with the metallicities in the range $-0.80 <$

$[Fe/H] \leq -0.20$. This group of stars was identified as a thick disk. Friel showed that the fit by three component models favoured small scale height values, 700 pc for the thick disk. The local density was fixed at the value of 5%. He believed that the age determination models would help to clearly separate the two disk components.

Norris[16] compared the results of several work and observations. Using number stellar count, he noticed that the velocity dispersion appeared to vary monotonically and continuously with the abundances. Thus, he suggested that a dispersive mechanism of the disk stars is responsible for the thick disk phenomenon.

Barbuy and Erdelyi-Mendes obtained spectra at the 1.4m Coude Auxiliary Telescope(CAT) at the European Southern Observatory(ESO) in Chile of 24 moderately metal-poor stars to derive their oxygen-to-iron ratio. They used the Coude Echelle Spectrometer(CES) and a Reticon at a resolution of R = 80000. The exposure time was set to obtain spectra with high S/N ratio of the order of 200. The authors conclude that oxygen seemed to be overabundant relative to iron at $[Fe/H] = -0.8$. In the range of metallicities corresponding to the thick disk $-0.8 < [Fe/H] < -0.5$, the oxygen-to-iron ratios showed a scatter, however the author noted that the error bars were big, which was related to the oxygen identification, and further method improvements were required.

Cesertano et al.[17] used the data from two survey with the available proper motions, photometry and line of sight velocities. Firstly, they tried to apply the classical disk+halo model to the kinematic data of stars. It was shown that this model is inadequate and the third intermediate component was required. Thus, they performed a three-component fit and identified the properties of the thick disk component. The asymmetric drift value was $50 \pm 15 km/s$, the velocity dispersions were $(66, 37, 38) km/s$, the local density was around $10\% \pm 5\%$ and the scale height was less than 1kpc.

The faint photometric survey covering about 1 square degree and consisting of 1238 objects was presented by Von Hippel[18]. In order to provide the survey for probing the thick disk population, he provided the catalog of observation with the photometric and metallicity information complete to 17-18 V-magnitude. He showed that the photometric metallicities derived for 508 stars indicated for the existence of metal-poor stellar population, which was identified as a mixture of thick disk and halo stars.

Yamagata and Yoshii[19] released their sample of 7600 stars in the 16 squared degree area centered at $l = 200°, b = 59°$ direction for the stars brighter than 18 V-magnitude. The photometric data was taken with The Kiso Schmidt telescope. The authors used their sample with a combination of the photometric sample of 21.46 square degree in the direction near

the North Galactic Pole $l = 81°, b = 87°$ from Yoshii et al.[20] and the photometric sample of 11.5 square degree in the direction of South Galactic Pole $l = 0°, b = -90°$ from Gilmore and Reid[21]. Additionally, in order to investigate the radial structure of the Galaxy, they added to the analysis one more sample of 17 square degrees towards the Galactic center $l = 37°, b = -51°$ from Gilmore et al.[22]. The authors used the star count technique with the three-component model of the Galaxy, where the density profile of disk components was approximated by the exponential function. The analysis showed that the obtained scale height of thick disk was 900pc with a thin-to-thick local ratio of 0.019. They also spotted the north-south asymmetry and suggested that the Sun is located 40pc northerner than the Galactic mid-plane.

Reid and Majewski[23] analysed the data from the survey of proper motions and multicolor photometry in the north Galactic pole[24]. They applied the star count technique to the observational data, trying several models for the Galaxy to obtain the best fit parameters. As they pointed none of the models fitted data perfectly, however, preferable numbers of the thick disk scale height and local density are bigger than was shown before. They found the thick disk scale height of 1400-1600pc with the local density of 2%.

Soubiran[25] used the sample of 2370 stars with proper motion information, V and B magnitudes and radial velocities in 7 square degree area in the direction of $b = 80°$. The distances were derived from B, V magnitudes. The author deconvolved three Galactic components by the Stochastic-Estimation-Maximization(SEM) algorithm. For each galactic component a Gaussian function was used. The data was separated into 5 bins in the vertical direction. Soubiran noted that for the first two bins, $(0 < Z \leq 500$ the algorithm always converged to a two-component solution with thin and thick populations only. For the such configuration, the thick disk was huge and thick-to-thin ratio was around 15%. Despite the stability of such separation, Soubiran indicated this solution as a non-physical one. The reported values for the thick disk are following: asymmetric drift of $41 \pm 16 km/s$, mean rotational velocity $V_{rot} = 179 \pm 16$ and dispersion of U velocity $\sigma_U = 56 \pm 11 km/s$.

Ojha [26] tried to find new constrains on the thick disk. He used the sample at intermediate latitude and North Galactic Pole. The sample consisted of the data from 6 surveys: the field of direction of Galactic anti-centre $l = 167°, b = 47°$,the field of direction of Galactic center $l = 3°, b = 47°$, the field of Galactic anti-rotation $l = 278°, b = 47°$, and three surveys of field towards North Galactic Pole ($l = 58°, b = 80°, l = 42°, b = 79°, l = 124°, b = 87°$. Then he deconvolve the stellar components up to large distances from the galactic plane by Stochastic-Estimation-Maximization (SEM) and qualified the thick disk observations by the multivariate

discriminant analisys (MDA). A thick disk component was identified by SEM algorithm for different vertical distance bins up to around 3.5 kpc. The dependence of rotational velocity (V) lag with respect to the vertical distance (z) was shown. Using MDA for the Besancon model of population synthesis [27] on two data sets from Galactic center and anti-centre directions with 5 parameters: three apparent magnitudes blue (B), visual (V) and ultraviolet (U) bands and two proper motions, he found the best fit, when the circular velocity of the thick disk around 180 km/s. He also found the dispersions of velocities of the thick disk stars $\sigma_U = 67$, $\sigma_V = 51$, $\sigma_W = 46 km/s$ and scale heights for the thin disk (around 260pc) and thick disk (around 770pc)

Beers and Sommer-Larsen[28] published the sample of 1936 Galactic stars with metallicities $[Fe/H] \leq -0.6$. The author studied the metal-poor stars and tried to divide them into thick disk and halo component. They showed that for the sample separated into components according to the distance from the Galactic plane there was indication of strong gradient in rotational velocity among the metal-poor stars. The two-component model (thick disk and halo) with the constant rotational velocity reproduced the observed sample for large and small vertical distances. The rotational velocity of the thick disk was derived as $195 \pm 7 km/s$. The model suggested by the authors predicted the fraction of the thick disk metal-poor $[Fe/H] \leq -1.5$ stars of around 30% in the solar neighborhood. Also, they derived the velocity ellipsoid values from the subsample associated with the thick disk component. The subsample consisted of 349 stars with $-1.0 \leq [Fe/H] \leq -0.6$ and $|Z| \leq 1 kpc$. The resulting velocity dispersions are the following: $\sigma_U = 63 \pm 7 km/s$, $\sigma_V = 42 \pm 4 km/s$ and $\sigma_W = 38 \pm 4 km/s$.

Chen[29] presented his analysis of Majewski data[24]. He found that the intrinsic stellar distribution departed from a continuous trend and a discrete thick disk component was required. The asymmetric drift was identified of $-14 \pm 5 km/s$. He pointed that his result are very close to Reid and Majewski[23], since they used the same data. The abundance gradient was not found. With absence of any clear age-abundance correlation, Chen tended to the model of the origin of the thick disk, in which the thick disk is the result of the heating event of the thin disk.

Robin et al. [30] used several stellar counts models and the observational data from four different sources. Various thick disk hypotheses were fitted to observational data through a maximum likelihood technique. They concluded that the thick disk population can be described by an exponential density law in the galactic plane with a scale height of 2.8kpc and a modified exponential law in the direction perpendicular to the galactic plane with a scale height of 760pc. The local number density was calculated to be around 5.6%. The mean metallicity of the thick disk was found to be $-0.7 \pm 0.2 dex$. They emphasized some key property of the thick disk: a

density profile slope change between thin and thick disk, the thick disk is kinematically distinct from thin disk (kinematic gradient was not found for the thick disk), thick disk stars showed no vertical abundance gradient. According to the findings, they favoured the disruptive accretion scenario

Wolfe and Prochaska[31] studied stellar formation for different populations. In this article, they combined the metallicity data and column density data of HI with the new kinematic data from Keck I 10 m telescope. They showed that the metal-rich systems with damped $Ly\alpha$ lines still contained enough baryonic matter to account for the thick disk mass. They noted that such systems with the largest profile velocity width, showed a narrow range of metallicities, while the wider range of metallicities was obtained for small velocity profile width. Thus, they conclude that such system dominated by stars rather than by gas.

Dahnen and Binney[32] reported their findings from the newest Hipparcos data. Using main-sequence stars from Hipparcos catalog with a 10% or fewer errors in parallaxes (16054 stars) they calculated the motion of the Sun with respect to the local standard of rest(LSR). $U_\odot = 10.00 \pm 0.36 km/s$, $V_\odot = -5.25 \pm 0.62 km/s$ and $W_\odot = 7.17 \pm 0.38 km/s$. They emphasized that by cross-correlation of Hipparcos and other catalogs such as Tycho it was possible to reproduce the full three-component velocity, since Hipparcos did not measure radial velocities. However, they doubted that the radial velocities obtained from ground-based telescopes were unbiased. The author calculated velocity dispersion, concluding the ratio of $\sigma_U : \sigma_V : \sigma_W = 2.2 : 1.4 : 1$ with varying absolute values from $\sigma_U = 20 km/s$ to $\sigma_U = 38 km/s$ increasing with the colour index B-V. Also, it was shown that there was a vertex deviation for late-type stars, which means that the Galactic potential is non-axisymmetric at the Solar radius.

Ojha et al.[33] published new survey consist of photometry and proper motions for the stars from 2 directions at intermediate latitude. The first area covered 7.19 degrees centred in the direction of $l = 167.5°, b = 47.4°$ and the second one covered 20.84 degrees in the direction centered at $l = 278°, b = 47°$. The limiting magnitude of 18.5 for V-band was reported. They derived the density vertical profile for the stars from the survey and applied the star count technique with the two exponential function model of the disk. They found the scale height of thin and thick disk to be 250pc and 790pc respectively. The local thick-to-thin ratio was about 6%. They reported dispersions of the thick disk velocities as well as lag velocity. The values were $\sigma_U = 67 km/s$, $\sigma_V = 3 km/s$, $\sigma_W = 40 km/s$ and $V_{lag} = -53 \pm 10 km/s$. Also, the authors indicated that evidences for a vertical gradient of kinematic of the thick disk was not found.

Phleps et al.[34] presented the result of deep star counts on the Calar Alto Deep Imaging Survey(CADIS). The CADIS survey was designed to identify galaxies, however stars were also

identified in order to avoid confusion with quasars. The author analysed the subsample of 300 faint stars $15.5 \leq R \leq 23$ from this survey. The stars were located in two areas: $l = 85°, b = 45°$ and $l = 175°, b = 45°$. The distances were estimated by photometric parallaxes. A three-component model of galaxy, which consisted of a thin disk, a thick disk and a de Vaucouleurs spheroid (halo) was assumed. Several models for the Galactic disk density distribution were used in this work. The first model was the sum of two exponential functions, which gave the scale height of the thin disk of $280 \pm 14pc$ for the first field and $267 \pm 9pc$ for the second one, while for the thick disk the scale heights were $1267 \pm 74pc$ and $1296 \pm 116pc$ with the thin-to-thick ration at the mid-plane of around 1-8%. The second model was the sum of two sech function. The values for this model are following: $286 \pm 20pc$ and $358 \pm 13pc$ for the thin disk scale heights, $1478 \pm 30pc$ and $1132 \pm 84pc$ for the thick disk, with the thin-to-thick ratio in the huge range from 2% to 25%. And finally square sech model with the values: $352 \pm 26pc$ and $360 \pm 13pc$ for the thin disk scale heights, $1158 \pm 112pc$ and $1047 \pm 71pc$ for the thick disk, with the thin-to-thick ratio in the range from 3% to 6%.

Detailed analysis of chemical abundances of the disk stars was given by Prochaska et al.[35]. The authors interpreted high-resolution spectra obtained with HIRES spectrograph on the 10 m Keck I telescope. The sample of 10 thick disk stars with high-resolution $R \approx 50000$ and high signal-to-noise ratio $S/N > 100$ was observed in the range of wavelengths $4400 - 9000$. They confirmed the enhancement of O and Mg for the thick disk stars, and also showed by others elemental abundances that thick disk population has a distinct chemical history from the thin disk one. The authors noted similarities in the spectra of thick disk stars and bulge stars, which leaded to the suggestion that thick disk and bulge formed from the same gas reservoir at a common epoch. The decreasing trend of over-abundances for some $\alpha$ elements with increasing [Fe/H] was found. They pointed that if such behaviour can be clearly explained by the onset of type Ia super novae, then the thick disk probably was formed during several Gyr and according to this scenario models of heating of initial thin disk are favoured.

The work of Nissen et al.[36] also devoted to elemental analysis. They used data from Beijing Astronomical Observatory with Coudé Echelle Spectrograph and attached to the 2.16m telescope and data from ESO NTT EMMI spectrograph. Both samples were obtained with a high resolution $R \geq 40000$. The stars from the samples were representing thin disk, thick disk and halo. They showed that the Sc abundance decreased with increasing metallicities, while Mn increased from $[Mn/Fe] \approx -0.5$ at $[Fe/H] = -1.4$ to zero at solar metallicity. They spotted a discontinuity of sharp increase of [Mn/Fe] at $[Fe/H] \approx -0.7$ that they associated as a transition between thin and thick disk.

Tautvaišienė et al.[37] studied spectroscopic data of 13 core helium-burning (red horizontal branch) stars in the thick Galactic disk. The data were obtained with the SOFIN spectrograph on the Nordic Optical Telescope(NOT). Analysing the results, they conclude that for these stars they did not find enhanced overabundance of Na and Al. Abundances of O, Mg, Eu and some other heavy elements with comparison to iron for stars studied by them showed that the thick disk population and thin disk population had a different chemical history. They proposed that metal enrichment timescale was short for the thick disk population.

Another result based on the spectroscopic data was published by Gilmore et al.[38]. The spectroscopic survey of about 2000 F,G stars located at vertical distances from 0.5 to 5kpc from Two Degree Field facility on the Anglo-Australian Telescope was used. The spectra resolution was about 2.5Åin the wavelength region from 3700 to 4700 Å. Radial velocity accuracy was about 15 km/s. Analysing the data, they noted that at the distance of few kpc from Galactic mid-plane the thick disk population behaved differently with comparison to predictions. The rotational velocity of this population was significantly lower. The value of about 100 km/s for the rotational velocity was obtained instead of the usual value of about 180 km/s. The author proposed that such strange behaviour can be caused of the existence of a population of stars from a disrupted satellite galaxy that merged with a Milky Way disk 10-12Gyr ago.

Nykytyuk and Mishenina[39] tried to reproduce the star formation rate for the thin and thick disk according to the model with the gas inflow. The main observational indicator is a chemical abundance. However, [Fe/H] measurements showed overlapping between thin and thick disk components. While for the Fe enrichment responsible to super nova Ia(SNIa), $\alpha$ elements are synthesized by massive stars. Thus, the amount of Fe in the interstellar medium reached maximum in the first Gyr after initiation of star formation, while $\alpha$ elements enrichment took place during several tens Myr. This idea was used by the authors to reconstruct star formation history be $[\alpha/Fe]$ ratio. They concluded that the star formation of the thin disk stars started 9-10 Gyr ago and had been going smoothly, while the majority of thick disk stars were formed during 2-3 Gyr and almost stopped about 10 Gyr ago. A bit later, Mishenina et al.[40] presented analysis of high-resolution spectra of FGK dwarfs and giants. Dividing the sample of 350 stars into thick and thin disk by available kinematical information, they showed that there are a few thin disk stars with $[Fe/H] < -0.30$. Metal-poor stars $[Fe/H] < -0.60$ have high Mg $[Mg/Fe] > 0.20$ and Si $[Si/Fe] > 0.15$ abundances, while at the solar metallicity the value is around 0.20 for both Mg and Si. Thick disk stars have on average higher $[Mg/Fe]$ than the thin disk stars. For metallicities $[Fe/H] > -0.30$ the dispersion of $[Si/Fe]$ is small, while it is high for low metallicities.

In order to improve our understanding of thin-thick disk separation, more attempts of kinematical and chemical division into components were made. Soubian and Girard[41] tried to reveal more chemical peculiarities of the disk using for separation into thin and thick disk populations kinematical data from the Hipparcos catalogue. The defined eight parameters for thin disk, thick disk and Hercules stream, according to which they used probabilistic way to obtain the stellar populations. They chose the star to belong to the subsample when there is more than 80% probability. Setting the density of 72%, 19% and 9% for the thin, thick and Hercules stream components, they obtained their final sample consisted of 428 thin disk stars, 84 thick disk stars and 44 Hercules stream stars. 81 stars were not classified. Performing the chemical analysis of these components, the authors concluded that the thin and thick disks overlap in metallicity and exhibit parallel slopes of $[\alpha/Fe]$ vs. $[Fe/H]$ in the range of metallicities from -0.80 to -0.30. The enhancement of $\alpha$ elements in the thick disk had been quantified to be +0.10 dex. They suggested to use $[AL/Fe]$ and $[Mg/Fe]$ for which offset between disks even bigger, about +0.15 dex. They estimated the age difference of thin and thick disks of about 4Gyr, so an interruption in star formation between their formation took place. The stars from Hercules stream span widely in metallicity and age. Their chemical properties are similar to the thin disk, which favors the hypothesis of resonance influence by the central bar. Also, it was reported that metal-rich stars assigned to the thick disk did not follow global trends and their nature remained unclear.

Famaye et al.[42] also used the Hipparcos catalog with additional radial velocities from CORAVEL and some more precise proper motions from Tycho-2 to investigate kinematics of 5311 type K giant stars and 719 type M giant stars. All the stars were single stars, the binary stars were excluded from sample before. They applied a maximum-likelihood method based on a Bayesian approach to estimate kinematical parameters and identify subgroups in the solar neighborhood. Hyades-Pleiades supercluster, the Sirius moving group and Hercules stream were identified. The authors reproduced be the isochrones the age of these subgroups to be in a very wide range, which leaded to the conclusion that these subgroups in velocity space are related to the dynamical perturbations of the spiral arms or of the bar. They presented their estimations of the kinematics of these groups, emphasising that the fine structure of phase space in the solar neighborhood can not be reproduced in terms of an asymmetric steady-state model, and more complex models and simulations were required.

Marsakov and Borkova[43] collected wide data of stellar parameters and chemical abundances from various surveys. Performing statistical averaging of this data with error estimation, they combined this data with distances and proper motions calculated from Hipparcos, Ty-

cho, PPM-N and PPM-S catalogs. Their final sample consisted of 847 dwarfs and subgiants. They divided the sample into thin, thick disk and halo in the following way: thin disk stars $\sqrt{U^2 + V^2 + W^2} < 85 km/s$ and $\sqrt{Z_{max}^2 + 4 * e^2} < 1.05$, thick disk stars $\sqrt{U^2 + V^2 + W^2} < 175 km/s$ and other, where $e$ is eccentricity of a star orbit. Analysing the chemical abundances and using the relations between iron and magnesium abundances to age, they concluded that the Galactic thick disk is older than the thin one. The majority of thick disks stars were formed within 1.1-1.6 Gyr after protogalactic cloud began to collapse, however the metal-rich tail of thick disk had born after the beginning of thin disk formation.

Bilir et al.[44] studied the data taken from Sloan Digital Sky Survey Data Release 5(SDSS DR5) for 36 high-latitude field $60 \leq b \leq 65$covering Galactic longitude range $0 \leq l \leq 360$. They analysed photometry and, applying an exponential density distribution model for the two disk components and de Vaucouleurs spheroid for the halo, they fitted the scale height parameters for every field. They spotted the variation of scale heights. The thick disk scale height changed from about 550 pc at $120 < l < 150$ to about 720 pc at $250 < l < 290$ and thin disk scale height changed from about 195 pc at $160 < l < 230$ to about 180 pc at about direction to the center. They suggested that such variation could be explained by the influence of gravitational effect of the Galactic long bar.

Karaali et al.[45] suggested "unified density law" to describe spatial density in the vertical direction up to 8 kpc from the Galactic plane. This unified density has the following form: $D(z) = exp[-(a_2 * z^2 + a_1 * z + a_0)]$. They fitted the obtained density distribution from the data[46] and showed the calculated parameters of $a_2, a_1$ and $a_0$. Thus, they voted that the widely discussed separation of disk into thin and thick populations was misleading, and the Galactic disk is a single structure.

Smiljanic et al.[47] proposed to use Beryllium abundances as a measure of age. For this purpose they took the sample from Venn et al.[48] with kinematic data and assigned probabilities for the thin disk, the thick disk and the halo components. Venn and co-authors selected 90 stars for their investigation, but instead of probabilities they considered a star to belong to the galactic component, for which the probability is highest. Thus, 9 thin disk stars, 30 thick disk stars and 49 halo stars were selected. They aimed to study stars from different populations, but with the similar abundances. The chosen stars of thin and thick disk are in the metallicity range of $-1.70 < [Fe/H] < -0.50$ and halo stars in the range of $-2.48 < [Fe/H] < -0.50$. Spectra for the stars were obtained from Ultraviolet and Visual Echelle Spectrograph(UVES) on the Very Large Telescope(VLT). They showed the linear increase in Be abundances with $[Fe/H]$ and $[\alpha/H]$. Their age estimate by Be was fairly good for the disk, but failed to repro-

duce halo population age. The better models of Be abundance, including galactic cosmic rays were required.

Spagna et al.[49] analysed the data from Second Guide Star Catalog based on the SDSS DR7. They selected the dwarf FGK stars according to the stellar parameters: the effective temperature in range of $4500 < T_{eff} < 7500K$ and surface gravity $log(g) > 3.5$. Distances were computed from isochrones, from dust extinction corrected magnitudes and metallicities observed by spectra. The final cuts imposed were: proper motion error less 10 mas/yr, error on the velocity less than 50 km/s, total velocity less 600 km/s, distance less than 5 kpc and magnitude 13.5<g<20.5. The 27000 low metallicity $-3 < [Fe/H] < -0.5$ dwarf stars were used as tracers of inner halo and thick disk. They fitted rotational velocity histogram by two Gaussian functions corresponding to the halo and the thick disk populations, and also plotted dependencies of rotational velocities on metallicity and vertical distance. They found the rotational velocity-metallicity correlation, with the gradient of $40 \div 50 km/s/dex$ among the thick disk stars with metallicities $-1 < [Fe/h] < -0.5$. Also, the vertical rotational velocity gradient of $-19 \pm 2 km/s/kpc$ was found.

Carollo et al.[50] explore the Galactic structure using from SDSS SEGUE survey. They derived the kinematical properties of thick disk and halo by sample of 16920 stars within 4 kpc from the Sun. They examined how many components are needed to describe the data. Additionally, to the halo component and thick disk, they studied metal wear thick disk population. The proposed metal wear thick disk population appeared chemically and kinematically distinct from the thick disk. They noted that the rotational velocity of this component as well as its metallicity were similar to the values derived for Monoceros stream. Also, scale heights for thick disk were computed and its value was $(\sigma_{V_R}, \sigma_{V_{Phi}}, \sigma_{V_Z}) = (53 \pm 2, 51 \pm 1, 35 \pm 1)$.

Lee et al.[51] used a sample of low-resolution spectra of initially about 63000 stars from SDSS DR8, obtained during the SEGUE sub-survey, which were originally targeted as G-dwarf candidates. They excluded stars with lack of information of stellar parameters, radial velocities or proper motions. To study the local dwarf star sample, the authors also excluded stars with distance more than 3 kpc from the Sun and surface gravity $log(g) < 4.2$. Accounting for dust extinction, the distances were estimated using a calibrated set of stellar isochrones. Considering the solar motion of $(U, V, W)_\odot = (11.10, 12.24, 7.25) km/s$ with the distance of Sun of 8kpc from the Galactic center and the rotational velocity of LSR of 220km/s, they reduced the contamination of halo stars in the sample imposing condition on rotational velocity $V_\Phi < 50 km/s$, metallicity $[Fe/H \leq -1.2]$ and distance from the Galactic center $7 < R < 10 kpc$. Thus, they chose the stars that are satisfying the following criteria: distance $d < 3 kpc$, surface gravity

$log(g) \geq 4.2$, signal-to-noise ration of spectra $S/N \geq 30^{-1}$, rotational velocity $V_\Phi > 50 km/s$, metallicity $[Fe/H] > 1.2$ and the radius in the galactic plane $7 < R < 10 kpc$. The final sample consisted of about 17300 stars. The authors separated the sample into thin disk and thick disk population according to $[Fe/H]$ and $[\alpha/Fe]$. For the stars with $[Fe/H] \geq -0.8$ the thin disk component was chosen to satisfy $[\alpha/Fe] < -0.08 * [Fe/H] + 0.15$ and the thick disk component for $[\alpha/Fe] < -0.08 * [Fe/H] + 0.25$. For the stars with $[Fe/H] < -0.8$ the thin disk component was chosen to satisfy $[\alpha/Fe] < +0.214$ and the thick disk component for $[\alpha/Fe] > 3.14$. The detailed analysis took place. They reported that the rotational velocity gradient with increasing $[Fe/H]$ for the thin disk was $-22.6 \pm 1.6 km/s/dex$, while the thick disk showed a positive slope $-45.8 \pm 2.9 km/s/dex$. They showed that the distribution of rotational velocity almost independent of radial distance for the thick disk and independent for the thin disk. The authors noted that the lag of rotational velocity between high-$[\alpha/Fe]$ (thick disk) and low-$[\alpha/Fe]$ (thin disk) was constant at a given vertical distance and its value was about 30km/s, implying that the populations were kinematically separated. The vertical gradient of rotational velocity for the thick disk found from the data was $-9.4 \pm 1.3 km/s$. There was no trace of correlation between orbital eccentricity and metallicity for the thin disk, while for the thick disk, eccentricity increased with decreasing metallicity. Summarising, the authors pointed that radial migration influenced the structural and chemical evolution of the thin disk, but it was not that significant for the formation and evolution of the thick disk.

Mishenina et al.[52] analysed the spectra of three different disk populations: thin disk, thick disk and Hercules moving group separated similar to their previous work[40]. The high resolution R=42000 and high signal-to-noise $S/N > 100$ spectra were obtained from ELODIE échelle spectrometer on the 1.93-m telescope of the Haute Provence Observatory. The authors determined the abundances of Cu, Zn, Na and Al in local thermal equilibrium approximation for the sample of 172 F,G,K dwarf stars. They reported that the Cu abundances are the same among all populations, while the mean Al and Zn abundances for the stars of thin and thick disk populations differ significantly.

Kordopatis et al.[53] presented their spectroscopic survey of F,G and K dwarf stars. The observations were done with VLT/FLAMES feeding the GIRAFEE spectrograph in MEDUSA mode. Low resolution spectra $R \approx 6500$ in the wavelength range $8206 < \lambda < 9400$ were obtained. The wavelength range dedicated to identification of Ca II line, Pashen lines, Mg I line and some molecular lines such as TiO and CN. The distance estimation was performed by isochrones method. The initial sample of 689 stars was reduced by 53 binary stars or low quality spectra, by 24 stars due to bad fit with the stellar parameters fit, by 11 due to bad distance

determination and some stars by data quality restriction. The final sample consisted of 479 stars, for 452 stars had full 6d phase-space coordinates. The authors used simulated Besançon stars[? ] to compare characteristics of their sample with the mock catalog from the simulation. The general trends were coincided, but some slight inconsistency was spotted. Then the author used two approaches to divide the sample into the thin disk, thick disk and halo components. The first approach was a probabilistic assigning to the specific component with the given kinematic characteristics. Following this procedure, 154 belonged to thin disk, 193 stars belonged to thick disk and 105 stars belonged to the halo component. The second approach based on the vertical distance divided the sample into 163 thin disk stars with $Z < 800pc$, 187 thick disk stars with $1 < Z < 4kpc$ and 5 halo stars above 5 kpc. They found the mean rotational velocity of -167km/s for the thick disk, the mean metallicity of -0.45 dex, with the metal-poor tail up to -1.8 dex, the vertical velocity gradient of $19 \pm 8km/s/kpc$, vertical metallicity gradient of $-0.14 \pm 0.05$ and the correlation between metallicity and rotational velocity of $\frac{\partial V_{phi}}{\partial [M/H]} = 43 \pm 11km/s/dex$. The scale height of $694 \pm 45pc$ was found for the thick disk.

Moni Bidin et al.[54] studied the variation of the kinematical properties of the Galactic thick disk with respect to the distance from the Galactic plane. The high-resolution spectra were observed by four different telescopes with similar characteristic instruments. They cleaned their sample from the dwarf stars and from the closest $|Z| < 1.3kpc$ stars to reduce thin disk contamination. Also, the cut on velocities was imposed to remove the halo stars from the sample. The final sample consisted of 412 stars. The distances were derived photometrically from reddening corrected magnitudes. The behavior of calculated U,V,W velocities with respect to the vertical distance Z was shown for distances up to 4.5 kpc. The mean vertical velocity component did not show deviation from zero in the whole range, the stars closer 3 kpc showed the motion in the direction of the anti-center $V \approx -20km/s$, while the stars from 3.5 kpc to 4.5 kpc showed the motion towards the Galactic center $V \approx 20km/s$. The rotational velocity steadily decreased with the vertical distance, with the gradient of about -30km/s/kpc. All the velocity dispersions smoothly increased with the distance from the mid-plane. Any significant change of the velocity dispersion ratios was not found. The authors also noted that the many kinematic value deviates from linear relation between 2.5 and 3.5 kpc height. An origin of this deviation was unknown and could be related to an unknown moving group.

Carrell et al.[55] published the article about the metallic gradient of thick disk stars. They, similarly to Lee et al.[51], used dwarf stars from SDSS DR8, also determining the distances by isochrone method. The authors did not divide stars according to their metallicity or another chemical information. They took all available stars in the range of vertical distances $1 < |Z| <$

$3kpc$ and measured their metallicity as a function of vertical distance and as a distance from the Galactic center. The found vertical metallicity gradient was $-0.113 \pm 0.010 dex/kpc$, and for the radial direction they found a metallicity gradient of about $0.03 dex$.

Bovy et al.[56] used a sample of G-dwarf stars with measured spectra from SDSS SEGUE survey. They divided the sample into narrow bins in the $([\alpha/Fe], [Fe/H])$ plane with 0.1 width in $[Fe/H]$ and with 0.05 width in $[\alpha/H]$. They called the subsample for the bins as mono-abundance component. The showed that each mono-abundance component exhibit nearly isothermal kinematics in the vertical direction and a slow outward decrease in the radial direction. The mean vertical velocity dispersion gradient is $0.3 \pm 0.2$, so each mono-abundance component is consistent with isothermality. They found the smooth variation of velocity dispersion from 15km/s for young component with abundance about solar ones to 50 km/s for old component for metal-poor $[\alpha]$-enhanced stars. The authors presented that according to this mono-abundance division the vertical parameters change smoothly and monotonically declining the usual separation of the disk into thin and thick components.

Williams et al. [57] studied the kinematical properties of red clump giant stars using RAVE data. The authors restricted the region to a volume within $6 < R < 10 kpc$ and $2 < Z < 2 kpc$. Their sample consists of 72365 stars. They found the difference between north and south in the radial velocity streaming motion $V_R$ as well as the complex behavior in the vertical velocity motion $V_Z$ in the solar vicinity. Stars inside the solar circle move upwards above the Galactic plane and downwards below the plane, while the stars outside the Solar circle move toward the Galactic plane from the both regions above and below the plane with velocities up to $|V_Z| = 17 km/s$. The authors connected such $V_Z$ structure to the wave of compression and rarefaction in the direction perpendicular to the Galactic plane, which could be causes by recently engulfed satellite galaxy or by the disk spiral arm, as Williams et al. [57] suggested.

Kawata and Chiappini[**?** ] analysed the literature related to the thick disk studies. They widely discussed the problem of thick disk selection. The thick disk selected geometrically shows different properties than the thick disk selected chemically. They noted that in the $([\alpha/H], [Fe/H])$ plane thin and thick disks are significantly distinct, while geometrically selected thick disk, even 1 kpc far from galactic plane, can be contaminated by the thin disk stars, and, as a result, the chemical properties of such sample differ.

Yan et al.[58] studied the kinematical and chemical distribution of the high-velocity stars with Gaia DR2 combined with the LAMOST and APOGEE spectroscopic surveys. The authors show that for such stars the rotational velocity distribution can be fitted by a two Gaussian function with the peaks at 164km/s and 3 km/s, which were associated with high-velocity

thick disk(HVTD) and metal-rich stellar halo(MRSH) respectively. The HVTD has the same rotational velocity and metallicity as the thick disk, however, HVTD has the same position as the halo in the Toomre diagram. The MRSH shows the same rotational velocity and position in the Lindblad and Toomre diagrams as a halo, but has metallicities similar to the thick disk. They also suggest that the properties of these structures imply that they were formed in-situ rather than were accreted from satellite galaxy.

## 2.4 Models and simulations

Bahcall and Soniera [59, 60, 61, 62] in the series of articles analysed the Galactic kinematics and suggested the first model for star counts. Their model of galaxy consisted of two different stellar components:a disk component and a de Vaucouleurs spheroid. The author, analysing luminosity function and its agreement to observation data, decided to use the luminosity function in the following form

$$\begin{aligned} \mathrm{N}(M) = \frac{n_* 10^{\beta(M-M^*)}}{[1+10^{-(\alpha-\beta)\delta(M-M^*)}]^{1}/\delta}, M_b \leq M \leq 15, \\ \mathrm{N}(M) = \mathrm{N}(15), 15 \leq M \leq M_d, \\ \mathrm{N}(M) = 0, M \leq M_b, or M \geq M_d, \end{aligned} \tag{2.1}$$

with $n_* = 4.03 * 10^{-3}, M^* = +1.28, M_b = -6, M_d = +19$ and $\alpha = 0.74, \beta = 0.04, \frac{1}{\delta} = 3.40$.

Combining the star vertical density profile

$$\rho_d^{\perp}(Z, M) \propto exp(-Z/H(M)) \tag{2.2}$$

where H is the scale height, with the star density profile within the Galactic plane

$$\rho_d^{\parallel} \propto exp(-(z - r_0)/h) \tag{2.3}$$

where $r_0$ is the distance of the Sun from the galactic center and h is the scale length, they chose the density profile in the form

$$\rho_d(r, M) = \rho_d^{\parallel} * \rho_d^{\perp} = exp(-Z/H(M) - (z - r_0)/h) \tag{2.4}$$

For the spheroid they took the projected surface brightness

$$\lg(\frac{I(\Theta)}{I(\Theta_e)}) = -3.3307 * (\frac{\Theta}{\Theta_e}^{1/4} - 1) \tag{2.5}$$

where $\Theta$ is the angular distance from the center and $\Theta_e$ is the angular distance with half luminosity enclosed, and the spatial density distribution

$$\rho_s(r) = C * \frac{exp(-b(r/r_e)^{1/4})}{(r/r_e)^{7/8}} \tag{2.6}$$

where C is the normalization constant, b = 7.669 and $r_e$ is the spatial distance of $\Theta_e$ projection.

Finally, the surface density of stars for each component can be expressed

$$A(m_1, m_2, l, b)d\Omega = \int_{m_1}^{m_2} dm \int_0^{\infty} \nu(M)\rho(R, M)R^2\, dRd\Omega \tag{2.7}$$

where R is the distance from the Sun, $m_1$ and $m_2$ are apparent magnitudes and $l$ and $b$ are galactic coordinates.

Since this model does not account for the complex structure of the galactic disk, we will not discuss the results of comparison of this model with observation, we just mention that they noted that disk function is steeper close to the galactic mid-plane. Nevertheless, this was the first attempt to fit stellar counts with the predicted model of the Galaxy. This work gave raise to more complex models of Galaxy.

Gilmore et al. [63] constructed his model for star count. The model was similar to Bahcall and Soniera model, but different luminosity function was used. Gilmore emphasised that with the poor observation data some nonphysical models may to be seen the best fit. Further, in the series of works [64, 21, 65, 66, 22] he with his colleagues showed the existence of complex structure of the thick galactic disk and pointed that the thick galactic disk could mistakenly be considered as a spheroidal halo component.

Pritchet [67] suggested his model for the star count. He built the model under several assumptions: two-component disk-spheroid model, with cylindrical symmetry near the Galactic center and symmetry with respect to the galactic plane. It should be noted that the disk in his model is allowed to consist of several subcomponents. The disk density was separated into radial and vertical component

$$\rho_d(R, Z) = \rho_0 * F(R) * g(z) \tag{2.8}$$

where $\rho_0$ is the local number density, R is distance from the center of the Galaxy and Z is distance from the galactic mid-plane. He chose exponential radial function

$$F(R) = exp(-(R - R_0)/h) \tag{2.9}$$

where $R_0$ is the distance of the Sun from the Galactic center, and h is ... (chosen to be 3.5kpc). He also applied the cutoff for the disk component for $R = 15kpc$. For the vertical density profile the author used two different function: exponential disk $g(Z) = exp(-|Z|/\beta$ and self-gravitating isothermal disk $g(Z) = sech^2(Z/2\beta)$, where $\beta$ depends on magnitude for exponential disk, but changes slightly (assumed to be around 80). The luminosity function was constructed according Luyten [68] and Jahreiß and Wielen [69]. For halo density profile, the following function was chosen

$$\rho_h(a) = f_h * \rho_0(a_0^n + R_0^n)/(a_0^n + a^n) \tag{2.10}$$

where $f_h$ is the fraction of number of stars in the solar neighborhood, $a_0$ is assumed to be 1 kpc and $a^2 = r^2cos^2(b) + R_0^2 + z^2/\alpha^2 - 2R_0cos(b)cos(l)$. r is the distance from the Sun, $\alpha$ is the axial ratio of the halo, and b,l are the galactic coordinates. Combining with the luminosity function, one can finally compute star counts being the number of stars with apparent magnitude per unit interval in magnitude within solid angle.

This model allows to calculate parameters of the model by comparing star counts with observations. The author performed such comparison. Among others, he found that the most probable model was the model with two-subcomponent disk. For the case of isothermal disk, the scale height of 150 and 600 pc were observed for the thin and thick disk, with the fraction of stars belonging to the thick disk components in solar neighborhood between 0.1 and 0.3. For the exponential model of disk the values of the scale height are slightly different, 100pc for the thin disk and 400pc for the thick one, with around the same fraction of the thick disk stars in the solar vicinity. However, they warned that their residuals of modeling were bigger than it was expected.

Robin and Creze [27] constructed their detailed model of the stellar content of the Milky Way. They started from the equation of stellar statistics for the apparent distribution in a given field of view.

$$A(m) = \int_r \nu(M)\rho(r)r^2\omega\, dr \tag{2.11}$$

where A(m) is a number of stars within apparent magnitude m in the solid angle $\omega$, M is an absolute magnitude, $\rho(r)$ is a density and r is a distance from the Sun, while $\nu(M)$ is a luminosity function. The equation breaks into a sum of components with different $\rho$ and $\nu$. To solve this equation, some assumptions were necessary. They started from a distribution for number of stars per cubic parsec in a given cell of the CMD, with ages in a given range, near the Sun.

$$\Phi(M_{bol}, T_{eff}, Age) \tag{2.12}$$

This distribution defines the stellar content in the solar vicinity. Chemical composition $\varphi(Z, Age)$ is set with a given metallicity for stars. After specifying the distribution of intrinsic properties for the solar vicinity, number of stars $N$

$$N = \Phi * \varphi * \rho * r^2 cos(b) dldbdr \tag{2.13}$$

can be obtained with the given density distribution. Where r,l,b are the coordinates. Then one can derive the distribution of these stars to observation from the Earth for any pass band.

This approach is very universal, since one can use any models to connect the theoretical values such as age, temperature with the observational ones such as magnitudes and colour index. The calibration values for the solar neighborhood are required. Robin and Creze showed that local date favors a three-component model of Galaxy.

Bahcall[70] chose a more theoretical approach to the galactic modelling. He combined the Boltzmann and Poisson equations for the motion of isothermal stars perpendicular to an axisymmetric galactic disk. Several assumptions, such as neglection of diagonal terms for velocity ellipsoid, decoupling of vertical and plane motion, Z-independence of halo density profile, were made in order to simplify the equations. He demonstrated the numerical solution for the vertical profile in case of one-component disk and multicomponent disk of the Galaxy.

Jenkins[71] was investigating the heating of the galactic disk through scattering by molecular clouds and spiral waves. For this reason, he presented his solution of orbit-averaged Fokker-Plank equation by Monte Carlo simulation. The vertical potential of the disk was described in two ways: by using a fixed realistic unharmonical potential and by self-consistent potential. He found that assumed strength of spiral heating did not significantly affect the shape of vertical density distribution and the vertical dispersion. He pointed that in his model for a coeval stellar disk there was lack of high-velocity stars and the density distribution wings were sub-isothermal. The resulting disk was closely isothermal when a gas disk converted into stars at a constant rate.

Dehnen[72, 73] performed a numerical simulation. The simulation includes the bar, which

is growing from the initially axisymmetric potential disk. He showed that according to the simulation, the outer Lindblad resonance of bar is responsible for the bimodal structure of the disk in the velocity space. The velocity of the division line depends on distance from the outer Lindblad resonance, the bar angle, the shape of the bar and the normalization of the rotation curve. Additionally, he measured the bar pattern speed of $53 \pm 3 km/s/kpc$, but the error is not accounted for the systematic error and there was uncertainty on the bar angle, which was also not accounted.

Fux[74] simulated the Galactic bar influence on the stellar orbits by analytical 2D modeling of barred potential and by N-body simulation. He modeled the galactic potential as a sum of axisymmetric component and bar component, and then studied the motion of test particles in the potential. He obtained that there are two regions:the region with a regular orbit motion and the region with a chaotic orbit motion. The chaotic part depends on only non-axisymmetric part of potential. He noted that the splitting into regular and chaotic parts depends on the value of the Hamiltonian and related to the bar resonance. The author concluded that the simulation of the test particle motion started from initially axisymmetric potential and evolved to the rotating bar potential reveal a decoupled evolution of the regular and chaotic disk phase space regions. For the regular regions the density of phase space almost conserves, while for the chaotic regions the stars evolves by chaotic mixing towards a uniform population of the phase space volume. The phase space within the corotation resonance represents the large part of the particle with chaotic orbits, which are further spread through the disk. Thus, the regions outside corotation become more crowded by chaotic orbit particles. The author showed the overdensity structures appeared in the phase space for the Sun position are similar to the observed Hercules stream. The N-body simulation confirmed the results obtained from the analysis of test-particle motion.

Sellwood and Binney[75] showed by their simulation that the spiral waves in galactic disks churn the gas and the stars preserving their angular momentum distribution and increasing their random motion. They based the model on the theory of horseshoe orbits and a steady potential. The majority of stars of the simulation were effected by the corotation resonance. They showed that the group of stars from different sides of the resonance just exchange their position without significant radial spreading or increase in non-circular motion. So, the transient spiral waves are responsible for the radial migrations, which caused the observed metallicity gradient. They noted that deflection of interstellar gas clouds at corotation should induce an anticyclonic circulation in the interstellar matter, which was detected in observations of interstellar velocity field.

Robin et al[76] published an article with description of Besançon model of the Galaxy. The main aim of creation of the model is to reproduce the stellar content of Milky Way, using scenario of formation and evolution with some physical assumption. The model consists of 4 population: disk, thick disk, stellar halo and bulge, with a set of evolutionary tracks and assumptions on density distributions. The stellar content of each epoch is computed from standard parameters: the initial mass function and the star formation rate. The detailed model for each component with the parameters used are presented. It should be noted that in the model the authors followed the thick disk formation scenario by a merger event at the beginning of the life of thin disk 11 Gyr ago.

Abadi et al.[77] presented analysis of the photometric and dynamic properties of the disk galaxy in the simulated $\Lambda CDM$ scenario. The 3D simulation of hydrodynamical and gravitational effects includes gas, stars and dark matter components. Transformation of cold dense gas was responsible for the star formation processes with the rate controlled by the density of gas. Energy feedback during the evolution of stars is also included. The galaxy was experienced a number of high-redshift mergers and then quiescent period. At actual moment galaxy consist of the old spheroid component, which can be fitted by superposition of $R^{1/4}$ functions, and the young disk component, which can be describe by exponential function. The total light is distributed almost evenly between these components. An about quarter of stars were formed after last merger. The authors found very similar galaxy UGC 615, however they noted that its dynamical properties differ significantly. Thus, they showed that galactic properties can be explained as a result of hierarchical clustering scenarios, where the spheroid components are results of mergers and disks are results of quiescent accretion.

De Simone et al.[78] studied the heating of the velocity distribution by spiral waves. The motion of the stars in the disk was modeled by external potential consisted of axisymmetric part and other sources. The kinematics of a population of stars was described by the distribution function. Assuming the flat rotational curve for the underlying axisymmetric Galaxy, they modeled the spiral structure as a superposition of waves. They were focused on effects of transient spiral arms, since these effects can heat stars over a large distance. Their approach was based on direct numerical integration of test-particle orbits in the sheared sheet. The authors confirmed that transient spiral arms can heat the galactic disk and spiral structure can lead to a wide range in age-velocity dispersion relation. They found their results of mean radial velocity, axis ratios of the velocity ellipsoid and variation of the vertex deviation consistent with observations for the solar neighborhood. The authors found that the existence of small-scale structures in the velocity distribution can be reproduced by transient spirals. Thus, they con-

cluded that transient spiral waves are the dominant heating mechanism of the disk in the solar neighborhood.

Sotnikova and Rodionov[79] connected the mass of spherical halo component with the minimum possible thickness of stable stellar disk. They first derived a theoretical relation and then test it in the N-body simulation. The global parameters are assumed to be stable against perturbations in the plane and in the vertical direction. The stability condition limits the radial and vertical velocity dispersion for a given halo mass. Thus, the disk thickness and the halo mass are related. Considering stability condition of the disk with isothermal density profile, square sech function along Z axis, and vertical equilibrium condition one can estimate how thickness of the disk related to the mass of spherical halo. The larger the relative mass of the spherical component within the fixed radius, the smaller the relative disk thickness in this radius. Then, the authors aimed to test the relation in N-body simulation. They used an algorithm based on the hierarchical tree algorithm with additions from the NEMO software package. The disk consisted of from 300000 to 500000 gravitating particles depending on model. The spherically symmetric component was described as an external static potential, which was presented as a superposition of the bulge potential and the dark halo potential. According to the equilibrium Jeans equation, the initial velocities were set. They tried several configurations with the mass ration of spherical component to the disk component from 0.25 to 4. Analysing the results of the simulation, they found that their theoretical estimation can be used as lower limit estimation for the dark matter halo mass. They pointed that the main cause of the differences between theoretical estimation and simulation is that saturation level of the bending instability in simulation can be much higher than the then the level given in the theoretical estimation by the linear criterion. They also concluded, that the more concentrated the spherical component toward the center of the galaxy the thinner stable disk can be observed.

Roškar et al.[80] by their self-consistent high-resolution N-body with smooth particle hydrodynamics simulation showed the importance of the radial migrations in the disk formation process. They traced that stars, being scattered by resonance of transient spiral arms, can migrate across significant galactocentric distances, at the same time preserving their circular orbits. The noted that the radial migration provides an explanation for the observed age-metallicity relation. Showing the importance of such an effect as radial migration, they concluded that further studies are required to estimate its prevalence in the galactic formation process.

Bournaud et al.[81] presented the simulation of gas-rich young galaxies. The simulation was based on the evolution of Jeans-unstable gas-rich galactic disks using a particle-mesh sticky-particle code. The spatial resolution of 35 pc was chosen. Two millions particles for each com-

ponent of gas, stars and dark matter was used. They ran three configurations with the different stellar mass and different gas fractions. The first model with stellar mass of $2 * 10^{10}$ with 60% fraction of gas, the second with stellar mass of $3 * 10^{10}$ with 50% fraction of gas and the last one stellar mass of $4 * 10^{10}$ with 40% fraction of gas were studied. The initial disk had constant surface densities for gas and stars. The external radius of 6 kpc and the scale height of 500pc were set, as well as dark matter to baryon ratio of 1:2. They studied the impact of minor mergers on these models. Analysing the results after isolated evolution phase and after the minor merger phase, they concluded that clumpy turbulent structures and instabilities, which are responsible for their creation, can make the thick disk, while minor mergers fail to explain some observable properties of the thick disk. Thus, they pointed that observed properties of thick disks suggest the existence of clumpy phase with rapid internal evolution for the spiral galaxies.

Schönrich and Binney[82] introduced their model of chemical evolution of the Milky Way, which included radial migration of stars and flow of gas through the disk. The model accounted for iron and $\alpha$ elements. The simulation consists of a series of discrete time-steps of 30 Myr. The disk separated into 80 rings of width 0.25 kpc. The presence of cold and warm gas is accounted for each ring. They set the star formation rate, gas inflow rate with its distribution. The radial mixing was modelled by the process of exchange of the mass of neighbor rings in the vicinity of the corotation resonance of spiral arms. To better model the disk heating, stars were oscillating around their center of orbits with steadily increasing amplitudes. The vertical motion they assumed decoupled and described it by relationship between time and vertical velocity dispersion and isothermal population for a given age. They pointed some weak places of the model such vertical motion decoupling and absence of any central component of the Galaxy such a bulge. Nevertheless, the model described the metallicity gradient in a good agreement with the observations of Milky Way and external galaxies.

Moster et al.[83, 84] showed that gas can prevent the destruction of thin stellar disk by minor mergers. They ran numerical simulation, which included stellar component and gas component. It was shown that when the gas in the thin disk is taken into account, the thickening by minor mergers reduces by 25% for the initial gas fraction of 20% and by 50% with initial disk fraction of 40%. They obtained the final scale height in the range of 500-1000 pc, regardless of the initial scale height. Thus, they concluded that the existence of a thin disk is not in obvious conflict with galactic hierarchic clustering, since it is possible to reproduce the observed thin disk of the Galaxy even after 1:10 recent merger, assuming 20% fraction of gas. The model computes the number of stars of a given type, age, effective temperature and absolute magnitude at any place in the Milky Way. Including calculation of Poisson noise of data, one can obtain

the mock catalog of stars from this model. Despite the fact that the model may not describe the fields close tho the Galactic plane due to the rough model of extinction, it is a very useful tool to compare observational data with modeled star counts.

Spitoni and Matteucci[85] studied an effect of radial inflows of gas on the chemical evolution model. They divided the galactic disk into several concentric rings, which evolve without a matter exchange. They defined infall law for the thin disk as an exponential function of time and coefficient depended on the radius. They assumed timescale for the mass accretion increase with the Galactic radius according to linear relation. The inner region, with the radius less than 4 kpc, was not accounted. They ran several simulations with one and two infalls with different parameters to trace how the changes influence the resulting metallicity gradient. For one-infall model with inside-out formation gradient was flat and failed to reproduce the observations, while when radial inflow with the speed of 1 km/s was included without inside-out formation, weak metallicity gradient was recovered. Assuming radial inflow varying in radius from 0 to 4 km/s and including inside formation, the authors reproduce the steepness of metallicity distribution. Two infall models were able to reproduce the gradient, but it was not steep enough. Thus, the authors concluded that radial gas flows can be important to reproduce metallicity gradient along the disk, however, inside-out formation is coupled, and it is not clear which process is more prevalent.

Curir et al.[86] built a N-body simulation for Milky Way-like disk to verify the observational relation of $\frac{\partial V_{phi}}{\partial [Fe/H]}$, which was found to be 40-50 km/s/dex. They used a dark matter halo containing a rotating stellar exponential disk. The stellar disk parameters were taken similar to observed parameters of Milky Way's disk. The disk was assumed in gravitational equilibrium with the dark matter halo. They also added second case of simulation, which include bulge. These two N-body simulation were evolving for 10 Gyr. The initial metallicities were assigned after 1 Gyr. Thus, the authors studied redistribution of the initial chemical properties after 9 Gyr. They noted that the bulgeless disk decays in a barred configuration. Migration processes were found in both cases, while in the barred case the impact of migration is bigger. The inner disk stars move towards the outer regions and settle layers at higher distances from the mid-plane. They measured that the rotation-metallicity relation of 60km/s/dex for particles at $1.5 < Z < 2.0 kpc$ persist up to 6 Gyr. They conclude that their pure N-body simulation can account for the rotation-metallicity correlation, which was observed in the thick disk. Thus, the internal disk processes such a heating and a radial migration contribute in the formation of the thick disk. The positive rotation-metallicity correlation of the thick disk population would represent the initial inverse chemical radial gradient in the inner parts of the Milky Way, which

suggest the accretion of primordial gas scenario.

Vera-Ciro and D'Onghi[87] aimed to study the effect of radial migration and its impact on the vertical action. They employed N-body simulations of two galaxies: one consisted of a dark matter halo and a disk, while another one had additionally bulge component. The stars evolved in an isolated disk of galaxies with different multi arm spiral morphology for the first model and with a developed bar after about 3.5 Gyr of evolution for the model with a bar. For the first case, the authors reported that the vertical action for an ensemble of stars was approximately conserved, with a dispersion of fractional changes around 20%. However, for the 6 Gyr of evolution this quantity conserves with less accuracy with increase of standard deviation up to 50% including stars which migrates radially by resonant scattering and corotation. For the second case, the barred case, large angular momentum changes occurred, with significant vertical heating. It was concluded that for this case, the vertical action can not be treated as conserved quantity. For the 6 Gyr evolution, this quantity increased with a standard deviation of about 80%.

Obreja et al.[88] presented the results of applying Gaussian Mixture Models in the kinematic space of stars of normalized angular momentum and binding energy on NIHAO high-resolution galaxies. They simulate an analogue galaxy of the Milky Way to reveal properties of different stellar components. They noted that the simulated mass density profile of two disk components are more centrally concentrated than exponential function, while halo and bulge can be described by exponent law. The authors, convincing that the stellar properties of the simulated galaxy are in agreement with observed ones, tracked back in time the Lagrangian mass of each component. They found that 98% of the thin disk component was formed in situ with a constant star formation rate at about $1.5 M_{\odot}/yr$ over the last 11 Gyr. The thick disk has an extended star formation rate with a peak at around $5 M_{\odot}/yr$.

Antoja et al.[89] studied the Milky Way disk comparing the data from Gaia with the modeled disk. They found the Galactic disk phase space to be full of substructures. Snail shells and ridges were observed. They reported that the nature of these substructures implies that the disk is not in equilibrium state and it is strongly affected by the Galactic bar and spiral arms. Accrediting to authors the disk was perturbed between 300 and 900 Myr ago, which is matching the estimation of the last pericentric passing of Sagitarius dwarf galaxy. The phase-wrapping by the satellite galaxies was predicted, but structures as snail shells or ridges were never examined before.

Bland-Hawthon[90] used the data from Gaia and GALAH survey to examine the Galactic disks in the distances up to 1 kpc from the Sun. They divided disk into $\alpha$-rich and $\alpha$-poor

components. $\alpha$-rich component is old, formed rather quickly and it has complex structure with metal-poor stars being on highly non-circular and low angular momentum orbits. $\alpha$-poor component is a product of gradually declining stars formation during 10 Gyr. For this component the stars on low angular momentum orbits tend to be more metal-rich and this component has larger dispersion for plane motion than the vertical one. The authors also noted the substructures showed by Antoja et al.[89]. They tried to reproduce the age of snail shell structure. Their estimation was 390 Myr using angle-action coordinates with Piffl potential and 515 Myr when McMillan potential was used. Thus, the disturbance of the disk took place at this time.

Arreaga-García[91] used the smoothed particle hydrodynamics technique for developing his numerical model of a galaxy composed of a dark matter halo, a rotational disk, a spherical bulge and a ring of molecular gas. He showed that the model was stable for 10 Gyr. He presented the characteristics, such as radial density profile, rotation curve and angular momentum distribution of the configuration after 10 Gyr. Additionally, he showed the results of simulation of a collision between equal mass galaxies for the four different cases of initial configuration. The mass density profiles and radial surface density profiles were presented for these cases.

Anguiano et al. [92] used cross-correlated information from the Sloan Digital Sky Survey Apache Point Observatory Galactic Evolution Experiment (APOGEE) survey's DR16 and Gaia DR2 to separate thin disk, thick disk and halo populations. They selected 211820 stars associated with the thin Galactic disk, 52709 stars associated with the thick disk and 5795 stars associated with the halo. The selection was employed by the help of chemical information from APOGEE. The sample studied by Anguiano et al. was enclosed in $6 < R < 10kpc$ and $1 < Z < 2kpc$. The authors found that the chemically selected thin disk has a velocity dispersion $(\sigma_R, \sigma_\varphi, \sigma_Z)$ of $(36.81, 24.35, 18.03) \pm (0.07, 0.04, 0.03)$ km/s, the thick disk has a velocity dispersion $(\sigma_R, \sigma_\varphi, \sigma_Z)$ of $(62.44, 44.95, 41.45) \pm (0.21, 0.15, 0.15)$ km/s. The mean rotational velocity of the chemically selected thick disk is equal to $191.82 \pm 0.24 km/s$ and their value of asymmetric drift between the Thick and thin disks is about 30 km/s.

Another recent work of Everal et al. [93, 94] consisted of analysing Gaia photometry and astrometry to estimate the spatial distribution of the Milky Way disk in the solar vicinity. The authors corrected the sample incompleteness using a solution for the selection function of the Gaia source catalogue [95, 96]. They recovered the densities of the thin and thick disks in the solar neighborhood, as well as the height scales of vertical distribution. The authors calculated the ratio of thick-to-thin disk local density of $0.147 \pm 0.005$ and a value of the surface density of the stellar disk $23.17 \pm 0.08 \pm 2.43 M_\odot pc^{-2}$, where the first error connects to the statistical error and the second one connects to the systematic error.

## 2.5 Theories of the thick origin

Spitzer and Schwarzschild[97] studied the mechanism of disk heating by interactions between stars and interstellar clouds. The star-cloud interaction relaxation time is shorter than for star-star interactions, so they tried to account for this type of interaction. The cloud mass should be much bigger than the star mass for such interaction to be effective. In this case, low-velocity stars may increase their velocity by the star-cloud encounters during, as the authors estimated, about $3 * 10^9 years$. They assumed that all the difference between velocities of Population 1 stars with the present velocity of interstellar clouds may be causes by star-cloud interaction. So such interactions could increase the average velocity of old groups such as late dwarf stars and red giant stars by a factor of 2, while they could not change velocity noticeably for the younger groups because of insufficient time of interactions.

Lacey[98] extended the understanding of the star-cloud interaction mechanism. He derived equations for velocity dispersion evolution of the stars in a galactic disk, when the motion is perturbed by massive gas clouds, which are moving in the circular orbits in the disk. He divided the evolution into two phases: initial relaxation and steady heating phase. During the steady heating phase velocity dispersion increase with the time, but the shape of the velocity ellipsoid is fixed. He pointed that for such mechanism, massive clouds with a mass about $10^6 M_\odot$ are required to effect the velocities of old star group, while for younger ones even more massive clouds are needed. However, measure value for the velocity dispersion ratio is different from expected one. The vertical dispersion is 10-30% larger. Thus, the author concludes that some other heating mechanisms might be involved.

Burkert et al.[99] constructed self-regulated dynamical and chemical evolution of a gaseous initially hot protodisk. The star formation as well as cooling and heating processes were taking into account. He showed that the collapse of this gaseous protodisk leads to three distinguishable components: an old thin disk, a young thin disk and a thick disk. According to the model, after a short thick disk formation stage of about few hundreds Myr long, the majority of stars form an old thin disk. Then at 4-6Gyr the young disk was formed. They also emphasised that the model predicts vertical metallicity gradient, the disk formation from inside out and the surface density of the young thin disk. Thus, they suggested that this formation scenario could take place in the formation of Milky Way.

Quinn et al. [100] suggested that the origin of the thick disk could be mergers with satellite galaxies. They used N-body simulation of interaction disk-halo system with the satellite galaxies with the mass in the range of 0.04-0.2 mass of the disk. The satellite galaxies were initially on

inclined circular orbits, merging with a similar to Galactic disk. They concluded that satellite orbit decay by sinking into the disk plane and then radially into the center of the disk. The debris disrupted by tidal forces can be found afterwords on inclined orbits at large distances, on orbits close to circular near to the disk plane and in the center of the disk. The result depends on initial mass density of the satellite. The initial galactic disk spread radially and vertically. The radial spreading is more notable for initially cool disk. The mean scale height increases by a factor of two. They showed that the resulting disk structure are comparable with the disk found in the Galaxy and in the external one. However, they noted that, since thin disk do not survive mergers, the galaxies with clearly evident thin disk must have reformed their thin disk by secondary processes. In this case, there would be clear separation in age of the disk components.

Sridhar and Touma[101] showed the influence of resonance on the galactic disk. Assuming collisionless stellar system, they derived the equations governing the behaviour of the distribution function in the region of resonance. 2:2 resonance between epicyclic and vertical oscillations was studied. They showed that resonant stars rise their high by converting their redial actions into vertical ones. By this mechanism, such stars can reach the distance from the galactic plane of several kpc. Thus, this resonance mechanism can be one of the causes of thick disk growing.

Schönrich and Binney[102] analysed the results of their model[82] to reconstruct the evolution process of the Galaxy. They presented in details all the parameters and normalisations which they used in order to simulate the Milky Way. They identified the thick disk by the extended vertical density and by chemical composition. They pointed that the kinematic selection misallocates many stars, adding old stars to the thin disk and young stars to the thin disk. They showed the results of chemical distribution of their model are consistent with observations. Thin disk stars are located in a narrow high density ridge in the $[Fe/H]$, $[\alpha/H]$ plane between metallicities from -0.65 to 0.15. The metal-rich thick disk lies in the big area of $[Fe/H]$, $[\alpha/H]$plane in [Fe/H] from -0.9 to well above 0 and higher in $\alpha/H$ than the thin disk, at about 0.3 dex. The metal-poor thick disk lies above the metal-rich thick disk in $[\alpha/H]$ and goes down to -1.4 dex in [Fe/H]. The metal-rich thick disk, an intermediate population, has a very low density, so the thin disk and the thick disk are clearly distinct structures. The thin disk stars are younger than 7 Gyr and have almost circular orbits, while the thick disk stars nearly all older than 8 Gyr and have significantly non-circular orbits, showing the rotation velocity lag up to 100km/s. Thus, they concluded that according to their model, which reproduce observations in the $[Fe/H]$, $[\alpha/H]$ plane, without any external effects, there is no evidence for a

violent origin of the thick disk. So, it formed internally because of resonant effects of the spiral structure and of the bar.

Wilson et al. [103] compared the observed stellar eccentricity distribution of Milky Way thick disk with the eccentricity distributions of a simulated disk formed via accretion, radial migration, and gas-rich mergers. They found that the broad peak at high eccentricities is inconsistent with the relatively narrow peak at low eccentricities for observed distribution. This fact indicates that the thick disk of Milky Way was formed predominantly in situ.

Park et al.[104] used two recent cosmological high-resolution zoom-in simulations NEWHORIZON and GALACTICA to trace a galactic disk formation process. The simulations are both running RAMSES Eulerian hydrodynamics code with adaptive mesh refinement and based on the same cosmological parameters. They investigate 18 disk galaxies from the NEWHORIZON simulation and one disk galaxy from GALACTICA simulation. Applying the widely accepted fit to the disk r-band vertical profile, they noted that the observed scale heights and luminosity ratios are consistent with observations. They decomposed the disk into thin and thick ones spatially to trace their age and the birthplace. Both disks are dominated by the stars formed in situ, while thick disks shows higher contribution of ex situ stars. The thin disks were found younger, rotating faster and more metal-rich than the thick ones. The authors noted that thin disks mostly consist of young stars with rotation dominated kinematics, while the thick disks in situ originated part much older and were formed before disk settling, which cause dispertion-dominated kinematics. According to their estimations, about half of thick disk stars were formed after disk settling. Thus, they concluded that the thin and thick disk are not entirely distinct components in terms of formation processes.

# 3

# Disk kinematics in the Solar neighborhood

## 3.1 Data selection

We consider the commonly used division of galactic disk into thin and thick component. In our work, we focus on the stellar component of the disk. To study the galactic disk, we aim to use whole sky distributed data in order to not be biased because of the coverage problem of telescope. This leads us to think of space-based telescopes. Precise positions and velocity are essential components, so we need instrument which measure positions, proper motions and radial velocities of stars. For our porpoises, Gaia ESO satellite [1] has been chosen as a perfect instrument. In this section we concentrate our attention on properties of the instrument on the Gaia satellite subsection 3.1.1, then discuss the Early Data Release 3 (EDR3) [105] of Gaia mission subsection 3.1.2 and in further parts of this section we describe a subset of stars which was used to perform kinematics analysis.

### 3.1.1 Gaia satellite

One of the biggest event of the last decade was launch of Gaia satellite [**?** ] 19th of December 2013. Gaia is a logical continuation of Hipparcos project, which was aimed to collect astrometric data. Precise distance measurement is clue ingredients in astronomy and Gaia does it by parallax method, which is purely geometrical one, i.e. does not require any knowledge of source, but distance measured by parallax are limited because of measurement errors. Hipparcos satel-

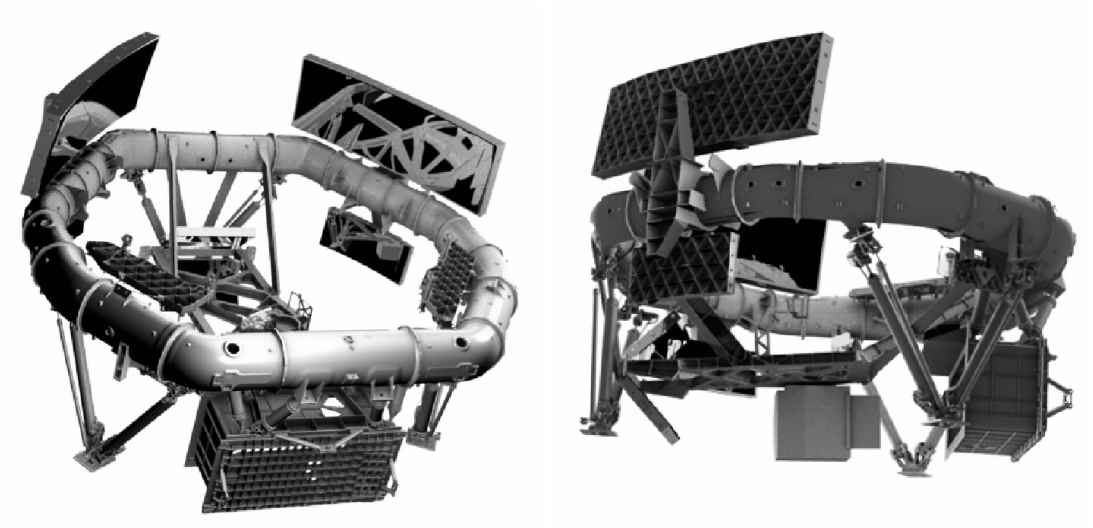

**Figure 3.1:** Schematic payload overview without protective tent [1].

lite launched in 1997 measured parallaxes with the precision of milliarcseconds for more than 100 000 stars. It leaded to the new level of understanding of our galaxy. Gaia as a descendant of Hipparcos continues measuring parallaxes with a breathtaking precision for more than billion objects. The aim of the Gaia satellite is measurements of locations and three-dimensional velocities of objects, as well as their astrophysical properties such as effective temperature and surface gravity. Improving our understanding of Milky Way with its complexity because of different contributions of satellite galaxies and stream as well as with its stellar age diversity is a main purpose of Gaia mission.

In order to use any scientific instrument one needs to know at least its basic properties, so in the following section we briefly recover the essential characteristic of the observational instrument on the Gaia satellite.

The satellite is fitted by two identical three-mirror anastigmatic telescopes. (can i add plot from literature?) The main mirror of each telescope has an aperture of 1.45×0.50m. Two mirrors are pointed in directions separated by an angle of 106.5 degrees (see Figure 3.1). Passing through the system of mirror, light beams from telescopes reach the focal plane, on which there are 106 charge-coupled device (CCD) detecrors 4050×1966 pixels each (plot again). Gaia is equipped with three instruments: astrometric instrument, photometric instrument and spectroscopic instrument.

The astrometric instrument performs measurements by 7 CCDs separate for each telescope and common area of two telescopes consisted of 62 CCDs. 7 CCDs row is used for sky map-

ping, while others 62 CCDs are devoted for the unfiltered white-light photometric band G (stands for Gaia), 330-1050nm measurements, which have high signal-to-noise ratio. It is possible to measure positions of stars brighter than 20 magnitude (mag). It was expected that more than 1000 millions stars would be measured and in third data release this number is bigger than 1800 stars. Combining several observations of one source a parallax and a proper motion can be identified.

The photometric instrument performs measurements of spectral energy distribution in the same time and with the same angular resolution as the astrometric instrument does. By this approach each object can be classified, and its astrophysical characteristics can be identified as well as chromatic corrections of the astrometric data can be accounted. The photometric instrument consists of two fused-silica prisms dispersing light. Thus, the first disperser BP (blue photometer) has wavelength rage 330-680 nm and the second one RP (red photometer) has 640-1050 nm. Bandpass can be defined, accounting also for the Optical coatings of prisms, telescope transmission and detector quantum efficiency.

The spectroscopic instrument also called radial-velocity spectrometer (RVS) collects data of spectra only for bright enough stars from Gaia sample. Radial velocity can be identified through Doppler-shift measurements for stars brighter than 16 mag. Rough stellar parameters can be obtained from spectra of stars brighter than 14.5 mag. Interstellar reddening, atmospheric parameters and rotational velocities can be identified for stars brighter than 12.5 mag and finally it is possible to trace individual element abundances of Fe, Ca, Mg, Ti and Si for stars brighter than 11 mag. The part of spectra, which is analysed, is in range of 845-872 nm. This spectral range was chosen to cover the Ca II triplet, which is used for radial velocity determination over a wide range of metallicities, signal-to-noise ratios, temperatures and luminosity classes (F,G,K). Hydrogen Pashen series lies in the wavelength range as well, which makes possible to derive radial velocity for early type stars. Also, the defuse interstellar band, which is used for accounting for interstellar reddening, is located at 862 nm.

The Gaia satellite is located in the second Lagrange (L2) point of system Sun-Earth-Moon around 1.5 million kilometers away from Earth in the anti-Sun direction and follows annual Earth rotation around the Sun. The satellite rotate around L2 in a Lissajous-type orbit with amplitudes of 120000 km × 340000km and 180000 km perpendicularly to the ecliptic plane. The orbital period is around 180 days. The Lissajous-type orbit has several advantages with respect to the orbit around the Earth, for example, stable thermal conditions, propitious radiation environment and high observing efficiency in which the field of view of telescope does not cover Earth, Sun and Moon.

The scanning law describes the pointing direction of the telescope as a function of time. The scanning function is one of the key ingredients of astrometric characteristics of the Gaia. The main principles of the scanning function were developed in the 1970s and had been used for Hipparcos in the 1990s [106]. Uniform revolving scanning is used for Gaia observation. Such a scanning law optimises the astrometric precision in terms of maximum uniformity of the sky coverage [107].

The scanning law is created in a way to give the maximum uniformity of the sky coverage after the nominal five-year mission. Nevertheless, the number of observations of one object depends on its location in the sky, particularly on its ecliptic latitude. At minimum for dimmest objects in Gaia sample (G > 20) the number of transits is 70, which still gives high enough quality of measurements for the positions and proper motions.

### 3.1.2 Gaia EDR3 catalog

The first intermediate Gaia data release called Gaia Early Data Release 3 (EDR3) /cite is the newest Gaia release at the date of this work. The catalog is based on the information collected for the first 34 months of the mission. The main difference between EDR3 and previous Data Release 2 (DR2) [108] lies in updated astrometry and photometry. The radial velocities in EDR3 mainly imported from the previous release. Now we brightly discuss the main improvements of new release and the limitations which one should be aware of while using the data.

The identification of spurious detections caused by spikes from bright stars, cosmic rays or the planets of Solar system passing field of view of the telescope has been improved, which means that the list of sources became was cleaned. Also, cleaning of the oservation-to-source matching results led to fewer sources with negative parallaxes or too large parallaxes. The separation limit of close source pairs below which two sources are considered duplicates was lowered to 180 mas from 400 mas in DR2. Thus, some sources which were considerate in DR2 as duplicate appear as two sources in EDR3. The source character may change from DR2 to EDR3 because of reassigning of sources and transits.

The Gaia team improved and extended astrometric calibration model to handle the locations of saturated images, the effect of change of transfer inefficiency and inaccuracies in point spread function and line spread function models. As a result, the Gaia EDR3 astrometry median uncertainties were decreased by a factor 0.71 for positions and parallaxes and by a factor 0.44 for the proper motions for the G = 15 mag. For faint and bright end of Gaia sample, the improvement is not so huge, but still significant. The parallax zero point has improved by

estimation from quasar parallaxes from -29 μas in DR2 to -17μas in EDR3.

The photometric data is much more homogeneous over the sky.Also, single passband for G, G_BP and G_RP are available over the entire magnitude and colour range, with no systematic errors above the level of 1%. The usage of the external calibration, which is based on a larger list of calibrators, covering a wider spectral range than in DR2, redetermines the passbands. New passnads and a larger set of input observations significantly improved photometry in precision and accuracy. Some peculiarity for faint red sources remains. Their flux in the BP band is overestimated, which means that they appear bluer in terms of colour index G_BP - G_RP. So, the G_BP flux of faint sources is biased. One should be careful using the colour index G_BP - G_RP for faint end of Gaia sample, or use color index G - G_RP instead. As in DR2 the magnitudes of the bright end of Gaia sample should be corrected by saturation effects [109].

Radial velocity information in EDR3 came from DR2 with slight changes. It was cleaned up from the potentially spurious values such as sources with unreliable or erroneous radial velocities, in particular radial velocities bigger than 600 km/s were removed. Radial velocities in DR2 are available only for stars with effective temperature in the range 3550-6900K. The radial velocities data set in DR2 contains the median radial velocities averaged over the 22 month of observations, mainly measured for the sources which are brighter than G 13 mag.

The completeness of EDR3 has slightly improved at the faint end between G 19 and G 21 and remained unchanged for bright end. The large scale completeness limit estimated by 99th percentile of the G magnitude distribution varies with galactic latitude between G 20 and G 22. The capability to observe all stars in crowded regions is reduces which means that the survey limit in this regions with density above 10$^5$ stars per square degree can be brighter than G = 20.

### 3.1.3 Solar vicinity

The most usual approach to select the thick disk stars is to impose the spacial condition on the distance from the galactic plane. Such way allows to study only thick disk subsystem since at the distance of 1-2kpc from galactic plane most of the stars represent thick disk (Girard Soubrian 2006, Kordopatis 2011). But there are obvious drawbacks of this approach, such as observation errors and sample completeness. Here we use different approach to select thick disk stars. Since thick disk stars locate not only below and above the galactic plane but also close to the midplane we can find them even in the solar neighborhood. The concentration of thick disk stars is expected to be highest in the midplane, which is the statistical advantage of this approach.

Observational errors are smaller for stars in the Solar vicinity and the completeness of sample selected in this area is significantly more reliable. Further, using the kinematical data for stars in the solar vicinity we can distinguish thick and thin disk stars by the velocity perpendicular to the galactic plane.

### 3.1.4 Red Giant Stars

Red Giant stars are stars at their late evolutionary stage. The hydrogen in the cores of these stars fully burned in to helium and this is hydrogen fusion only in shell source. These stars have radiuses of tens or hundreds of solar radius, but effective temperature is usually lower than solar one. Despite the fact that the energy density of emission is smaller than solar, they are bright because of their size. We use Red Giant stars, because they are relatively old stars, which have already relaxated and do not trace a birth cloud kinematics. Of course, any speed of evolution of the star depends on its mass, however, stars with big masses evolve very fast and do not remain in a stage of red giants. Thermonuclear fusion of helium in the core starts for such stars, and they leave the stage of red giants. Thus, if there is a part of young stars in the red giant stage, this part is tiny. Majority of red giant stars has masses lower than the solar mass and the lifetime of red giant stage is about a billion years. Another advantage of using Red Giant stars is strongly observational. They are bright enough for the Gaia spectroscopic instrument, so we have radial velocities for these stars.

### 3.1.5 Subset of stars

The following section is based on the newest at the time of the begging of this work, Gaia EDR3 catalog. First restriction was implemented to study the solar vicinity. For this reason we are aimed to choose stars within the cylinder centered at the Sun which has radius 1 kpc and height $\pm 0.5$ kpc, which means that the farthest distance will be $\sqrt{1.25} \approx 1.12$ kpc, i.e. all stars with parallax $> 1/\sqrt{1.25} \approx 0.89$ mas. The Gaia team strongly recommend use only astrometrically good behaved data for which $ruwe < 1.4$ [110]. The parameter *ruwe* (Renormalised Unit Weight Error) indicates that the single-star model provides a good fit to the astrometric observations. A value greater than 1.4 could indicate that the source is non-single or otherwise problematic for the astrometric solution. In order to safety use parallaxes as a measure of distance, the Gaia team recommends selecting sources with error in parallaxes less or equal to 10% and within 1 kpc from the Sun [111]. Otherwise, distances could be biased, in particularly, overestimated. Also, to avoid dim sources for which redial velocity measurements can not be

performed, we impose the cut on apparent magnitudes $G < 13.5$ mag. Summarizing, the first selection from Gaia EDR3 catalog was done by imposing $ruwe < 1.4$, $parallax > 0.89$, apparent magnitude $G < 13.5$ and $paralax_over_error > 10$. Additionally, we divided stars into north and south components by galactic latitude $b > 0$ and $b < 0$ respectively (see Algorithm 3.1 and Algorithm 3.2). The total number of sources is 4863317 (2553317 for north sample and 2310000 for south sample).

**Algorithm 3.1** The query of the north sample in Astronomical Data Query Language for the Gaia server

```
SELECT *
FROM gaiaedr3.gaia_source
WHERE parallax > 0.89
AND parallax_over_error > 10
AND ruwe < 1.4
AND phot_g_mean_mag < 13.5
AND b > 0
```

**Algorithm 3.2** The query of the north sample in Astronomical Data Query Language for the Gaia server

```
SELECT *
FROM gaiaedr3.gaia_source
WHERE parallax > 0.89
AND parallax_over_error > 10
AND ruwe < 1.4
AND phot_g_mean_mag < 13.5
AND b < 0
```

The next cut was done to select all sources within the abovementioned cylinder volume. Then we selected sources which have not null photometric measurements, in particularly, B-R colour index *bp_rp* and not null radial velocities *dr2_radial_velocity*. We have got 2387462 sources ($\approx 56\%$ ).

Using inverted parallaxes as a distance we constructed the distance modulus for all the sources which allows us to calculate absolute magnitude $G_(abs)$ and build colour-magnitude diagram (see Figure 3.4). One can see at the plot the presence of the red clump (RC) stars, as an overdensity at $G_(abs) \approx 0.5$ on its blue end and tilted toward to fainter and redder direction due to the effect of interstellar extinction. We chose all the RGB stars by selection $B - R > 1$ and $G_(abs) - 1.85 * (B - R) < -0.7$ which is following the direction of extinction from the

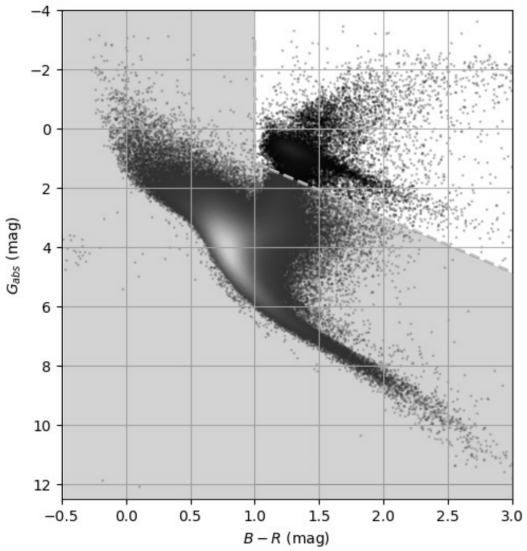


**Figure 3.2:** $G_{abs}$ vs. $B - R$ for all the Gaia data in the cylinder studied in this investigation, colour-coded by density of points (the whiter the denser, every 20 stars plotted). Our Gaia RGB sample was selected from the area delimited by the grey dashed line.

RC tilt. A final sample consists of 278228 stars named Gaia RGB in table (reference of table). The full number of stars from Gaia EDR3 located in the volume of the cylinder and consistent with the same colour and magnitude selection is 296879 stars. Thus, we are missing only 6% of the total number of such stars observed by Gaia within the cylinder due to the lack of radial velocity information.

The computation of rectangular coordinates and velocities was performed by Topcat [112] functions astromXYZ() and astromUVW(). X coordinate oriented in the direction of Galactic center, Y coordinate points Galactic rotation, Z coordinate directed towards North Galactic Pole and their corresponding velocities U, V and W. Another Topcat function icrsToGal() was used to compute the Galactocentric velocities in the cylindrical coordinate system $(V_R, V_\Phi, V_Z)$ considering solar motion $(U, V, W)_\odot = (11.1, 12.2, 7.3) km/s$ with respect to the local standard of rest (LSR) [113], which correspond to the Galactic rotation of -244.5 km/s [114]. $V_R$ velocity points away from the Galactic center, $V_\Phi$ velocity oriented against the Galactic rotation and $V_Z$ points to the North Galactic Pole. According to the $V_R$ velocity value we constructed samples called "thin disk" and "Thick disk" in a sense that these samples should be dominated by thin disk stars and Thick disk stars respectively. We impose the restriction $|V_Z| < 15 km/s$ and heights $|Z| < 200 pc$ for the thin disk sample and for the Thick disk sam-

ple $40 < |V_Z| < 80km/s$. More details about the separation one can see in the next section section 3.2. The final number of stars for each sample is shown in the Table 3.1

| Sample name | North | South | Total |
|---|---|---|---|
| Gaia RGB | 133,218 | 145,010 | 278,228 |
| Gaia RGB thin disk | 54,197 | 55,628 | 109,825 |
| Gaia RGB Thick disk | 6,776 | 7,022 | 13,798 |

**Table 3.1:** Samples names and sizes.

### 3.1.6 Completeness

In order to check that our sample of stars is not biased and that it is reliable for all the RGB stars within mentioned above volume, we perform here a completeness analysis.

Our calculation is based on the assumption that the stellar density changes only vertically and that it is distributed symmetrically with respect to the Galactic plane. In a complete sample, uniformly distributed number of stars in a cylinder should grow as a square of radius of a cylinder. The empirical cumulative distribution function (CDF) of normalized cylindrical radius $R_xy/1000 = \sqrt{X^2 + Y^2}/1000$ should grow parabolic or empirical CDF of normalized cylindrical radius squared $(R_xy/1000)^2$ should grow linearly following the identity function. The CDF is constructed by sorting $(R_xy/1000)^2$ data and computing the percentile of each bin versus the data itself. A completeness is reach when the CDF is indistinguishable from the identity function, i.e. the number of stars grow linearly with the radius of the cylinder. A deviation means the sample is nor or homogeneous, either complete. The plot (add plot) of CDF minus identity function versus the radius $(R_xy/1000)^2$ shows how much the data deviates from ideal complete and homogeneous sample. The location of the CDF below the identity function means that some stars are missing. Also, one can see it from the plot $G_abs$ versus distance (add plot and some words). The incompleteness occur at faint end of RGB stars at small values of radius.

Let us focus on the qualitative estimation of completeness. For a uniformly distributed sample $\{X_i\}_{i=1}^n$ within an interval, $[0, 1]$ empirical CDF is an identity function in this interval within statistical noise. So, the corresponding percentile $p_i$ is $p_i \sim X_i$ for $i = 1, \ldots, n$. An incompleteness occurs when a systematic difference between CDF and underlying distribution is found. As shown above (pic) the percentile of the data is generally below the data. $\hat{X} \neq 1$ can be computed as the area of the data CDR would correspond to the uniform distribution CDF

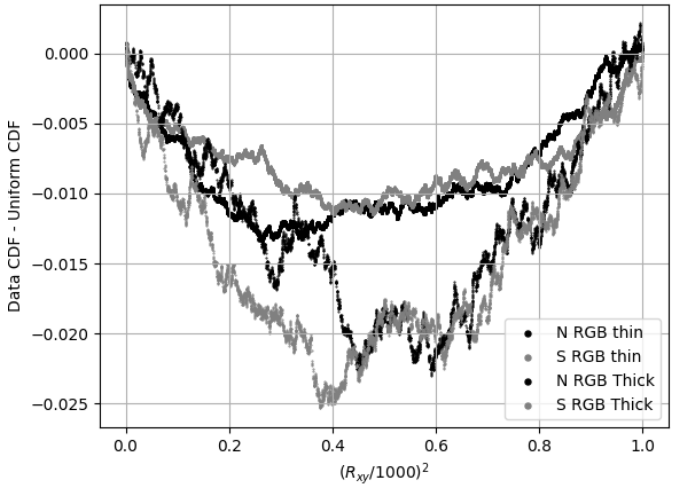


**Figure 3.3:** Cumulative distribution function (CDF) of the normalized cylindrical radius squared minus the identity function, for the samples studied in this work.

in the interval $[0, \hat{X}]$. Thus, $\hat{X} \neq 1$ is the value up to which the current $n$ data points would homogeneously sample a uniform distribution, then

$$\sum_{i=1}^{n-1}(X_{i+1} - X_i)p_i = \frac{\hat{X}^2}{2} \Longrightarrow \hat{X} = \sqrt{2\sum_{i=1}^{n-1}(X_{i+1} - X_i)p_i} \tag{3.1}$$

If we sample the same population but over the interval $[0, 1]$ with $N \neq n$ points, then trivially $\frac{N}{1} = \frac{n}{\hat{X}}$. Finally, the incompleteness percentage can be computed as

$$\text{Incompleness \%} = \left(1 - \frac{n}{N}\right) \times 100 = (1 - \hat{X}) \times 100 = \left(1 - \sqrt{2\sum_{i=1}^{n-1}(X_{i+1} - X_i)p_i}\right) \times 100 \tag{3.2}$$

The result of this computation are shown in Table 3.2.

| Sample name | North | South |
|---|---|---|
| Gaia RGB | 1.02 | 0.91 |
| Gaia RGB thin disk | 0.84 | 0.77 |
| Gaia RGB Thick disk | 1.19 | 1.46 |

**Table 3.2:** Samples incompleteness percentages

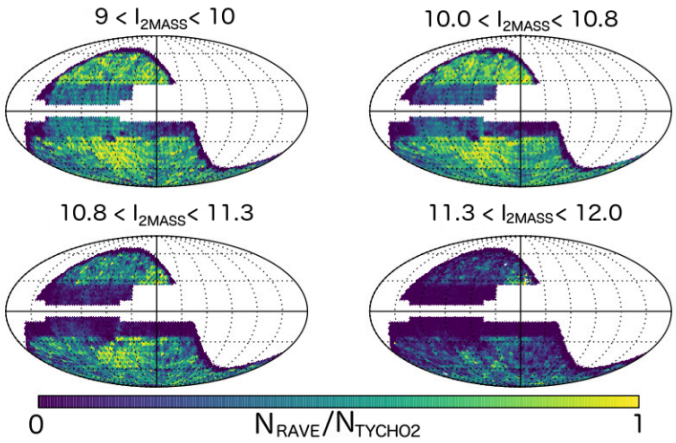


**Figure 3.4:** Mollweide projection of Galactic coordinates of the completeness of the stars in Tycho-2 for which RAVE DR5 radial velocity measurements are available for the core sample. Each panel shows the completeness over a different magnitude bin, where the HEALPix pixels are colour-coded by the fractional completeness ($N_{RAVE}/N_{TYCHO2}$) [2]

### 3.1.7 RAVE DR5 METALLICITIES

To add information about the metallicities and elemental abundances, we matched the Radial Velocity Experiment Data release 5 (RAVE DR5) catalogue [2] with discussed above Gaia EDR3 catalogue. However, RAVE is a ground-based survey, so the coverage of the sky can not be uniform and the total number of stars is significantly smaller in RAVE DR5. Thus, the aim of using RAVE DR5 is to get the general trend of metallicities for the disk components. First, we briefly mention main aspects of RAVE mission and particularly RAVE DR5 catalogue, and then we focus on the cross-matching procedure.

The sky coverage of RAVE is far from uniform (see, since it is a ground-based survey located in the Southern Hemisphere. The target selection for the survey is purely photometrical, thus, RAVE DR5 is free from kinematical bias. The I-band apparent magnitude is the main section criteria. The survey mostly have stars with apparent I magnitude $9 < I < 12$. Another restriction on colour index ($J - K_s >= 0.5$) was applied later for the directions close to the Galactic Plane to bias the survey towards giants. As a result, total number of stars is 448 948 stars.

Spectra for the RAVE survey are performed by the multi-object spectrograph 6dF (6 degree field) on the 1.2 meter UK Schmidt Telescope of the Austrian Astronomical Observatory. The covered spectral region is similar to that Gaia mission uses. The spectral region is 8410-8795 Å. The main feature is calcium triplet. For hot stars, the Paschen series of hydrogen is present in the region. Also, weaker metallic lines for the Solar type stars can be identified.

Despite difficulties with subtraction of air-glow emission lines, the RAVE team reached typical precision of about 2km/s for radial velocity identification. The stellar atmospheric parameters such as effective temperature, surface gravity and metallicity indicator were determined for the observed spectra. The RAVE team calibrated these parameters using a set of reference stars. For such reference stars, the parameters are available in the literature and usually derived from high-resolution spectra. Also, elemental abundances for Aluminium, Magnesium, Nickel, Silicon, Titanium, and Iron are available for a subset of stars in RAVE DR5 catalogue. The values were implemented by best-fitting model spectrum by minimizing $\chi^2$ between the models and observations. To have elemental abundances the star should fit the following requirements: good quality of spectra (Signal-to-Noise ratio > 20), effective temperature in the interval from 4000K and 7000K, rotational velocity lover then the 50 km/s and $\chi^2 < 2000$, which means that the observed spectra is fitted good enough by the model.

Thus, the fifth data release of RAVE catalogue has 520 701 entries, but only 457 558 of them are unique ones. The notable part of these entries is several observations of the same stars, and these observations may or may not have the same RAVEID in the catalogue, since the IDs are based on coordinates, which can slightly change from one observation to another. Firstly, we reject all the entries with repeated RAVEID. And then we deleted all clusters or groupings of stars that were within 1 arcsecond from each other to exclude repeated observations with different RAVEID. Therefore, 405 231 stars are in the final clean version of RAVE DR5 catalogue.

A threshold of 1.7 arcsends was set for positional matching by angular distance between the clean version of RAVE DR5 and Gaia EDR3 as the best one. The subset of 536 stars with the radial velocity offset $\Delta RV$ of about $+100 km/s$ with respect to Gaia EDR3 was found. As was indicated [115] these stars were located close to the plate edges during the observation, but since there is not any information about this in catalogue, they can not be discarded safely. So, we imposed one more condition for cross-matching $\Delta RV < 90 km/s$. And finally, we discarded a few cases of multiple matches: 96 Gaia EDR3 stars were matched to two different RAVE DR5 stars and 409 RAVE DR5 stars were matched to two different Gaia EDR3 stars. After all, the final matched catalogue RAVE DR5 $\times$ Gaia EDR3 (RAVE $\times$ Gaia) has 356 270 sources, which is 88% of the clean version of the RAVE DR5 catalogue. Some low signal-to-noise ratio ($STN\_SPARV$ 1) RAVE DR5 entries exhibit way too large uniform distributed $\Delta RV$ within the imposed limit. We did not use them for the further analysis.

Despite the fact that the cross-matched RAVE x Gaia catalogue is a small subsample of Gaia EDR3, we used it in order to additionally check our results with a chemical constrain. We did not split RAVE $\times$ Gaia sample into northern and southern parts. Metallicity value [Fe/H]

(Met_K) was used to select thin disk stars having $[Fe/H] > -0.4$additionally to kinematical restriction and the thick disk stars having $-1.0 < [Fe/H] < -0.4$. The number of stars in each sample is shown in Table 3.3. We repeated the completeness analysis on these sample (see Table 3.4 and Figure 3.5).

| Sample name | Total |
|---|---|
| Gaia×RAVE RGB | 30,170 |
| Gaia×RAVE RGB thin disk | 3,381 |
| Gaia×RAVE RGB Thick disk | 1,113 |

**Table 3.3:** Sample names and sizes used in this work with RAVE DR5 data

| Sample name | incompleteness |
|---|---|
| Gaia×RAVE RGB | 4.87 |
| Gaia×RAVE RGB thin disk | 3.36 |
| Gaia×RAVE RGB Thick disk | 5.84 |

**Table 3.4:** Samples incompleteness percentages with RAVE DR5 data

## 3.2 Velocity distribution

### 3.2.1 Radial velocities

The normalized histograms were constructed for the samples described above. Figure 3.6 shows the distribution of radial velocity $V_R$ for the samples, which consist only of Gaia EDR3 data, computed with bins of $5km/s$ separately for the thin and thick disk samples and separately for the northern and southern parts of the cylinder. As was expected, the dispersion of the thick disk is bigger than the dispersion of the thin one. To get a qualitative result of each distribution we estimated it by using a Gaussian fit from the Python *scipy* package and using the standard algebraic equations of mean values and standard deviations. The results of the fitting procedures for the samples is shown in the Table 3.5. While the mean velocities and the standard deviations are shown in the table Table 3.6.

Then we performed the same procedure for the samples of cross-matched catalogues RAVE DR5×Gaia EDR3 which have the chemical abundances information. The histograms are shown in the Figure 3.7 and the qualitative estimations are shown in the Table 3.7 and Table 3.8.

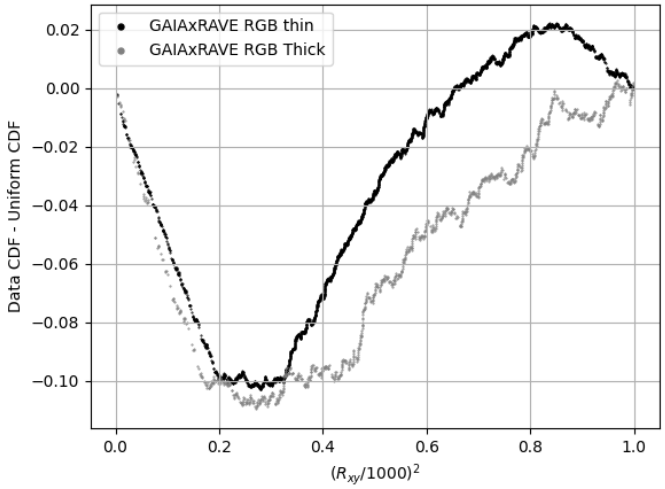


**Figure 3.5:** Cumulative distribution function (CDF) of the normalized cylindrical radius squared minus the identity function, for the samples studied in this work with RAVE DR5 data

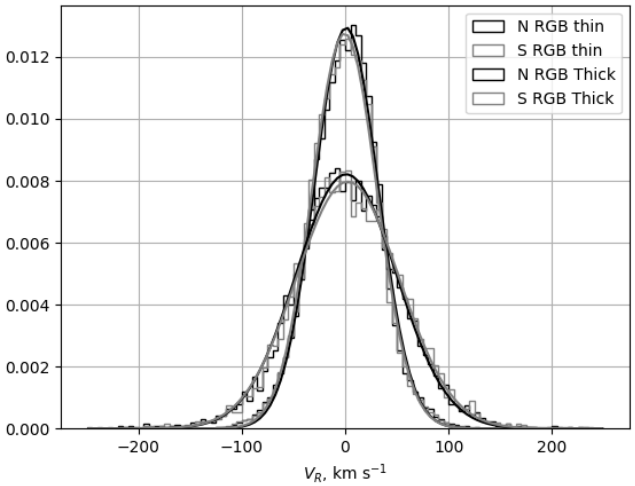


**Figure 3.6:** Histogram of $V_R$ and its Gaussian fit. See also Table 3.5 and Table 3.6.

| | $\mu$ | | $\sigma$ | |
|---|---|---|---|---|
| Sample name | North | South | North | South |
| Gaia RGB thin disk | $1.05 \pm 0.30$ | $-0.64 \pm 0.27$ | $30.81 \pm 0.25$ | $31.26 \pm 0.22$ |
| Gaia RGB Thick disk | $0.98 \pm 0.48$ | $2.50 \pm 0.57$ | $48.58 \pm 0.39$ | $50.04 \pm 0.47$ |

**Table 3.5:** $V_R$ mean $\mu$ and dispersion $\sigma$ values from a Gaussian fit ( Figure 3.6) with their respective errors.

| | Mean | | StdDev | |
|---|---|---|---|---|
| Sample name | North | South | North | South |
| Gaia RGB thin disk | $0.01 \pm 0.14$ | $-1.04 \pm 0.14$ | $32.65 \pm 0.10$ | $32.64 \pm 0.10$ |
| Gaia RGB Thick disk | $1.67 \pm 0.64$ | $3.53 \pm 0.63$ | $52.54 \pm 0.45$ | $52.48 \pm 0.44$ |

**Table 3.6:** $V_R$ mean and standard deviation values for the samples. Errors are computed as StdDev/$\sqrt{n-1}$ and StdDev/$\sqrt{2n}$ respectively.

The samples with the chemical abundances show the similar results. So, the lack of chemical abundances for the pure Gaia samples does not bias the conclusions. As one can see from the table, mean velocities in all samples for the thin and thick disk are of an order of $1-2km/s$. The radial velocity dispersion for the thin disk sample is $\sim 30km/s$ and for the thick disk sample is $\sim 50km/s$.

### 3.2.2 Azimuthal velocities

We performed the same procedure for the azimuthal velocity. The histograms and the Guassian fits are shown on the Figure 3.8 for the samples without RAVE data and on the plot Figure 3.9 for the samples from cross-correlated catalogue.The results of the Gaussian fit and algebraic estimation can be found in the Table 3.9 and Table 3.11 and for the samples using RAVE data in the Table 3.11 and Table 3.12. The distribution of azimuthal velocity is noticeably non-symatric, we fitted azimuthal velocity histograms by symmetric Gaussian function to see a general trend and to estimate the value of the difference between our samples. The values estimated from the kinematically selected sample are comparable to the value from smaller samples from cross-correlated catalogue, performed by the stellar abundance. Once again, it proves that the lack of chemical information does not bias the results.

Analyzing the results, one can see that the mean velocity of the thin disk is lagging from the assumed velocity of LSR (-244.5 km/s) by from 5 to 8 km/s, while the Thick disk is lagging by about 20 km/s. The observed lag of the rotational velocity can be explained by main two causes. The first one is asymmetric drift (some words). And the second one is that the thin and thick

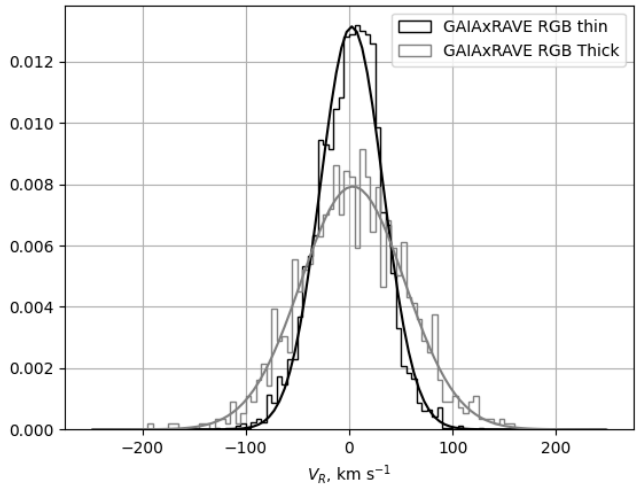


**Figure 3.7:** Histogram of $V_R$ and its Gaussian fit for the samples using RAVE data. See also Table 3.7 and Table 3.8.

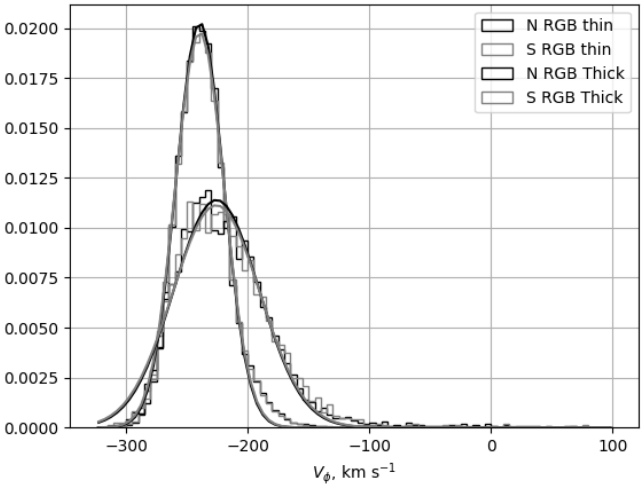


**Figure 3.8:** Histograms and Gaussian fit of $V_\varphi$. See also Tables 3.9 and 3.10. .

| Sample name | $\mu$ | $\sigma$ |
|---|---|---|
| Gaia×RAVE RGB thin disk | $2.51 \pm 0.70$ | $30.33 \pm 0.57$ |
| Gaia×RAVE RGB Thick disk | $3.56 \pm 1.41$ | $50.31 \pm 1.15$ |

**Table 3.7:** $V_R$ mean $\mu$ and dispersion $\sigma$ values from a Gaussian fit (Figure 3.7) with their respective errors for the samples using RAVE data.

| Sample name | Mean | StdDev |
|---|---|---|
| Gaia×RAVE RGB thin disk | $0.48 \pm 0.54$ | $31.29 \pm 0.38$ |
| Gaia×RAVE RGB Thick disk | $4.00 \pm 1.52$ | $50.85 \pm 1.08$ |

**Table 3.8:** $V_R$ mean and standard deviation values for the samples studied for the samples using RAVE data. Errors are computed as StdDev/$\sqrt{n-1}$ and StdDev/$\sqrt{2n}$ respectively.

disk components are mixed (more details in the next section subsection 3.2.3)

### 3.2.3 Vertical velocities and density ratio

The vertical velocity distribution for the Gaia RGB sample cannot be fitted by a single Gaussian function. We tried to reconstruct a double Gaussian distribution by using our separation of the vertical velocity for the thin and the thick disk stars. To recall, the restriction for the thin disk sample is $|V_z| < 15 km/s$ and the restriction for the thick disk sample is $40 < |V_z| < 80 km/s$. The results of the double Gaussian fit one can find in the table Table 3.13 and in the figure Figure 3.10. And also the same fit was done for the cross-matched samples Table 3.14 and Figure 3.11. As one can see from these plots, the thin disk sample can be strongly contaminated by the thick disk stars, also taking into account that the thin disk samples have $|Z| < 200$ pc while the thick disk samples have $|Z| < 500$ pc.

Of course, for a valuable estimation of portions of the thin and the thick disks, we should take the same volume for both samples. Also, we tried to perform the fit of $V_Z$ distribution by the sum of two Gaussian functions, which for simplicity have zero mean ($\mu = 0$). The Gaussian function with the smaller dispersion corresponds to the thin disk and other one, which has bigger dispersion, corresponds to the thick disk population. The third parameter of the fit is the portion of Thick disk stars within the whole volume sample. The size of bins of 2 km/s for the histogram of vertical velocity was chosen. The fit was performed with optimize.curve_fit from the Python scipy package (ref?). One can see the obtained results for different heights in the table Table 3.15 and in the figure Figure 3.12 and Figure 3.13,where sample for $|Z| < 500$ pc and subsample for $|Z| < 200$ pc are plotted respectively.

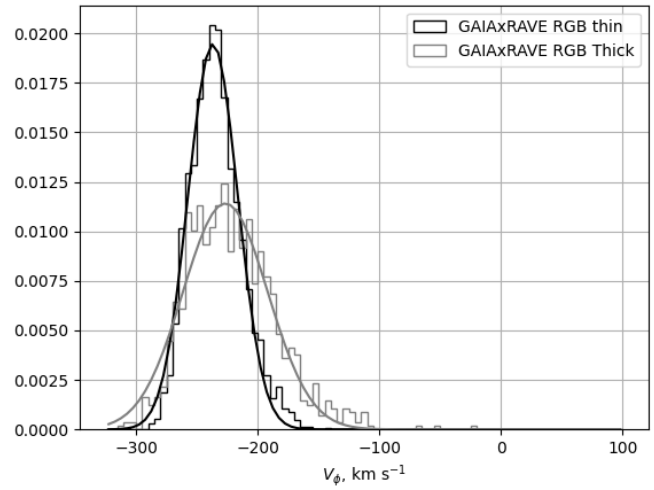


**Figure 3.9:** Histograms and Gaussian fit of $V_\varphi$ for the samples using RAVE data. See also Tables 3.11 and 3.12. .

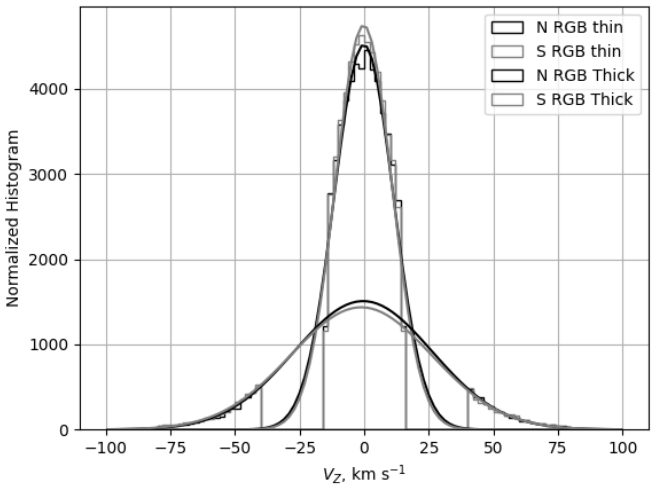


**Figure 3.10:** Histograms and Gaussian fit of $V_Z$. See also the table 3.13.

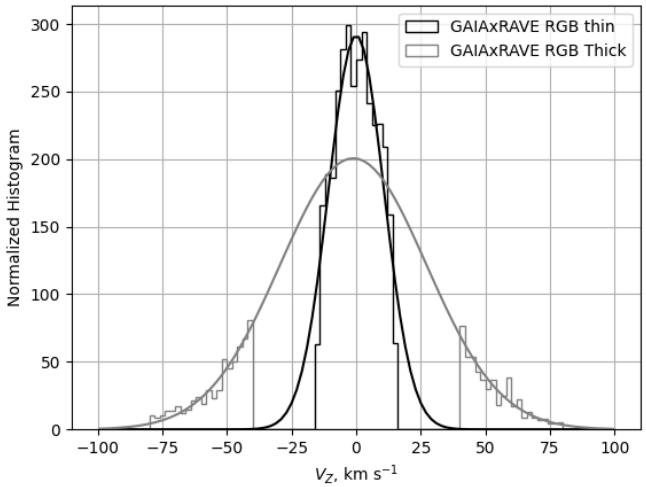


**Figure 3.11:** Histograms and Gaussian fit of $V_Z$. See also the table 3.14.

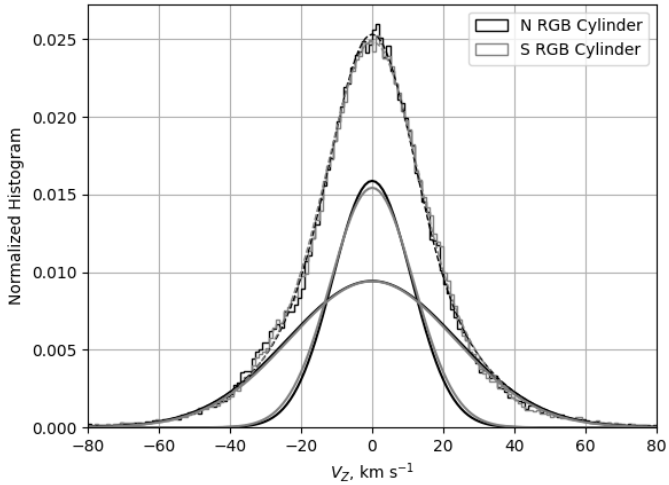


**Figure 3.12:** Histogram and Sum-of-two-Gaussians fit for $V_Z$ for the samples $|Z| < 500$ pc .

| | $\mu$ | | $\sigma$ | |
|---|---|---|---|---|
| Sample name | North | South | North | South |
| Gaia RGB thin disk | -239.31 $\pm$ 0.23 | -239.40 $\pm$ 0.19 | 19.67 $\pm$ 0.19 | 20.15 $\pm$ 0.15 |
| Gaia RGB Thick disk | -225.67 $\pm$ 0.70 | -225.80 $\pm$ 0.79 | 35.01 $\pm$ 0.57 | 35.84 $\pm$ 0.65 |

**Table 3.9:** $V_\varphi$ mean $\mu$ and dispersion $\sigma$ values from a Gaussian fit with their respective errors.

| | Mean | | StdDev | |
|---|---|---|---|---|
| Sample name | North | South | North | South |
| Gaia RGB thin disk | -236.80 $\pm$ 0.09 | -237.11 $\pm$ 0.09 | 22.06 $\pm$ 0.07 | 22.32 $\pm$ 0.07 |
| Gaia RGB Thick disk | -218.07 $\pm$ 0.52 | -218.26 $\pm$ 0.50 | 43.07 $\pm$ 0.37 | 42.19 $\pm$ 0.36 |

**Table 3.10:** $V_\varphi$ mean and standard deviation values for the samples. Errors are computed as StdDev/$\sqrt{n-1}$ and StdDev/$\sqrt{2n}$ respectively.

According to the fitting results we can say that around a half of the stars in the cylinder is actually the thick disk stars.

Also, one can clearly see that there is asymmetry between north and south samples in the numbers of stars. It is more evident for the $|Z| < 200pc$ cylinder sample.

There is an excess of stars at $-40 < V_Z < -20$ and a dearth at $25 < V_Z < 50$, which occurs for both north and south samples, which levels up to 41% for the samples $|Z| < 500pc$ for both north and south.

From the fit now we are able to estimate the thin disk sample contamination by the thick disk stars. For a normal distribution $N(\mu, \sigma)$ the cumulative distribution function (CDF) is given by

$$CDF(x) = \frac{1}{2}\left[1 + \text{erf}\left(\frac{x-\mu}{\sigma\sqrt{2}}\right)\right] \tag{3.3}$$

The area under $N(0, \sigma)$ in the interval [-15,15] is given by

$$CDF(15) - CDF(-15) = \frac{1}{2}\left[1 + \text{erf}\left(\frac{15}{\sigma\sqrt{2}}\right)\right] - \frac{1}{2}\left[1 + \text{erf}\left(\frac{-15}{\sigma\sqrt{2}}\right)\right] = \text{erf}\left(\frac{15}{\sigma\sqrt{2}}\right) \tag{3.4}$$

then the contamination of the thick disk stars in the thin disk sample is

$$\frac{p_T \text{erf}\left(\frac{15}{\sigma_T\sqrt{2}}\right)}{p_T \text{erf}\left(\frac{15}{\sigma_T\sqrt{2}}\right) + (1-p_T)\text{erf}\left(\frac{15}{\sigma_t\sqrt{2}}\right)} \tag{3.5}$$

| Sample name | $\mu$ | $\sigma$ |
|---|---|---|
| Gaia×RAVE RGB thin disk | -236.82 ± 0.54 | 20.50 ± 0.44 |
| Gaia×RAVE RGB Thick disk | -226.61 ± 1.31 | 34.97 ± 1.07 |

**Table 3.11:** $V_\varphi$ mean $\mu$ and dispersion $\sigma$ values from a Gaussian fit with their respective errors, for the samples using RAVE data.

| Sample name | Mean | StdDev |
|---|---|---|
| Gaia×RAVE RGB thin disk | -234.22 ± 0.37 | 21.30 ± 0.26 |
| Gaia×RAVE RGB Thick disk | -221.13 ± 1.09 | 36.38 ± 0.77 |

**Table 3.12:** $V_\varphi$ mean and standard deviation values for the samples using RAVE data. Errors are computed as StdDev/$\sqrt{n-1}$ and StdDev/$\sqrt{2n}$ respectively.

where $0 \leq p_T \leq 1$ is the portion of thick disk stars with velocity distribution $N(0, \sigma_T)$. $N(0, \sigma_t)$ is the velocity distribution for the thin disk stars. Restricting to the interval [-15,15] we can conclude that in the $|Z| < 200pc$ samples there is a 27% for north sample and 42% for south sample contamination by thick disk stars in the thin disk samples ($|V_Z| < 15km/s$) samples. For the samples $|Z| < 500pc$ this value levels up to 41% for both north and south samples.

As summarized by Bland-Hawthorn Gerhard(2016) the scale height of thick disk is around three times bigger ($900 \pm 180pc$) than the thin disk one ($300 \pm 15pc$). Thus, it is expected that the portion of the thick disk stars decreases at smaller height samples. Keeping this thought in mind, we limited our thin disk samples to $|Z| < 200pc$ attempting to reduce the thick disk contamination.

### 3.2.4 North-south asymmetry and excess and dearth of stars in $V_Z$

To make the excess and dearth of stars clearer and also give the quantitative estimation of this effect we built the residual plot Figure 3.14. The residuals do not look random with $V_Z$ and the excess from negative values of $V_Z$ as well as the dearth from positive side go clearly beyond the Poisson noise computed for each histogram bin. The smaller excess one can see also for larger velocities in the sample with $|Z| < 500pc$, which is likely caused by halo star contamination. Speaking of the number of stars for the excess and the dearth for their $V_Z$ locations we can compute that for samples with $|Z| < 500pc$ 1254 stars in the excess and 1319 stars in the dearth for the north sample, from which only 265 and 368 stars can be considered as a noise

| | $\mu$ | | $\sigma$ | | $A$ | |
|---|---|---|---|---|---|---|
| Sample name | North | South | North | South | North | South |
| Gaia RGB thin disk | -0.14 ± 0.47 | -0.21 ± 0.41 | 11.44 ± 0.65 | 10.94 ± 0.55 | 129609 ± 5584 | 130213 ± 5008 |
| Gaia RGB Thick disk | -0.39 ± 0.18 | -0.11 ± 0.26 | 26.73 ± 0.36 | 27.22 ± 0.50 | 101016 ± 3103 | 98312 ± 3991 |

**Table 3.13:** $V_Z$ mean $\mu$, dispersion $\sigma$ and amplitude $A$ values from a Gaussian fit (Figure 3.10) with their respective errors.

| | $\mu$ | $\sigma$ | $A$ |
|---|---|---|---|
| Gaia×RAVE RGB thin disk | 0.02 ± 0.55 | 10.74 ± 0.73 | 7849 ± 410 |
| Gaia×RAVE RGB Thick disk | -1.13 ± 0.46 | 28.34 ± 0.88 | 14251 ± 905 |

**Table 3.14:** $V_Z$ mean $\mu$, dispersion $\sigma$ and amplitude $A$ values from a Gaussian fit (Figure 3.11) with their respective errors for the samples using RAVE data.

respectively. 768 stars in the excess and 1451 stars in the dearth for the south sample, from which 276 and 379 stars can be taken as a noise. For the samples with $|Z| < 200$ the numbers are following: for the north sample 754 and 576 stars with a maximum possible noise of 188 and 258 stars, for the south sample 338 and 711 stars with a maximum possible noise of 198 and 268 stars respectively. The numbers are just a small percentage of the whole sample, less than 1%, yet the presence is visible.

In the Figure 4.5 a kernel density estimate plot $|Z|$ versus $|V_Z|$ is shown for the Gaia RGB samples. From this plot it is evident that the outermost and lowest (10%) isodensity level for both hemispheres extends farther in distance at $40 < V_Z < 20$ than at $25 < V_Z < 50$. This explains the excess at $40 < V_Z < 20$ and the dearth at $25 < V_Z < 50$ in Figure 3.14.

There are two main differences between north and south sample which can be seen from the Figure 4.5. These differences are clearly visible at isodensity level 30% ($300 < |Z| < 450$) and 90% ($|Z| < 100$). The stars of south hemisphere extend farther in height from the disk plane than in the north hemisphere. The first one means that there are more stars in the south hemisphere than in the north one for $|Z| > 250pc$, which can be also seen from the histogram of $|Z|$ Figure 3.16, while the second one may explain the excess of thick disk stars in the south $|Z| < 200pc$ sample that is shown also in the Figure 3.13.

## 3.3 Results

In this section, we will conclude the results of this chapter. We compare our work to the respectively recent articles in the section subsection 3.3.1 and we briefly repeat the main findings in section subsection 3.3.2

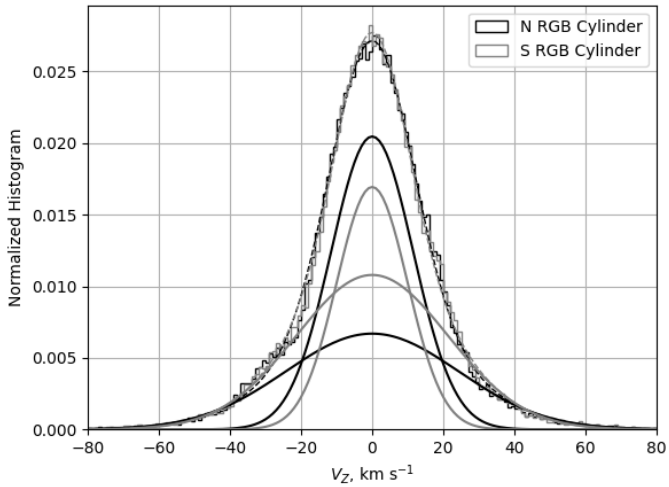


**Figure 3.13:** Histogram and Sum-of-two-Gaussians fit for $V_Z$ for the subsamples $|Z| < 200$ pc .

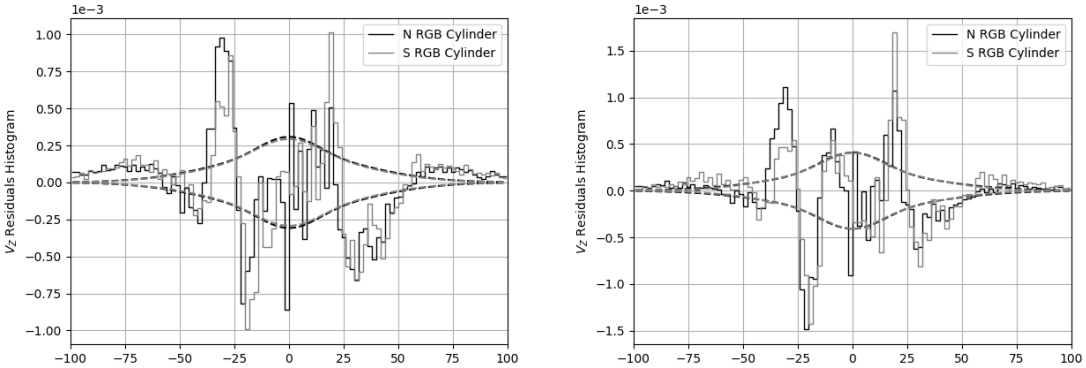


**Figure 3.14:** Residuals from the $V_Z$ sum-of-two-Gaussian fit for the $|Z| < 500pc$ sample (left panel) and the $|Z| < 200pc$ sample (right panel). Dashed lines mark the corresponding Poisson noise ($1\sigma$) for each histogram bin. The excess at $-40 < V_Z < -20$ and dearth at $25 < V_Z < 50$ visibly extend beyond the expected noise. Another smaller excess unaccounted for by the fit is also visible at larger velocities in the $|Z| < 500pc$ sample.

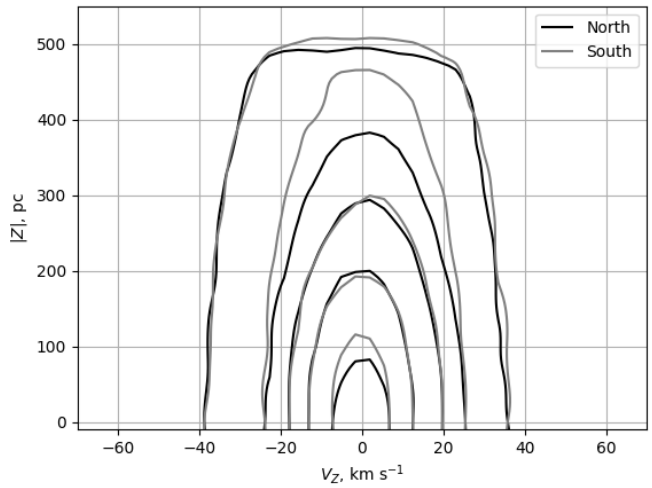


**Figure 3.15:** Kernel density estimation for |Z| vs. V Z on the Gaia Cylinder RGB sample. This was implemented using the function kdeplot of the Python Seaborn package, isodensity levels shown are 10% (outermost) to 90% (innermost) in steps of 20%.

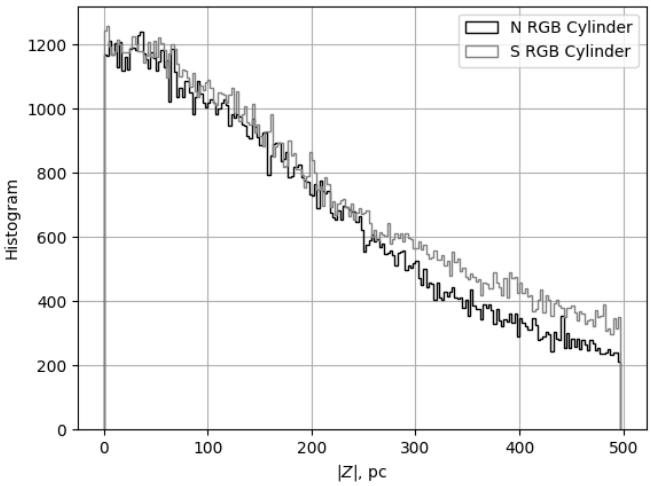


**Figure 3.16:** Histogram of |Z| for the Gaia Cylinder RGB North and South samples.

| Gaia Cylinder RGB | $\sigma_{thin}$ | | $\sigma_{Thick}$ | | Thick Disk % | |
|---|---|---|---|---|---|---|
| Sample height | North | South | North | South | North | South |
| $\|Z\| < 500$ pc | $11.09 \pm 0.28$ | $11.78 \pm 0.33$ | $23.90 \pm 0.64$ | $23.49 \pm 0.73$ | $55 \pm 3$ | $53 \pm 4$ |
| $\|Z\| < 200$ pc | $11.68 \pm 0.28$ | $10.25 \pm 0.31$ | $24.76 \pm 1.22$ | $21.81 \pm 0.72$ | $39 \pm 4$ | $55 \pm 4$ |
| $\|Z\| < 100$ pc | $11.51 \pm 0.31$ | $10.15 \pm 0.29$ | $24.27 \pm 1.31$ | $21.73 \pm 0.77$ | $39 \pm 4$ | $51 \pm 4$ |
| $\|Z\| < 50$ pc | $10.90 \pm 0.32$ | $10.32 \pm 0.31$ | $23.19 \pm 1.12$ | $22.02 \pm 0.89$ | $44 \pm 4$ | $49 \pm 4$ |

**Table 3.15:** $V_Z$ dispersion $\sigma$ values and errors from the sum of two zero-centered Gaussians fit.

### 3.3.1 Comparison with another resent articles

An excces of stars with the vertical velocities at about -40 km/s could be trace of the wave of compression and rarefaction in the direction perpendicular to the Galactic plane studied by Williams et al.[57]

The complex structure of $V_Z$ is present also in our analysis. The distribution of the vertical velocity $V_Z$ of red giant stars shows the excess of stars with velocities $-40 < V_Z < -20 km/s$ and the dearth of stars with velocities $25 < V_Z < 50 km/s$. Also, from the figure Figure 4.5 it is obvious that the north and the south hemispheres are not equal in terms of the vertical velocity distribution, while two other components of velocity $V_R$ and $V_\Phi$ do not show anomalies. Observed structure in the vertical stellar velocity distribution in the solar neighborhood can be caused by several mechanisms. An influence on the Galactic disk by the Galactic bar and spiral arms is quite strong and can lead to complex structure of the disk kinematics [89]. Also, Nonequilibrium-phase mixing can occur due to the tidal disturbance of the Galactic disk by the crossing of a Sagittarius-like satellite [90]. Further study is needed to identify the mechanism responsible for these features.

Lee et al. [51] analysed the sample of 17277 G-dwarfs stars from SEGUE survey with a measured metallicity information as well as $[\alpha/Fe]$ ratio. They separated the disk onto thin and thick disk population. A distance to individual stars were estimated by calibrated stellar isochrones, while proper motion information of their sample has errors about 3-4 mas/yr. Using this data, Lee et al. [51] measured the velocity lag between chemically separated thin and thick disk populations. The value of the lag is nearly constant at about 30 km/s almost irrelevant of the distance from the Galactic plane $|Z|$. However, our value is almost twice smaller, 14km/s. Using cross-matched samples for Gaia EDR3 and RAVE DR5 catalogues, we found that the metallicity information does not change, essentially the value of the velocity lag.

Our analysis of red giant stars kinematics in the solar neighborhood showed a smaller value of asymmetric drift of about 19 km/s. The discrepancy may be a cause of the fact that Anguiano

et al. [92] selected stars in the larger volume, comparing to samples used in our work. Also, the difference could be due to the incompleteness of the sample used by the authors, since the completeness issue was not discussed.

There is even bigger discrepancy between our work and Anguiano et al.[92] in the estimation of proportion of stars that belong to the different subsystems of Galactic disk. Their estimated values are: 81.9% for the thin disk and 16.6% for the thick disk. So the local thick-to-thin density normalization is about 2% for this value, which is very far from our results (90%). As Kawata and Chiappini [116] noticed, the thick disk selected kinematically and chemically are strictly speaking two different objects. Our selection criterion for the thick disk was purely kinematic for the complete samples, but the comparison with the cross-matched samples with RAVE data, where we used chemically based selection for the thin disk $[Fe/H] > 0.4$ and for the Thick disk $1 < [Fe/H] < 0.4$, showed that kinematical properties do not change in the solar neighborhood.

Our result of the thick-to-thin ratio is in agreement with already mentioned work of Kawata and Chiappini [116]. The authors determined the star formation history of our Galaxy using the chemical abundances of long-lived stars. They found that there was an intense star formation phase for our Galaxy between 9 and 12.5Gyr ago than was followed by a dip in star formation rate lasting about 1Gyr. According to them, the formation of massive thick disk occurred during this intense phase.

Lehnert et al. [13] studied the star formation history of the Milky Way in comparison with properties of distant high-redshift galaxies. They found that the Milky Way formed stars with the high formation rate during the first 4Gyr of evolution, which resulted to the formation of the thick disk with the mass approximately equal to the mass of thin disk.

Park et al. [104] analysed high-resolution simulations GALACTICA and HEWHORIZON. They found that the thin and thick disks contain overlapping components, and even in the Galactic midplane stars of the thick disk contribute on average around 30% in total density of stars and about 10% of luminosity. The conclusion of these authors was that the thin and thick disks are not entirely distinct components, when they are defined spatially, in terms of formation process. The two disks represent parts of a single disk that evolves with a time due to continuous star formation and disk heating.

### 3.3.2 The main results

We studied the kinematical properties of the Milky Way disk in the solar neighborhood. Spatially restricted complete sample of 296879 red giant stars in the cylinder with the center in the solar position, with the radius of 1kpc and the half-height of 0.5kpc was analysed by two-component fit to the velocity distribution of the $V_Z$ velocity component. Our results can be summarized as follows.

1. The kinematical properties of the selected stars point at the existence of two distinct components: the thin disk with mean velocities $V_R$, $V_\varphi$, $V_Z$ of -1, -239, 0 km/s, and velocity dispersions $\sigma_R$, $\sigma_\varphi$, $\sigma_Z$ of 31, 20 and 11 km/s, correspondingly. The Thick disk component has, on the other hand, mean velocities $V_R$, $V_\varphi$, $V_Z$ of +1, -225, 0 km/s, and velocity dispersions $\sigma_R$, $\sigma_\varphi$, $\sigma_Z$ of 49, 35, and 22 km/s. Completeness of our RGB sample of stars allows to estimate the density ratio of the thin and Thick disks in the solar neighborhood. We find that Thick disk stars comprise about half the stars of the disk. Such high density of the stars with Thick disk kinematics points at an *in situ* rather than *ex situ* formation of the Thick disk.

2. $V_Z$ velocity field has **small but real** anomaly in the solar neighborhood. Velocity distribution of red-giant stars in the direction perpendicular to the galactic plane has an excess of stars with $V_Z$ velocities of $-40 < V_Z < -20$ km/s and a dearth of stars with $25 < V_Z < 50$ km/s. Anomaly is observed both in the Northern and in the Southern Galactic hemispheres.

The result of this work was published in The Astrophysical Journal [117].

# 4

# Vertical structure of the disk

## 4.1 Data selection

For the reasons described in the previous chapter section 3.1, we are certain that the data from the Gaia satellite is in a perfect match with our further aim, which major part consists of the analysis of positions and proper motions of stars to reveal the vertical structure of the Milky Way disk. In the work described in the previous chapter chapter 3 we used the data from EDR3 catalogue, since it was the newest release of the Gaia team at the beginning moment of the work. Here we will use the next data release Gaia DR3 catalogue. The main difference between the Gaia EDR3 and Gaia DR3 catalogues is the radial velocity information, which we will barely use in the following chapter, however it is necessary to mention the main improvement and direct the reader of this work to the source with the fully described information.

In this section we mention the specialities of the Gaia DR3 catalogue subsection 4.1.1, then in subsection 4.1.2 we describe why we decided to exclude the radial velocities from our analysis, then we explain our restriction on a magnitude of the sources subsection 4.1.3 and then we present the final subset subsection 4.1.4 and its completeness subsection 4.1.5.

### 4.1.1 Gaia DR3 catalog

Gaia EDR3 was the first installment of the full Gaia DR3. It was included astrometry and photometry based on 34 months of satellite operations, while the radial velocity information

was copied from Gaia DR2, with some specialities, which are mentioned in subsection 3.1.2. Gaia DR3 has the same source catalogue, where astronomy and photometry repeated from Gaia EDR3. Mean low-resolution blue and red photometer spectra and high-resolution radial velocity spectrometer spectra were added. Also, information related to radial velocity spectrometer and blue and red photometer spectra was reestemated or added, as well as new estimates of mean radial velocities to a fainter limiting magnitudes. Also, some useful information about source classification and characterisation was added.

Regarding astrometry and photometry, which come from Gaia EDR3, some systematic errors, which are mostly connected to the bright stars ($G < 13$), were found [118].

Mean low-resolution BP/RP spectra for about 220 million sources were released. The source should be bright enough $G < 17.65$ to have spectra with sufficient signal-to-noise ratio. Only few faint specific objects have G up to 21.43. The signal-to-noise ratio of spectra depends on the magnitude and varies in the range from 100 for the faintest sources $G \approx 15$ to 1000 for the central part of some RP spectra for $9 < G < 12$.

New radial velocity information based on 34 months of satellite operations, while radial velocities in Gaia EDR3 were from Gaia DR2, which is based on 22 months of data and contains information for stars $G_{RVS} \leq 12$ and with effective temperatures $3500 < T_{eff} < 6900$K. New radial velocities in Gaia DR3 are available for about 33.8 million stars with $G_{RVS} \leq 14$ and with $3100 \leq T_{eff} \leq 14500$K. An additional type of data such as the line broadening velocity for about 3.5 million stars, $G_{RVS}$ magnitudes for more than 32 million stars, mean spectra for almost 1 million stars and epoch radial velocities for RR Lyrae and Cepheids were published for the first time.

The transit RVS spectra are extracted, cleaned, deblended (if necessary), wavelength calibrated and normalised to their pseudo-continuum or by scaling with a constant. Then the spectra shifted to the rest frame using radial velocity information for the same epoch for the bright stars $G_{RVS} \leq 12$ or using combined radial velocities for faint stars. Then the spectra are interpolated into a common wavelength array in the range 846-870 nm with a step of 0.01 nm and averaged. The spectra which were released have signal-to-noise ratio more than 20 for the star spectral types A, F, G and K. It should be mentioned that the published spectra are not uniformly distributed over the sky. The known issue of spurious population of stars with high radial velocity from previous Gaia date release can occur because of flux contamination of target source by the flux of nearby bright source. Also, when a bright source and a target source are separated by 1.8" in the direction perpendicular to the scan, it can produce biased radial velocities. These effects were accounted and radial velocities for such stars were deleted

from the catalogue. Radial velocity uncertainties are of the order of a few km/s, but it should be noted that they are slightly underestimated for bright stars.

### 4.1.2 Projection on the Galactic plane

We want to extend our sample in terms of the vertical coordinate. In other words, we want to include stars which have |Z| up to 2kpc, which is a value around twice of scale height of thick disk. This approach allows tracing the significant decreasing of stellar density not only because of the thin disk population, but also due to the thick disk component. However, at such big distances the 3d velocity can be reproduced for a small part of the stars, since the radial velocity measurements have restrictions mentioned above. Thus, it leads to incomplete sample, which can be the cause of biased results.

In our analysis we decided to use only proper motions to avoid completeness problem due to the lack of radial velocities. To do so, we need that proper motions represent plane motion in the Galactic disk. To reach this condition we need that the difference between proper motion and the projection of proper motion on the plane was smaller than the error of proper motion measurements. According to the schematic plot Figure 4.1 we can write the following condition:

$$pm - pm * sin(b) < pm\_error \tag{4.1}$$

Where $pm$ is a proper motion, $b$ is a fixed angle of Galactic latitude, $pm\_error$ is error of proper motion measurements and $pm * sin(b)$ is a projected proper motion on the Galactic plane.

### 4.1.3 Main sequence stars

In the previous chapter chapter 3 we analysed the kinematics of red giant stars, however here we will use the main sequence (MS) stars. The main reason is that the population of MS stars is vast, and it allows us to perform statistical estimations. One of the reasons of using red giant stars in previous chapter was the fact that they are bright enough for the radial velocity spectrometer instrument of the Gaia satellite. Since here we will not use radial velocities, this is no longer an advantage. Thus, we can use the MS stars up to maximum $G \leq 21$ mag, which is the limiting apparent magnitude for the Gaia DR3 catalogue.

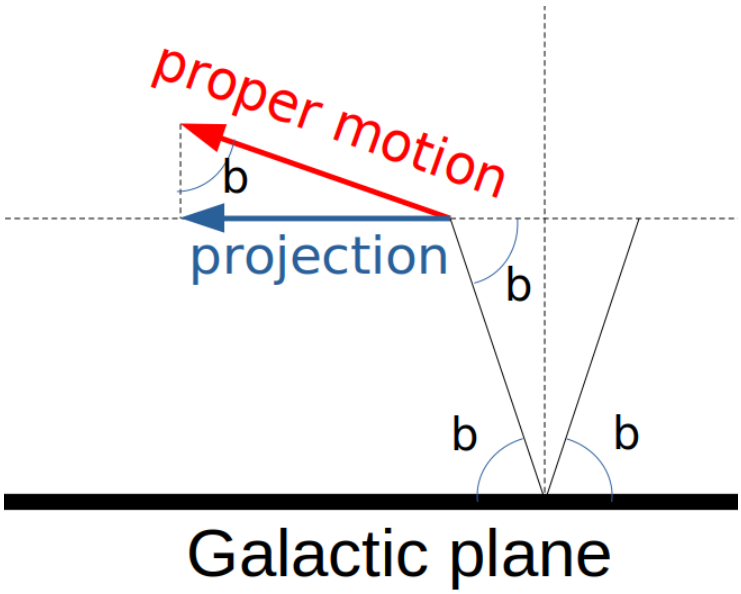


**Figure 4.1:** Schematic plot of the geometry of edge on view on the Galaxy.

Our cut is based on the absolute magnitude reproduced from the apparent one also accounting for the extinction by the ag_gspphot column in the Gaia DR3 catalogue.

$$G_0 = phot\_g\_mean\_mag + 5 * log(parallax) - 10 - ag\_gspphot \tag{4.2}$$

The imposed cut is $4 < G_0 < 8$. The graphical representation is shown in colour-magnitude diagram Figure 4.2.

The completeness of Gaia DR3 is estimated to be between 19 and 21 apparent magnitude. Assuming that the dimmest sources ($G_0 = 8$) from our subsample are at the 2 kpc, they will have apparent magnitude $G \approx 19.5$, which is in the range of Gaia astrometric and photometric instruments.

### 4.1.4 Final subset of stars

We selected the data from the Gaia DR3 catalogue with the following requests **??**. We selected stars in a volume of two cones with the Sun in the apex point, height of 2.5 kpc and within the solid angle of 15 degrees. The good quality data was chosen only $ruwe < 1.4$ according to the Gaia team (for more details check the previous chapter subsection 3.1.5) and error in parallaxes less than 10%. Also, proper motion should be non Null value.

Than we imposed some additional parameters which the Gaia DR3 catalogue allows us to do,

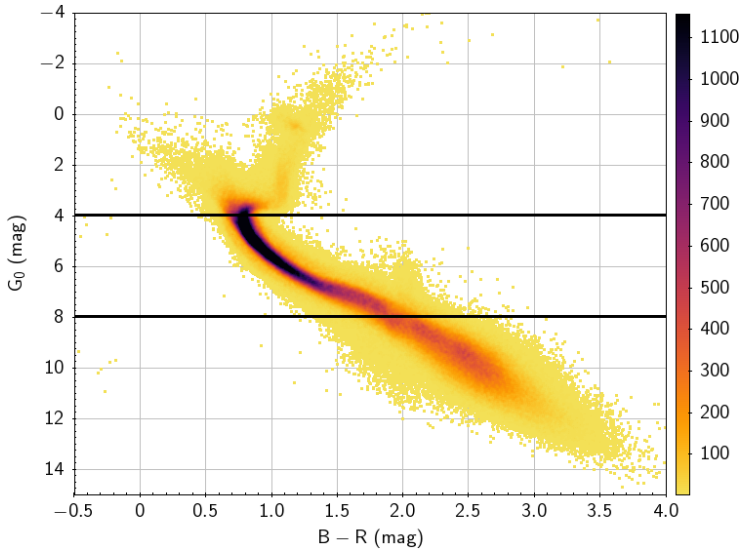


**Figure 4.2:** Color magnitude diagram, colour coded by density for the sample chosen by the Algorithm 4.1 query. The black lines represent an imposed cut on absolute magnitude.

**Algorithm 4.1** The query of the north sample in Astronomical Data Query Language for the Gaia server

```
SELECT *
FROM gaiadr3.gaia_source
WHERE ruwe < 1.4
AND ABS(parallax_over_error) > 10
AND (1.0/parallax) < 2.5
AND pmISNOTNULL
AND b < 75
```

**Algorithm 4.2** The query of the north sample in Astronomical Data Query Language for the Gaia server

```
SELECT *
FROM gaiadr3.gaia_source
WHERE ruwe < 1.4
AND ABS(parallax_over_error) > 10
AND (1.0/parallax) < 2.5
AND pmISNOTNULL
AND b < −75
```

such as *in_qso_candidates* = *false*, *in_galaxies_candidate* = *false* and *non_single_stars* = 0, which means that there are no quasars, galaxies or non-single stars in our sample. The total number of sources is 703272 for the both north and south cones.

We computed approximated UV velocities with only parallaxes and proper motions by assuming that the radial velocity is zero, since the contribution of projection to these velocities is small and below the estimated velocity error. We compared this UV velocities with the full UV velocities, with include radial velocity information over the subsample, for which Gaia DR3 catalogue has radial velocities, to check the difference. The difference is below 10% for 96% of subsample stars. And it should be noted that the stars with the biggest difference have the biggest redial velocity components and, according to the projection, they have the biggest vertical velocities. Such stars could be a halo stars and do not represent the disk-like motion.

From UV velocities, where U points towards the galactic center and V points to the direction of galactic rotation, we compute galactocentric cylindrical velocities $V_R$, which points away from the galactic center, and $V_\varphi$, which follows the opposite direction of the galactic rotation. The computation was done assuming the following values for the solar motion of the LSR and the solar galactocentric coordinates: $(U, V, W)_\odot = (11.10, 12.24, 7.25) km/s$, $V_{g,LRS} = -244.5 km/s$ and $R_\odot = 8 kpc$ [113].

The analysis of the UV velocities with respect to the LSR showed a small but notable number of halo stars, lagging in the rotation behind the LSR. We impose the restriction on the velocities $\sqrt{U^2 + V^2} \geqslant 180 km/s$ to exclude them from further analysis Figure 4.3. Our sample of stars is reduced to 683059 stars after this additional cut. Two open clusters visible in the polar caps were found in our sample. They are the Coma Cluster (97 stars) in the north and the Blanco 1 (457 stars) in the south. However, their presence does not disturb our results since their number of stars is negligible compared to the all sample. The final cut is made as in extinction-corrected absolute magnitude, $4 < G_0 < 8$ as described above subsection 4.1.3. The final sample consists of 334642 stars.

### 4.1.5 Completeness

Gaia GR3 completeness is based on already known from Gaia EDR3 estimation to be complete between 19 and 21 apparent magnitude $G$, since we do not use the radial velocity information. Our sample selection is based on the absolute magnitude $G_0$ between 4 and 8, which is in a save region of apparent magnitudes, taking into account the possible maximum distance of stars. This is described in more details in subsection 4.1.3. However, since we applied quality cuts

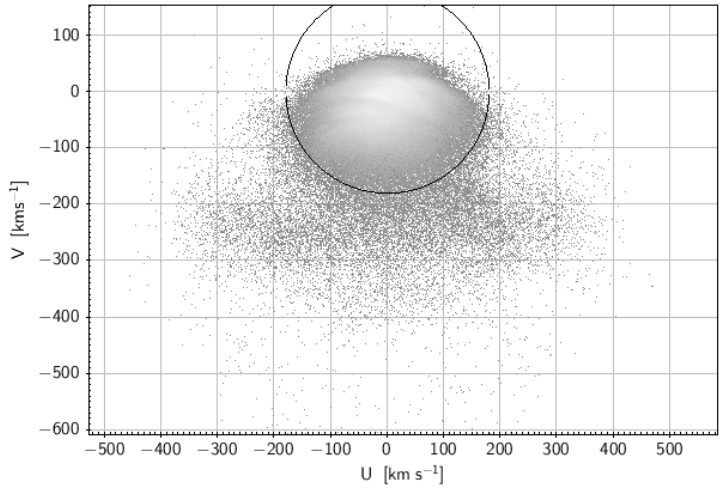


**Figure 4.3:** The plot of the UV velocities of the stars from the sample. The black circle is restriction $\sqrt{U^2 + V^2} \geqslant 180 km/s$.

such as cut on *ruwe*, cut on *paralax_over_error*, cut on *non_single_stars*, and also cut on velocities to exclude halo stars, the completeness can be compromised. Thus, we also perform completeness analysis here, as we have done in the previous chapter subsection 3.1.6. The cumulative distribution of the cylindrical radius centered at the Sun position within a thin cylinder volume, at various vertical heights from the galactic plane. These volumes in fact are truncated cones, but, since the difference between the base radius and the radius of the top surface is small, we can treat the thin cones as cylinders, or better say "coins" to emphasise their small height. As before, we assume that the star distribution is uniform within the volume of the coin. So, the number of stars should grow as a second power of the radius from the center. Repeating the computation from the previous chapter Equation 3.2, we plot the completeness for each coin Figure 4.4.

The incompleteness of our sample is below 1% within 2 kpc vertically from the galactic plane, but the incompleteness grows significantly further away. The grey line in Figure 4.4 is the histogram of vertical positions of stars. It shows the expected two peaks of distribution for the two cones volume sample. From the galactic plane to the height of about 300pc our sample volume is quite small, because of the enclosed angle of 15 degree. Thus, the number of stars within the coin increases because of increasing of volume of the coin for the first coins from the galactic plane. The distribution reach its peak at around 800 pc and then decrease, since the number of stars decreases far away from the galactic plane even if the volume of coins increases far and far away from the galactic plane. Also, one can see the north-south asymmetry of the

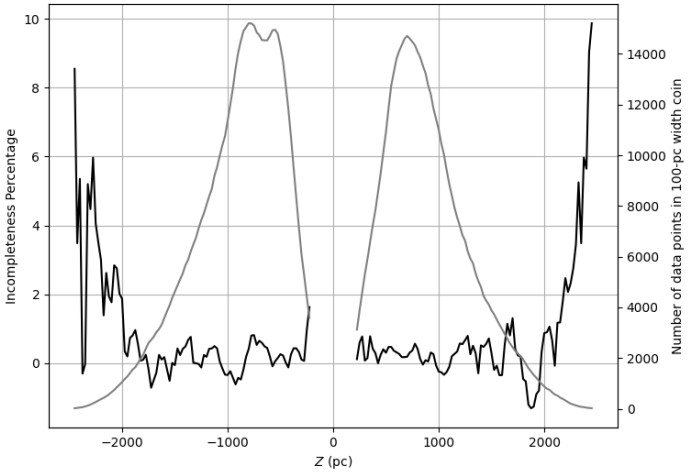


**Figure 4.4:** Completeness evaluation of the sample of 334642 stars divided into "coins" with the height of 100pc. The grey line is the histogram of the vertical positions of the stars. The black line is the estimation of incompleteness.

distribution, which was detected in the previous chapter subsection 3.2.4. We also notice that there are very few stars within the height of 100pc, therefore all calculations involving Z avoid this region. Considering the large variations of completeness beyond the height of 2 kpc, we limit our sample to $|Z| < 2kpc$. Thus, our final complete sample consists of 331273 main sequence stars.

## 4.2 Dependence physical values on the distance from the disk plane

### 4.2.1 $V_\varphi$ separation of thin and thick disk.

We tried to understand how rotational velocity depends on vertical structure or vise versa, how vertical structure changes with different $V_\varphi$ interval subsets. To do so, we first divided our sample into the subsamples with 20 km/s step starting from -300km/s and finishing at 40km/s. For each subset, we made a kernel density estimation plot of the vertical profile by the Python *seaborn.kdeplot* method with parameters $bw\_mathod = 0.1$ and $cut = 0$. In the Figure 4.5 one can see the lines for each subsample. From the plot, it is evident that the vertical distribution becomes wider when the subsample's absolute rotational velocity decrease.

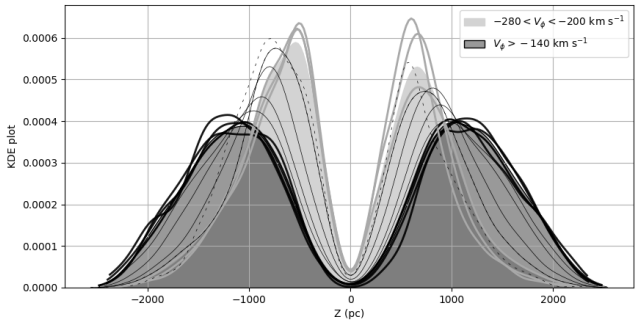


**Figure 4.5:** KDE plot of the vertical profile at various $V_\varphi$ intervals. Each curve corresponds to a $V_\varphi$ bin of 20 km/s width, centered at -290 to -50 km/s. The bold grey lines are the subsamples dominated by the thin disk, and the bold black lines are the subsamples dominated by the thick disk. The black lines are a mix of subsamples of both thin and thick disks, and the dashed line is the fastest rotating sample that exhibits significant asymmetry. The filled light and dark grey plots represent subsamples as defined in the legend, and correspond respectively to the thin $280 < V_\varphi < 200 km/s$ and thick disk $V_\varphi > -140 km/s$ dominated samples.

Particularly, we noticed that the subsamples in the range $-280 < V_\varphi < -200 km/s$ share a similar shape concentrated around the galactic plane, thin disk, while the subsamples in the range $-140 < V_\varphi < -60 km/s$ share a much wider shape, thick disk. The subsamples in between exhibit changing profiles with mixed characteristics. Also, it should be noted that the fastest subsample in the range $-300 < V_\varphi < -280$ shows significant north-south asymmetry, which is the cause to not include it into thin disk. The KDE for this subset is represented by the dashed line in the Figure 4.5. We combined the subsets in the range $-280 < V_\varphi < -200 km/s$ to build the KDE for our thin disk sample (light grey area in the Figure 4.5) and we combined the subsets in the range $-140 < V_\varphi < -60 km/s$ to build the KDE for the thick disk sample (dark grey area in the Figure 4.5).

### 4.2.2 Scale height estimation

For the samples of the thin and thick disks we computed the number density at each height. Using selected in the previous subsection subsection 4.2.1 samples of the thin and the thick disk, we perform a fit by commonly used for thin-thick spatial distribution separation square sech function, where there are two free parameters: $\rho_0$ is density at the galactic midplane and $H_Z$ is scale height of the disk component.

$$\rho(Z) = \rho_0^2(Z/H_Z) \tag{4.3}$$

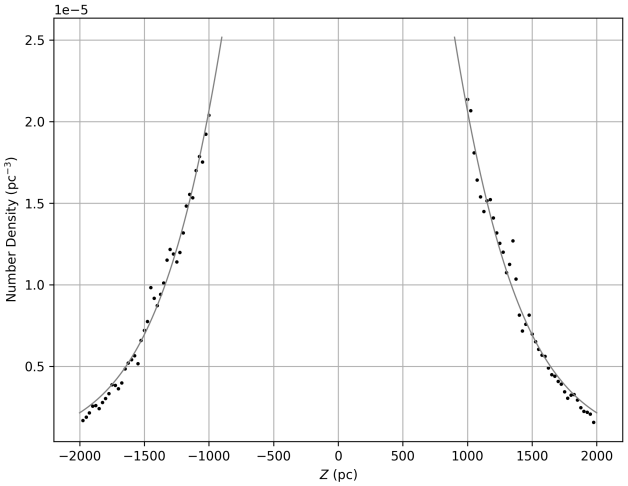


**Figure 4.6:** Number density fit for the thick disk sample. The obtained scale height is $826.60 \pm 12.14pc$

First, let us do so for the thick disk sample. By considering 6781 dwarf main sequence stars with $1000 > |Z| > 2000pc$ and $V_\varphi > -140km/s$ we use the Python package *scipy.optimize.curve_fit* to fit a function Equation 4.3 to the number density computed every $25pc$ over truncated cones of height $50pc$. The resulting densities are shown as black points and the fit is shown as a grey curve Figure 4.6. The fitting yields $\rho_0 = 6.884 \times 10^{-5} \pm 2.683 \times 10^{-6}$ pc$^{-3}$ and $H_Z = 826.60 \pm 12.14$ pc.

The same fitting procedure was done for the thin disk sample with a slight change. Several intervals of |Z| were studied in order to obtain a safe fit. In the previous chapter, we showed that the kinematically-selected thin disk sample may have non-negligible thick disk contamination. Therefore, we restrict the calculations to the interval $100 > |Z| > 200pc$ and $-280 < V_\varphi < -200km/s$, which gives us 5244 dwarf main sequence stars. Computing the thin disk number density every 5 pc over truncated cones of height 20pc, we perform a single square sech profile fit as we did for the thick disk. The results are $\rho_0 = 6.933 \times 10^{-3} \pm 1.681 \times 10^{-4}$ pc$^{-3}$ and $h_Z = 271.56 \pm 11.94$ pc. As before, the resulting densities are shown as black points and the fit is shown as a grey curve Figure 4.7

### 4.2.3 Thin-to-thick number density ratio

To calculate thin-to-thick number density ratio at the galactic plane $\rho_t/\rho_T$ we use the whole sample in the two cones volume, considering all the main sequence dwarf stars with $100 <$

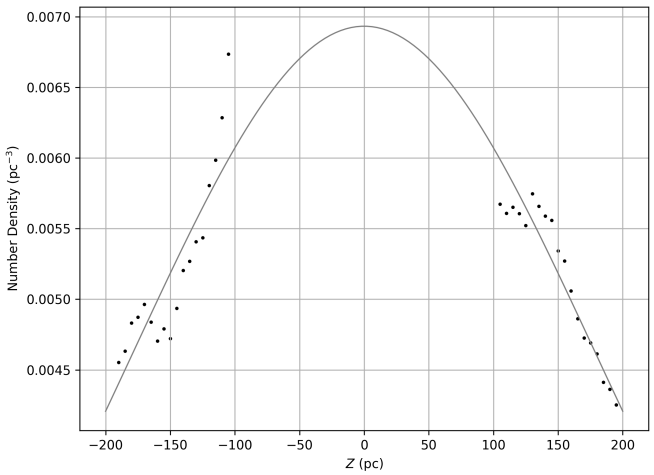


**Figure 4.7:** Number density fit for the thin disk sample. The obtained scale height is $271.56 \pm 11.94pc$

$|Z| < 2000pc$ without any restrictions implied on $V_\varphi$. We fit the vertical number density profile computed every 50 pc over truncated cones of height 100 pc in the range $-2 < Z < 2kpc$ excluding the closest to the galactic plane region ($-100 < Z < 100$) by the sum of two square sech functions Equation 4.4, where $\rho_t$ and $h_Z$ are the number density at the galactic plane and the scale height of the thin disk and $\rho_T$ and $H_Z$ are values for the thick disk respectively.

$$\rho(Z) = \rho_t^2 \left(\frac{Z}{h_Z}\right) + \rho_T^2 \left(\frac{Z}{H_Z}\right) \tag{4.4}$$

It should be noted that here free parameters are only number densities, scale heights were taken from the previous subsection subsection 4.2.2. The results are shown in the Table 4.1 and also can be seen in the Figure 4.8. The root mean square deviation (RMSD) of the fitting is a measure of the residuals between the data points and the fitted function. $RMSD = 8.191 \times 10^{-4}$.

| $h_Z$ (pc) | $H_Z$ (pc) | $\rho_t$ | $\rho_T$ | $\rho_t/\rho_T$ |
|---|---|---|---|---|
| 271.56 | 826.60 | $4.229 \times 10^{-3}$ | $2.786 \times 10^{-3}$ | 1.518 |
| $\pm$ 11.94 | $\pm$ 12.14 | $\pm$ $2.127 \times 10^{-4}$ | $\pm$ $1.019 \times 10^{-4}$ | $\pm$ 0.094 |
| 4% | 1% | 5% | 4% | 6% |

**Table 4.1:** The results of the fit for the disk sample in the two-cones volume. The second row shows the parameter errors and the third row shows the percentage errors.

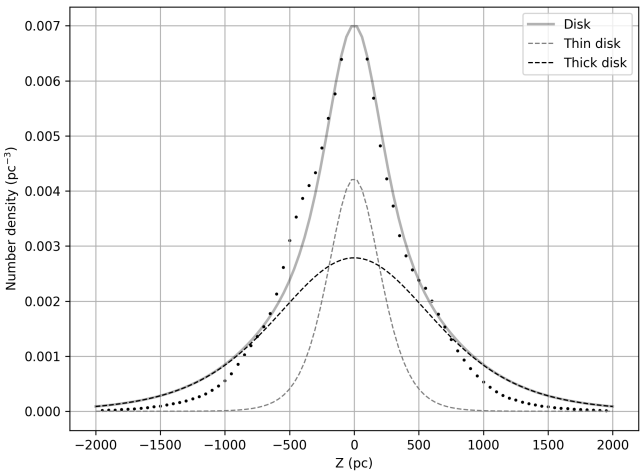


**Figure 4.8:** The vertical number density fit of the sample. Black points are the computed number densities at each truncated cone. The solid line represents the fit of the sum of the two square sech functions and the dashed lines represent the of the square sech function for the thin and thick disk respectively.

We notice that the fitting procedure with the fixed scale heights leads to the biggest values of the fitting line for $|Z| \gtrsim 700pc$ than the measured number densities. Thus, we decided to do several tests in which we fit the number density data with the function Equation 4.4 where $H_Z$, $h_Z$ or both of them are the free parameters.

In all of these three cases, the fitted scale heights are significantly different from the ones we obtain from $V_\varphi$ analysis and their percentage errors are significantly higher as well, however, their RMSD are smaller. The case with the all free parameters gives the smallest RMSD and the closest to the data points fit.

In all the cases, the thin disk has a smaller scale height than what we estimated from the fast rotating subsample, while the thick disk has a bigger scale height than was observed from the slow rotating subsample.

When the all parameters are free, the scale heights reach their extreme values, but the percentage errors are the biggest as well. For example, for the thin disk scale height, the value is 160.52 pc with the error of 121%. Therefore, for the fit with the all free parameters, the algorithm has a hard time finding stable reliable values. Thus, the best fit in terms of parameter errors is obtained when we take the fixed value of the scale heights from the $V_\varphi$ separated subsamples, although the fit is not properly follow the data points at height $|Z|$. We believe that estimates of the scale heights of the thin and thick disks listed in Table 4.1 are trustable, because

the subsamples are dominated by these populations despite not having further information to improve that data selection, so we use these values to estimate thin-to-thick ratio.

Thin-to-thick vertical number density ratio $\frac{\rho_t}{\rho_T}\frac{^2(Z/h_Z)}{^2(Z/H_Z)}$ is maximum at the $Z = 0$ and equal to $\frac{\rho_t}{\rho_T}$. This value decreases with the distance from the galactic plane and at about $|Z| \sim 700pc$ this value is about 4% of the midplane one and it tends to zero further away.

This could mean that the fitting values are driven mainly from the data points within $|Z| < 700pc$ and if we take points beyond, the results do not change significantly.

Playing with the fitting process a bit more and restricting our data sample to $|Z| < 700, 1000, 2000pc$ we found that the both midplane number density values $\rho_t$ and $\rho_T$ are changing within the corresponding $3\sigma$ level.

Probably our separation into fast and slow rotation samples may not properly gauge the vertical profiles of the thin and the thick disk or the fit function is needed to improved. Also, we did not account for the observed north-south asymmetry, which is significant to be considered.

The fitting of the sum of the thin disk and the thick disk with the generally accepted square sech model for the Milky Way galaxy fails to reproduce data points for $|Z| > 700pc$ of the complete and high quality Gaia DR3 data.

We believe that the approximation of using data within two cones without line-of-sight velocities is a good approach to increase completeness of more distant samples.

### 4.2.4 Density ratio. Comparison with the previous chapter

With the obtained scale heights and number densities we can compare this results with the results from the previous chapter subsection 3.2.3, where we found that within a height of 500pc from the galactic plane and cylindrical radius of 1kpc from the Sun, the both components of the disk have about the same number of red giant stars. Using the following equations:

$$\begin{aligned}
\int^2 \left(\frac{z}{h}\right) dz &= h \tanh\left(\frac{z}{2h}\right) + constant \\
\int_{-z_{lim}}^{z_{lim}} {}^2\left(\frac{z}{h}\right) dz &= 2h \tanh\left(\frac{z_{lim}}{h}\right) \\
\int_{-\infty}^{+\infty} {}^2\left(\frac{z}{h}\right) dz &= \lim_{z_{lim}\to+\infty} \int_{-z_{lim}}^{+z_{lim}} {}^2\left(\frac{z}{h}\right) dz = \lim_{z_{lim}\to+\infty} 2h \tanh\left(\frac{z_{lim}}{h}\right) = 2h
\end{aligned}$$

the fraction can be defined as

$$N_{cyl,thin}(|Z| < z_{lim}) = f(z_{lim}) N_{cyl,thick}(|Z| < z_{lim})$$

$$f(z_{lim}) = f(z_{lim}; h, H, \rho_t, \rho_T) = \frac{h}{H}\frac{\rho_t}{\rho_T}\frac{\tanh\left(\frac{z_{lim}}{h}\right)}{\tanh\left(\frac{z_{lim}}{H}\right)} \Longrightarrow f(500; h, H, \rho_t, \rho_T) = 0.88 \pm 0.06$$

Using a Monte-Carlo method assuming Gaussian $1\sigma$ errors for the parameters from the Table 4.1 the computed value f is consistent with f = 1 within $3\sigma = 0.18$. Thus, it supports our conclusion from the previous chapter that close to the galactic plane there is a significant number of the thick disk stars compatible with the number of the thin disk stars.

## 4.3 Results

In this section, we will conclude the results of this chapter. We compare our work to the respectively recent articles in the section subsection 4.3.1 and we briefly repeat the main findings in section subsection 4.3.2

### 4.3.1 Comparison with another resent articles

Park et al. [104] studied the vertical density distribution of the thin and thick disks to understand the disk components are really distinct components which are formed by different formation mechanisms and at different time. The authors used the simulations New Horizon and GALACTICA. They studied the results of evolution of 18 massive galaxies from New Horizon simulation together with one disk galaxy from GALACTICA simulation. The authors studied luminosity and mass distribution. To do so, they applied the two component fit to the r-band vertical profiles, which showed that two-component disk structures are well presented in the simulations. The result of the work [104] is that about 30% of the mass and about 10% of luminosity in r-band close to mid-plane of the disk are represented by thick disk stars. This result is in agreement with previous works on simulated galaxies [77, 88]. They found that kinematic decomposition of the disk stars leads to the comparable mass of the thick disk and of the thin disk stars.

### 4.3.2 The main results

We showed the dependence of $V_\Phi$ velocity on the distance from the galactic plane. The estimated from the sum of square sech function fit scale heights and densities at the mid-plane for

the thin and thick disk components were presented. As our analysis showed in the Milky Way there are more stars at higher scale heights than those of the thin disk that need to be accounted for. The result of this work was accepted for publishing in Galaxies Journal.

# 5

# Conclusion

The kinematical properties of the Milky Way disk in the solar neighborhood was studied. Spatially restricted complete sample of 296879 red giant stars in the cylinder with the center in the solar position, with the radius of 1 kpc and the half-height of 0.5kpc was analysed by two-component fit to the velocity distribution of the $V_Z$ velocity component. The kinematical properties of the selected red giant stars point at the existence of two distinct components of the disk of Milky Way: the thin disk and the thick disk. The thin disk has mean velocities $(V_R, V_\varphi, V_Z) = (-1, -239, 0)km/s$, and velocity dispersions $(\sigma_R, \sigma_\varphi, \sigma_Z) = (31, 20, 11)km/s$. The thick disk component has mean velocities $(V_R, V_\varphi, V_Z) = (1, -225, 0)km/s$, and velocity dispersions $(\sigma_R, \sigma_\varphi, \sigma_Z) = (49, 35, 22)km/s$. Completeness of our RGB sample of stars allows to estimate the density ratio of the thin and Thick disks in the solar neighborhood. We find that thick disk stars comprise about half the stars of the disk. Such high density of the stars with thick disk kinematics points at an *in situ* rather than *ex situ* formation of the thick disk. $V_Z$ velocity field has the anomaly in the solar neighborhood. Velocity distribution of red giant stars in the direction perpendicular to the galactic plane has an excess of stars with $V_Z$ velocities of $-40 < V_Z < -20$ km/s and a dearth of stars with $25 < V_Z < 50$ km/s. Anomaly is observed both in the Northern and in the Southern Galactic hemispheres. The dependence of $V_{Phi}$ velocity on the distance from the galactic plane was shown. The estimated scale heights for the thin and thick disk components were presented as well as their densities at the mid-plane. We conclude that in the Milky Way there are more stars at higher scale heights than those of the thin disk that need to be accounted for. Considering that most of the thick disk stars are lo-

cated in the galactic plane, then a separation of thin and thick disk populations close to the Sun, based only on detailed chemical abundances, and entirely independent of kinematic selections will provide a clearer answer.

# References

[1] Gaia Collaboration, T. Prusti, J. H. J. de Bruijne, A. G. A. Brown, A. Vallenari, C. Babusiaux, C. A. L. Bailer-Jones, U. Bastian, M. Biermann, D. W. Evans, L. Eyer, F. Jansen, C. Jordi, S. A. Klioner, U. Lammers, L. Lindegren, X. Luri, F. Mignard, D. J. Milligan, C. Panem, V. Poinsignon, D. Pourbaix, S. Randich, G. Sarri, P. Sartoretti, H. I. Siddiqui, C. Soubiran, V. Valette, F. van Leeuwen, N. A. Walton, C. Aerts, F. Arenou, M. Cropper, R. Drimmel, E. Høg, D. Katz, M. G. Lattanzi, W. O'Mullane, E. K. Grebel, A. D. Holland, C. Huc, X. Passot, L. Bramante, C. Cacciari, J. Castañeda, L. Chaoul, N. Cheek, F. De Angeli, C. Fabricius, R. Guerra, J. Hernández, A. Jean-Antoine-Piccolo, E. Masana, R. Messineo, N. Mowlavi, K. Nienartowicz, D. Ordóñez-Blanco, P. Panuzzo, J. Portell, P. J. Richards, M. Riello, G. M. Seabroke, P. Tanga, F. Thévenin, J. Torra, S. G. Els, G. Gracia-Abril, G. Comoretto, M. Garcia-Reinaldos, T. Lock, E. Mercier, M. Altmann, R. Andrae, T. L. Astraatmadja, I. Bellas-Velidis, K. Benson, J. Berthier, R. Blomme, G. Busso, B. Carry, A. Cellino, G. Clementini, S. Cowell, O. Creevey, J. Cuypers, M. Davidson, J. De Ridder, A. de Torres, L. Delchambre, A. Dell'Oro, C. Ducourant, Y. Frémat, M. García-Torres, E. Gosset, J. L. Halbwachs, N. C. Hambly, D. L. Harrison, M. Hauser, D. Hestroffer, S. T. Hodgkin, H. E. Huckle, A. Hutton, G. Jasniewicz, S. Jordan, M. Kontizas, A. J. Korn, A. C. Lanzafame, M. Manteiga, A. Moitinho, K. Muinonen, J. Osinde, E. Pancino, T. Pauwels, J. M. Petit, A. Recio-Blanco, A. C. Robin, L. M. Sarro, C. Siopis, M. Smith, K. W. Smith, A. Sozzetti, W. Thuillot, W. van Reeven, Y. Viala, U. Abbas, A. Abreu Aramburu, S. Accart, J. J. Aguado, P. M. Allan, W. Allasia, G. Altavilla, M. A. Álvarez, J. Alves, R. I. Anderson, A. H. Andrei, E. Anglada Varela, E. Antiche, T. Antoja, S. Antón, B. Arcay, A. Atzei, L. Ayache, N. Bach, S. G. Baker, L. Balaguer-Núñez, C. Barache, C. Barata, A. Barbier, F. Barblan, M. Baroni, D. Barrado y Navascués, M. Barros, M. A. Barstow, U. Becciani, M. Bellazzini, G. Bellei, A. Bello García, V. Belokurov, P. Bendjoya, A. Berihuete, L. Bianchi, O. Bienaymé, F. Billebaud, N. Blagorodnova, S. Blanco-Cuaresma, T. Boch, A. Bombrun, R. Borrachero, S. Bouquillon, G. Bourda, H. Bouy, A. Bragaglia, M. A. Breddels, N. Brouillet, T. Brüsemeister, B. Bucciarelli, F. Budnik, P. Burgess, R. Burgon, A. Burlacu, D. Busonero, R. Buzzi, E. Caffau, J. Cambras,

H. Campbell, R. Cancelliere, T. Cantat-Gaudin, T. Carlucci, J. M. Carrasco, M. Castellani, P. Charlot, J. Charnas, P. Charvet, F. Chassat, A. Chiavassa, M. Clotet, G. Cocozza, R. S. Collins, P. Collins, G. Costigan, F. Crifo, N. J. G. Cross, M. Crosta, C. Crowley, C. Dafonte, Y. Damerdji, A. Dapergolas, P. David, M. David, P. De Cat, F. de Felice, P. de Laverny, F. De Luise, R. De March, D. de Martino, R. de Souza, J. Debosscher, E. del Pozo, M. Delbo, A. Delgado, H. E. Delgado, F. di Marco, P. Di Matteo, S. Diakite, E. Distefano, C. Dolding, S. Dos Anjos, P. Drazinos, J. Durán, Y. Dzigan, E. Ecale, B. Edvardsson, H. Enke, M. Erdmann, D. Escolar, M. Espina, N. W. Evans, G. Eynard Bontemps, C. Fabre, M. Fabrizio, S. Faigler, A. J. Falcão, M. Farràs Casas, F. Faye, L. Federici, G. Fedorets, J. Fernández-Hernández, P. Fernique, A. Fienga, F. Figueras, F. Filippi, K. Findeisen, A. Fonti, M. Fouesneau, E. Fraile, M. Fraser, J. Fuchs, R. Furnell, M. Gai, S. Galleti, L. Galluccio, D. Garabato, F. García-Sedano, P. Garé, A. Garofalo, N. Garralda, P. Gavras, J. Gerssen, R. Geyer, G. Gilmore, S. Girona, G. Giuffrida, M. Gomes, A. González-Marcos, J. González-Núñez, J. J. González-Vidal, M. Granvik, A. Guerrier, P. Guillout, J. Guiraud, A. Gúrpide, R. Gutiérrez-Sánchez, L. P. Guy, R. Haigron, D. Hatzidimitriou, M. Haywood, U. Heiter, A. Helmi, D. Hobbs, W. Hofmann, B. Holl, G. Holland, J. A. S. Hunt, A. Hypki, V. Icardi, M. Irwin, G. Jevardat de Fombelle, P. Jofré, P. G. Jonker, A. Jorissen, F. Julbe, A. Karampelas, A. Kochoska, R. Kohley, K. Kolenberg, E. Kontizas, S. E. Koposov, G. Kordopatis, P. Koubsky, A. Kowalczyk, A. Krone-Martins, M. Kudryashova, I. Kull, R. K. Bachchan, F. Lacoste-Seris, A. F. Lanza, J. B. Lavigne, C. Le Poncin-Lafitte, Y. Lebreton, T. Lebzelter, S. Leccia, N. Leclerc, I. Lecoeur-Taibi, V. Lemaitre, H. Lenhardt, F. Leroux, S. Liao, E. Licata, H. E. P. Lindstrøm, T. A. Lister, E. Livanou, A. Lobel, W. Löffler, M. López, A. Lopez-Lozano, D. Lorenz, T. Loureiro, I. MacDonald, T. Magalhães Fernandes, S. Managau, R. G. Mann, G. Mantelet, O. Marchal, J. M. Marchant, M. Marconi, J. Marie, S. Marinoni, P. M. Marrese, G. Marschalkó, D. J. Marshall, J. M. Martín-Fleitas, M. Martino, N. Mary, G. Matijevič, T. Mazeh, P. J. McMillan, S. Messina, A. Mestre, D. Michalik, N. R. Millar, B. M. H. Miranda, D. Molina, R. Molinaro, M. Molinaro, L. Molnár, M. Moniez, P. Montegriffo, D. Monteiro, R. Mor, A. Mora, R. Morbidelli, T. Morel, S. Morgenthaler, T. Morley, D. Morris, A. F. Mulone, T. Muraveva, I. Musella, J. Narbonne, G. Nelemans, L. Nicastro, L. Noval, C. Ordénovic, J. Ordieres-Meré, P. Osborne, C. Pagani, I. Pagano, F. Pailler, H. Palacin, L. Palaversa, P. Parsons, T. Paulsen, M. Pecoraro, R. Pedrosa, H. Pentikäinen, J. Pereira, B. Pichon, A. M. Piersimoni, F. X. Pineau, E. Plachy, G. Plum, E. Poujoulet, A. Prša, L. Pulone, S. Ragaini,

S. Rago, N. Rambaux, M. Ramos-Lerate, P. Ranalli, G. Rauw, A. Read, S. Regibo, F. Renk, C. Reylé, R. A. Ribeiro, L. Rimoldini, V. Ripepi, A. Riva, G. Rixon, M. Roelens, M. Romero-Gómez, N. Rowell, F. Royer, A. Rudolph, L. Ruiz-Dern, G. Sadowski, T. Sagristà Sellés, J. Sahlmann, J. Salgado, E. Salguero, M. Sarasso, H. Savietto, A. Schnorhk, M. Schultheis, E. Sciacca, M. Segol, J. C. Segovia, D. Segransan, E. Serpell, I. C. Shih, R. Smareglia, R. L. Smart, C. Smith, E. Solano, F. Solitro, R. Sordo, S. Soria Nieto, J. Souchay, A. Spagna, F. Spoto, U. Stampa, I. A. Steele, H. Steidelmüller, C. A. Stephenson, H. Stoev, F. F. Suess, M. Süveges, J. Surdej, L. Szabados, E. Szegedi-Elek, D. Tapiador, F. Taris, G. Tauran, M. B. Taylor, R. Teixeira, D. Terrett, B. Tingley, S. C. Trager, C. Turon, A. Ulla, E. Utrilla, G. Valentini, A. van Elteren, E. Van Hemelryck, M. van Leeuwen, M. Varadi, A. Vecchiato, J. Veljanoski, T. Via, D. Vicente, S. Vogt, H. Voss, V. Votruba, S. Voutsinas, G. Walmsley, M. Weiler, K. Weingrill, D. Werner, T. Wevers, G. Whitehead, Ł. Wyrzykowski, A. Yoldas, M. Žerjal, S. Zucker, C. Zurbach, T. Zwitter, A. Alecu, M. Allen, C. Allende Prieto, A. Amorim, G. Anglada-Escudé, V. Arsenijevic, S. Azaz, P. Balm, M. Beck, H. H. Bernstein, L. Bigot, A. Bijaoui, C. Blasco, M. Bonfigli, G. Bono, S. Boudreault, A. Bressan, S. Brown, P. M. Brunet, P. Bunclark, R. Buonanno, A. G. Butkevich, C. Carret, C. Carrion, L. Chemin, F. Chéreau, L. Corcione, E. Darmigny, K. S. de Boer, P. de Teodoro, P. T. de Zeeuw, C. Delle Luche, C. D. Domingues, P. Dubath, F. Fodor, B. Frézouls, A. Fries, D. Fustes, D. Fyfe, E. Gallardo, J. Gallegos, D. Gardiol, M. Gebran, A. Gomboc, A. Gómez, E. Grux, A. Gueguen, A. Heyrovsky, J. Hoar, G. Iannicola, Y. Isasi Parache, A. M. Janotto, E. Joliet, A. Jonckheere, R. Keil, D. W. Kim, P. Klagyivik, J. Klar, J. Knude, O. Kochukhov, I. Kolka, J. Kos, A. Kutka, V. Lainey, D. LeBouquin, C. Liu, D. Loreggia, V. V. Makarov, M. G. Marseille, C. Martayan, O. Martinez-Rubi, B. Massart, F. Meynadier, S. Mignot, U. Munari, A. T. Nguyen, T. Nordlander, P. Ocvirk, K. S. O'Flaherty, A. Olias Sanz, P. Ortiz, J. Osorio, D. Oszkiewicz, A. Ouzounis, M. Palmer, P. Park, E. Pasquato, C. Peltzer, J. Peralta, F. Péturaud, T. Pieniluoma, E. Pigozzi, J. Poels, G. Prat, T. Prod'homme, F. Raison, J. M. Rebordao, D. Risquez, B. Rocca-Volmerange, S. Rosen, M. I. Ruiz-Fuertes, F. Russo, S. Sembay, I. Serraller Vizcaino, A. Short, A. Siebert, H. Silva, D. Sinachopoulos, E. Slezak, M. Soffel, D. Sosnowska, V. Straižys, M. ter Linden, D. Terrell, S. Theil, C. Tiede, L. Troisi, P. Tsalmantza, D. Tur, M. Vaccari, F. Vachier, P. Valles, W. Van Hamme, L. Veltz, J. Virtanen, J. M. Wallut, R. Wichmann, M. I. Wilkinson, H. Ziaeepour, and S. Zschocke, "The Gaia mission," , vol. 595, p. A1, Nov. 2016.

[2] A. Kunder, G. Kordopatis, M. Steinmetz, T. Zwitter, P. J. McMillan, L. Casagrande, H. Enke, J. Wojno, M. Valentini, C. Chiappini, G. Matijevič, A. Siviero, P. de Laverny, A. Recio-Blanco, A. Bijaoui, R. F. G. Wyse, J. Binney, E. K. Grebel, A. Helmi, P. Jofre, T. Antoja, G. Gilmore, A. Siebert, B. Famaey, O. Bienaymé, B. K. Gibson, K. C. Freeman, J. F. Navarro, U. Munari, G. Seabroke, B. Anguiano, M. Žerjal, I. Minchev, W. Reid, J. Bland-Hawthorn, J. Kos, S. Sharma, F. Watson, Q. A. Parker, R.-D. Scholz, D. Burton, P. Cass, M. Hartley, K. Fiegert, M. Stupar, A. Ritter, K. Hawkins, O. Gerhard, W. J. Chaplin, G. R. Davies, Y. P. Elsworth, M. N. Lund, A. Miglio, and B. Mosser, "The radial velocity experiment (rave): Fifth data release," *The Astronomical Journal*, vol. 153, no. 2, p. 75, jan 2017. [Online]. Available: https://dx.doi.org/10.3847/1538-3881/153/2/75

[3] R. J. Allen, J. E. Baldwin, and R. Sancisi, "Radio continuum observations of the edge-on disc galaxy NGC 891." , vol. 62, pp. 397–409, Jan. 1978.

[4] D. Burstein, "Structure and origin of So galaxies. III. The luminosity distribution perpendicular to the plane of the disks in So's." , vol. 234, pp. 829–836, Dec. 1979.

[5] V. Tsikoudi, "Photometry and structure of lenticular galaxies. I - NGC 3115," , vol. 234, pp. 842–853, Dec. 1979.

[6] E. Hummel, R. Sancisi, and R. D. Ekers, "Radio continuum observations of the edge-on spiral galaxies NGC 4244,4565, and 5907." , vol. 133, pp. 1–10, Apr. 1984.

[7] N. Reid and G. Gilmore, "New light on faint stars. II. A photometric study of the low luminosity main sequence." , vol. 201, pp. 73–94, Oct. 1982.

[8] A. Sandage and G. Fouts, "U ,V, W Velocity Components for the Old Disk Using Radial Velocities of 1295 Stars in the Three Cardinal Galactic Directions," , vol. 93, p. 592, Mar. 1987.

[9] A. Sandage, "The Disk and Halo Densities at the Plane from Star Counts in the Galactic Poles," , vol. 93, p. 610, Mar. 1987.

[10] P. G. van Dokkum, R. F. Peletier, R. de Grijs, and M. Balcells, "The vertical stellar distribution in NGC 6504: detection of a thick disk." , vol. 286, pp. 415–425, Jun. 1994.

[11] N. A. Tikhonov and O. A. Galazutdinova, "Stellar subsystems of the galaxy NGC 2366," *Astronomy Reports*, vol. 52, no. 1, pp. 19–26, Jan. 2008.

[12] S. Comerón, J. H. Knapen, K. Sheth, M. W. Regan, J. L. Hinz, A. Gil de Paz, K. Menéndez-Delmestre, J.-C. Muñoz-Mateos, M. Seibert, T. Kim, E. Athanassoula, A. Bosma, R. J. Buta, B. G. Elmegreen, L. C. Ho, B. W. Holwerda, E. Laurikainen, H. Salo, and E. Schinnerer, "The Thick Disk in the Galaxy NGC 4244 from $S^4G$ Imaging," , vol. 729, no. 1, p. 18, Mar. 2011.

[13] M. D. Lehnert, P. D. Matteo, M. Haywood, and O. N. Snaith, "The milky way as a high-redshift galaxy: The importance of thick disk formation in galaxies," *The Astrophysical Journal Letters*, vol. 789, no. 2, p. L30, jun 2014. [Online]. Available: https://dx.doi.org/10.1088/2041-8205/789/2/L30

[14] J. A. Rose, "Red horizontal-branch stars in the galactic disk." , vol. 90, pp. 787–802, May 1985.

[15] E. D. Friel, "A Spectroscopic Survey of High-Latitude Fields and Comparison to Galaxy Models," , vol. 93, p. 1388, Jun. 1987.

[16] J. Norris, "Population Studies: The Nature of the Thick Disk," , vol. 314, p. L39, Mar. 1987.

[17] S. Casertano, K. U. Ratnatunga, and J. N. Bahcall, "Kinematic Modeling of the Galaxy. II. Two Samples of High Proper-Motion Stars," , vol. 357, p. 435, Jul. 1990.

[18] T. A. von Hippel, "Galactic Structure From Faint Stromgren Photometry: The Catalog of Observations," , vol. 104, p. 1765, Nov. 1992.

[19] T. Yamagata and Y. Yoshii, "UBV Starscounts in SA54 and Global Structure of the Galaxy," , vol. 103, p. 117, Jan. 1992.

[20] Y. Yoshii, K. Ishida, and R. S. Stobie, "Galactic Structure Towards the North Galactic Pole Based on an Analysis of UBV Star-Count Data," , vol. 93, p. 323, Feb. 1987.

[21] G. Gilmore and N. Reid, "New light on faint stars - III. Galactic structure towards the South Pole and the Galactic thick disc." , vol. 202, pp. 1025–1047, Mar. 1983.

[22] G. Gilmore, N. Reid, and P. Hewett, "New light on faint stars - VII. Luminosity and mass distributions in two high galactic latitude fields." , vol. 213, pp. 257–278, Mar. 1985.

[23] N. Reid and S. R. Majewski, "Star Counts Redivivus. I. A New Look at the Galaxy at Faint Magnitudes," , vol. 409, p. 635, Jun. 1993.

[24] S. R. Majewski, "A Complete, Multicolor Survey of Absolute Proper Motions to B approximately 22.5: Galactic Structure and Kinematics at the North Galactic Pole," , vol. 78, p. 87, Jan. 1992.

[25] C. Soubiran, "Kinematics of the galaxy's stellar populations from a proper motion survey." , vol. 274, pp. 181–188, Jul. 1993.

[26] D. Ojha, "Kinematical properties of the thick disk of the Galaxy." in *The Formation of the Milky Way*, Jan. 1995, pp. 215–218.

[27] A. Robin and M. Creze, "Stellar populations in the milky way: a synthetic model." , vol. 157, pp. 71–90, Mar. 1986.

[28] T. C. Beers and J. Sommer-Larsen, "Kinematics of Metal-poor Stars in the Galaxy," , vol. 96, p. 175, Jan. 1995.

[29] B. Chen, "Kinematics and Chemical Properties of the Galaxy in the Vicinity of the North Galactic Pole," , vol. 113, pp. 311–320, Jan. 1997.

[30] A. C. Robin, M. Haywood, M. Creze, D. K. Ojha, and O. Bienayme, "The thick disc of the Galaxy: sequel of a merging event." , vol. 305, p. 125, Jan. 1996.

[31] A. M. Wolfe and J. X. Prochaska, "On The Evolution of Damped Ly$\alpha$ Systems to Galactic Disks," , vol. 494, no. 1, pp. L15–L18, Feb. 1998.

[32] W. Dehnen and J. J. Binney, "Local stellar kinematics from HIPPARCOS data," , vol. 298, no. 2, pp. 387–394, Aug. 1998.

[33] D. K. Ojha, O. Bienaymé, V. Mohan, and A. C. Robin, "New surveys of UBV photometry and absolute proper motions at intermediate latitude," , vol. 351, pp. 945–953, Nov. 1999.

[34] S. Phleps, K. Meisenheimer, B. Fuchs, and C. Wolf, "CADIS deep star counts: Galactic structure and the stellar luminosity function," , vol. 356, pp. 108–117, Apr. 2000.

[35] J. X. Prochaska, S. O. Naumov, B. W. Carney, A. McWilliam, and A. M. Wolfe, "The Galactic Thick Disk Stellar Abundances," , vol. 120, no. 5, pp. 2513–2549, Nov. 2000.

[36] P. E. Nissen, Y. Q. Chen, W. J. Schuster, and G. Zhao, "Sc and Mn abundances in disk and metal-rich halo stars," , vol. 353, pp. 722–728, Jan. 2000.

[37] G. Tautvaišienė, B. Edvardsson, I. Tuominen, and I. Ilyin, "Chemical composition of red horizontal branch stars in the thick disk of the Galaxy," , vol. 380, pp. 578–589, Dec. 2001.

[38] G. Gilmore, R. F. G. Wyse, and J. E. Norris, "Deciphering the Last Major Invasion of the Milky Way," , vol. 574, no. 1, pp. L39–L42, Jul. 2002.

[39] T. V. Nykytyuk and T. V. Mishenina, "The Magnesium Abundance in the Thin and Thick Disk of the Galaxy," *Odessa Astronomical Publications*, vol. 17, p. 63, Jan. 2004.

[40] T. V. Mishenina, T. I. Gorbaneva, C. Soubiran, O. Bienayme, V. V. Kovtyukh, and S. A. Korotin, "The Behavior of $\alpha$-Elements Abundances in the Thin and Thick Disks of the Galaxy," *Odessa Astronomical Publications*, vol. 18, p. 78, Jan. 2005.

[41] C. Soubiran and P. Girard, "Abundance trends in kinematical groups of the Milky Way's disk," , vol. 438, no. 1, pp. 139–151, Jul. 2005.

[42] B. Famaey, A. Jorissen, X. Luri, M. Mayor, S. Udry, H. Dejonghe, and C. Turon, "Local kinematics of K and M giants from CORAVEL/Hipparcos/Tycho-2 data. Revisiting the concept of superclusters," , vol. 430, pp. 165–186, Jan. 2005.

[43] V. A. Marsakov and T. V. Borkova, "Formation of Galactic Subsystems in Light of the Magnesium Abundance in Field Stars: The Thick Disk," *Astronomy Letters*, vol. 31, no. 8, pp. 515–527, Aug. 2005.

[44] S. Bilir, A. Cabrera-Lavers, S. Karaali, S. Ak, E. Yaz, and M. López-Corredoira, "Estimation of Galactic Model Parameters in High Latitudes with SDSS," , vol. 25, no. 2, pp. 69–84, Jan. 2008.

[45] S. Karaali, E. Hamzaoğlu, and S. Bilir, "A universal vertical stellar density distribution law for the Galaxy," , vol. 324, no. 1, pp. 23–30, Nov. 2009.

[46] S. Karaali, S. Bilir, and E. Hamzaoğlu, "A different approach for the estimation of Galactic model parameters," , vol. 355, no. 1, pp. 307–320, Nov. 2004.

[47] R. Smiljanic, L. Pasquini, P. Bonifacio, D. Galli, R. G. Gratton, S. Randich, and B. Wolff, "Beryllium abundances and star formation in the halo and in the thick disk," , vol. 499, no. 1, pp. 103–119, May 2009.

[48] K. A. Venn, M. Irwin, M. D. Shetrone, C. A. Tout, V. Hill, and E. Tolstoy, "Stellar Chemical Signatures and Hierarchical Galaxy Formation," , vol. 128, no. 3, pp. 1177–1195, Sep. 2004.

[49] A. Spagna, M. G. Lattanzi, P. Re Fiorentin, and R. L. Smart, "Evidence of a thick disk rotation-metallicity correlation," , vol. 510, p. L4, Feb. 2010.

[50] D. Carollo, T. C. Beers, M. Chiba, J. E. Norris, K. C. Freeman, Y. S. Lee, Ž. Ivezić, C. M. Rockosi, and B. Yanny, "Structure and Kinematics of the Stellar Halos and Thick Disks of the Milky Way Based on Calibration Stars from Sloan Digital Sky Survey DR7," , vol. 712, no. 1, pp. 692–727, Mar. 2010.

[51] Y. S. Lee, T. C. Beers, D. An, Željko Ivezić, A. Just, C. M. Rockosi, H. L. Morrison, J. A. Johnson, R. Schönrich, J. Bird, B. Yanny, P. Harding, and H. J. Rocha-Pinto, "Formation and evolution of the disk system of the milky way: [α/fe] ratios and kinematics of the segue g-dwarf sample," *The Astrophysical Journal*, vol. 738, no. 2, p. 187, aug 2011. [Online]. Available: https://dx.doi.org/10.1088/0004-637X/738/2/187

[52] T. V. Mishenina, T. I. Gorbaneva, N. Y. Basak, C. Soubiran, and V. V. Kovtyukh, "The copper and zinc abundances in stars of galactic sub-structures," *Astronomy Reports*, vol. 55, no. 8, pp. 689–703, Aug. 2011.

[53] G. Kordopatis, A. Recio-Blanco, P. de Laverny, G. Gilmore, V. Hill, R. F. G. Wyse, A. Helmi, A. Bijaoui, M. Zoccali, and O. Bienaymé, "A spectroscopic survey of thick disc stars outside the solar neighbourhood," , vol. 535, p. A107, Nov. 2011.

[54] C. Moni Bidin, G. Carraro, and R. A. Méndez, "Kinematical and Chemical Vertical Structure of the Galactic Thick Disk. I. Thick Disk Kinematics," , vol. 747, no. 2, p. 101, Mar. 2012.

[55] K. Carrell, Y. Chen, and G. Zhao, "Metallicity Gradients of Thick Disk Dwarf Stars," , vol. 144, no. 6, p. 185, Dec. 2012.

[56] J. Bovy, H.-W. Rix, D. W. Hogg, T. C. Beers, Y. S. Lee, and L. Zhang, "The vertical motions of mono-abundance sub-populations in the milky way disk," *The Astrophysical Journal*, vol. 755, no. 2, p. 115, aug 2012. [Online]. Available: https://dx.doi.org/10.1088/0004-637X/755/2/115

[57] M. E. K. Williams, M. Steinmetz, J. Binney, A. Siebert, H. Enke, B. Famaey, I. Minchev, R. S. de Jong, C. Boeche, K. C. Freeman, O. Bienaymé, J. Bland-Hawthorn, B. K. Gibson, G. F. Gilmore, E. K. Grebel, A. Helmi, G. Kordopatis, U. Munari, J. F. Navarro, Q. A. Parker, W. Reid, G. M. Seabroke, S. Sharma, A. Siviero, F. G. Watson, R. F. G. Wyse, and T. Zwitter, "The wobbly Galaxy: kinematics north and south with RAVE red-clump giants," *Monthly Notices of the Royal Astronomical Society*, vol. 436, no. 1, pp. 101–121, 10 2013. [Online]. Available: https://doi.org/10.1093/mnras/stt1522

[58] Y. Yan, C. Du, H. Li, J. Shi, J. Ma, and H. J. Newberg, "Existence of the Metal-rich Stellar Halo and High-velocity Thick Disk in the Galaxy," , vol. 903, no. 2, p. 131, Nov. 2020.

[59] J. N. Bahcall and R. M. Soneira, "The universe at faint magnitudes. I. Models for the Galaxy and the predicted star counts." , vol. 44, pp. 73–110, Sep. 1980.

[60] ——, "The distribution of stars to V = 16th magnitude near the north galactic pole - Normalization, clustering properties, and counts in various bands." , vol. 246, pp. 122–135, May 1981.

[61] ——, "Predicted star counts in selected fields and photometric bands Applications to galactic structure, the disk luminosity function, and the detection of a massive halo." , vol. 47, pp. 357–403, Dec. 1981.

[62] ——, "Comparisons of a standard galaxy model with stellar observations in five fields." , vol. 55, pp. 67–99, May 1984.

[63] G. Gilmore, "The significance of deep star counts for models of the Galaxy and the surface density of faint quasars." , vol. 195, pp. 183–196, Apr. 1981.

[64] N. Reid and G. Gilmore, "New light on faint stars. II. A photometric study of the low luminosity main sequence." , vol. 201, pp. 73–94, Oct. 1982.

[65] ——, "New light on faint stars - V. Infrared photometry and the H-R diagramfor very low mass dwarfs." , vol. 206, pp. 19–35, Jan. 1984.

[66] G. Gilmore, "New light on faint stars - VI. Structure and evolution of the Galactic spheroid." , vol. 207, pp. 223–240, Mar. 1984.

[67] C. Pritchet, "Application of star count data to studies of galactic structure." , vol. 88, pp. 1476–1488, Oct. 1983.

[68] W. J. Luyten, "A new determination of the luminosity function," , vol. 139, p. 221, Jan. 1968.

[69] H. Jahreiß and R. Wielen, "Leuchtkraftfunktion und Massendichte der sonnennahen Sterne," *Mitteilungen der Astronomischen Gesellschaft Hamburg*, vol. 35, pp. 212–214, Jan. 1974.

[70] J. N. Bahcall, "The distribution of stars perpendicular to galactic disk," , vol. 276, pp. 156–168, Jan. 1984.

[71] A. Jenkins, "Heating of galactic discs with realistic vertical potentials," , vol. 257, no. 4, pp. 620–632, Aug. 1992.

[72] W. Dehnen, "The Pattern Speed of the Galactic Bar," , vol. 524, no. 1, pp. L35–L38, Oct. 1999.

[73] ——, "The Effect of the Outer Lindblad Resonance of the Galactic Bar on the Local Stellar Velocity Distribution," , vol. 119, no. 2, pp. 800–812, Feb. 2000.

[74] R. Fux, "Order and chaos in the local disc stellar kinematics induced by the Galactic bar," , vol. 373, pp. 511–535, Jul. 2001.

[75] J. A. Sellwood and J. J. Binney, "Radial mixing in galactic discs," , vol. 336, no. 3, pp. 785–796, Nov. 2002.

[76] A. C. Robin, C. Reylé, S. Derrière, and S. Picaud, "A synthetic view on structure and evolution of the Milky Way," , vol. 409, pp. 523–540, Oct. 2003.

[77] M. G. Abadi, J. F. Navarro, M. Steinmetz, and V. R. Eke, "Simulations of galaxy formation in a Λ cold dark matter universe. i. dynamical and photometric properties of a simulated disk galaxy," *The Astrophysical Journal*, vol. 591, no. 2, p. 499, jul 2003. [Online]. Available: https://dx.doi.org/10.1086/375512

[78] R. De Simone, X. Wu, and S. Tremaine, "The stellar velocity distribution in the solar neighbourhood," , vol. 350, no. 2, pp. 627–643, May 2004.

[79] N. Y. Sotnikova and S. A. Rodionov, "Estimating the dark halo mass from the relative thickness of stellar disks," *Astronomy Letters*, vol. 32, no. 10, pp. 649–660, Oct. 2006.

[80] R. Roškar, V. P. Debattista, T. R. Quinn, G. S. Stinson, and J. Wadsley, "Riding the Spiral Waves: Implications of Stellar Migration for the Properties of Galactic Disks," , vol. 684, no. 2, p. L79, Sep. 2008.

[81] F. Bournaud, B. G. Elmegreen, and M. Martig, "The Thick Disks of Spiral Galaxies as Relics from Gas-rich, Turbulent, Clumpy Disks at High Redshift," , vol. 707, no. 1, pp. L1–L5, Dec. 2009.

[82] R. Schönrich and J. Binney, "Chemical evolution with radial mixing," , vol. 396, no. 1, pp. 203–222, Jun. 2009.

[83] B. P. Moster, A. V. Macciò, R. S. Somerville, P. H. Johansson, and T. Naab, "Can gas prevent the destruction of thin stellar discs by minor mergers?" , vol. 403, no. 2, pp. 1009–1019, Apr. 2010.

[84] B. P. Moster, A. V. Macciò, R. S. Somerville, T. Naab, and T. J. Cox, "The effects of a hot gaseous halo on disc thickening in galaxy minor mergers," , vol. 423, no. 3, pp. 2045–2057, Jul. 2012.

[85] E. Spitoni and F. Matteucci, "Effects of the radial flows on the chemical evolution of the Milky Way disk," , vol. 531, p. A72, Jul. 2011.

[86] A. Curir, M. G. Lattanzi, A. Spagna, F. Matteucci, G. Murante, P. Re Fiorentin, and E. Spitoni, "The thick disk rotation-metallicity correlation as a fossil of an "inverse chemical gradient" in the early Galaxy," , vol. 545, p. A133, Sep. 2012.

[87] C. Vera-Ciro and E. D'Onghia, "On the Conservation of the Vertical Action in Galactic Disks," , vol. 824, no. 1, p. 39, Jun. 2016.

[88] A. Obreja, A. V. Macciò, B. Moster, A. A. Dutton, T. Buck, G. S. Stinson, and L. Wang, "Introducing galactic structure finder: the multiple stellar kinematic structures of a simulated Milky Way mass galaxy," *Monthly Notices of the Royal Astronomical Society*, vol. 477, no. 4, pp. 4915–4930, 04 2018. [Online]. Available: https://doi.org/10.1093/mnras/sty1022

[89] T. Antoja, A. Helmi, M. Romero-Gómez, D. Katz, C. Babusiaux, R. Drimmel, D. W. Evans, F. Figueras, E. Poggio, C. Reylé, A. C. Robin, G. Seabroke, and C. Soubiran, "A dynamically young and perturbed milky way disk," *Nature*, vol. 561, no. 7723, pp. 360–362, sep 2018. [Online]. Available: https://doi.org/10.1038%2Fs41586-018-0510-7

[90] J. Bland-Hawthorn, S. Sharma, T. Tepper-Garcia, J. Binney, K. C. Freeman, M. R. Hayden, J. Kos, G. M. De Silva, S. Ellis, G. F. Lewis, M. Asplund, S. Buder, A. R. Casey, V. D'Orazi, L. Duong, S. Khanna, J. Lin, K. Lind, S. L. Martell, M. K. Ness, J. D. Simpson, D. B. Zucker, T. Zwitter, P. R. Kafle, A. C. Quillen, Y.-S. Ting, and R. F. G. Wyse, "The GALAH survey and Gaia DR2: dissecting the stellar disc's phase space by age, action, chemistry, and location," *Monthly Notices of the Royal Astronomical Society*, vol. 486, no. 1, pp. 1167–1191, 01 2019. [Online]. Available: https://doi.org/10.1093/mnras/stz217

[91] G. Arreaga-García, "A thick-disk galaxy model and simulations of equal-mass galaxy pair collisions," *Research in Astronomy and Astrophysics*, vol. 20, no. 11, p. 189, Nov. 2020.

[92] B. Anguiano, S. R. Majewski, C. R. Hayes, C. A. Prieto, X. Cheng, C. M. Bidin, R. L. Beaton, T. C. Beers, and D. Minniti, "The stellar velocity distribution function in the milky way galaxy," *The Astronomical Journal*, vol. 160, no. 1, p. 43, jun 2020. [Online]. Available: https://dx.doi.org/10.3847/1538-3881/ab9813

[93] A. Everall, N. W. Evans, V. Belokurov, D. Boubert, and R. J. J. Grand, "The Photo-Astrometric vertical tracer density of the Milky Way – I. The method," *Monthly Notices of the Royal Astronomical Society*, vol. 511, no. 2, pp. 2390–2404, 11 2021. [Online]. Available: https://doi.org/10.1093/mnras/stab3325

[94] A. Everall, V. Belokurov, N. W. Evans, D. Boubert, and R. J. J. Grand, "The photo-astrometric vertical tracer density of the Milky Way – II. Results from Gaia,"

*Monthly Notices of the Royal Astronomical Society*, vol. 511, no. 3, pp. 3863–3880, 02 2022. [Online]. Available: https://doi.org/10.1093/mnras/stac305

[95] D. Boubert and A. Everall, "Completeness of the Gaia verse II: what are the odds that a star is missing from Gaia DR2?" *Monthly Notices of the Royal Astronomical Society*, vol. 497, no. 4, pp. 4246–4261, 08 2020. [Online]. Available: https://doi.org/10.1093/mnras/staa2305

[96] ——, "A selection function toolbox for subsets of astronomical catalogues," *Monthly Notices of the Royal Astronomical Society*, vol. 510, no. 3, pp. 4626–4638, 12 2021. [Online]. Available: https://doi.org/10.1093/mnras/stab3665

[97] J. Spitzer, Lyman and M. Schwarzschild, "The Possible Influence of Interstellar Clouds on Stellar Velocities." , vol. 114, p. 385, Nov. 1951.

[98] C. G. Lacey, "The influence of massive gas clouds on stellar velocity dispersions in galactic discs," , vol. 208, pp. 687–707, Jun. 1984.

[99] A. Burkert, J. W. Truran, and G. Hensler, "The Collapse of Our Galaxy and the Formation of the Galactic Disk," , vol. 391, p. 651, Jun. 1992.

[100] P. J. Quinn, L. Hernquist, and D. P. Fullagar, "Heating of Galactic Disks by Mergers," , vol. 403, p. 74, Jan. 1993.

[101] S. Sridhar and J. Touma, "Adiabatic evolution and capture into resonance: vertical heating of a growing stellar disc," , vol. 279, p. 1263, Apr. 1996.

[102] R. Schönrich and J. Binney, "Origin and structure of the Galactic disc(s)," , vol. 399, no. 3, pp. 1145–1156, Nov. 2009.

[103] M. L. Wilson, A. Helmi, H. L. Morrison, M. A. Breddels, O. Bienaymé, J. Binney, J. Bland-Hawthorn, R. Campbell, K. C. Freeman, J. P. Fulbright, B. K. Gibson, G. Gilmore, E. K. Grebel, U. Munari, J. F. Navarro, Q. A. Parker, W. Reid, G. Seabroke, A. Siebert, A. Siviero, M. Steinmetz, M. E. K. Williams, R. F. G. Wyse, and T. Zwitter, "Testing formation mechanisms of the Milky Way's thick disc with RAVE," *Monthly Notices of the Royal Astronomical Society*, vol. 413, no. 3, pp. 2235–2241, 05 2011. [Online]. Available: https://doi.org/10.1111/j.1365-2966.2011.18298.x

[104] M. J. Park, S. K. Yi, S. Peirani, C. Pichon, Y. Dubois, H. Choi, J. Devriendt, S. Kaviraj, T. Kimm, K. Kraljic, and M. Volonteri, "Exploring the origin of thick disks using the newhorizon and galactica simulations," *The Astrophysical Journal Supplement Series*, vol. 254, no. 1, p. 2, apr 2021. [Online]. Available: https://dx.doi.org/10.3847/1538-4365/abe937

[105] Gaia Collaboration, Brown, A. G. A., Vallenari, A., Prusti, T., de Bruijne, J. H. J., Babusiaux, C., Biermann, M., Creevey, O. L., Evans, D. W., Eyer, L., Hutton, A., Jansen, F., Jordi, C., Klioner, S. A., Lammers, U., Lindegren, L., Luri, X., Mignard, F., Panem, C., Pourbaix, D., Randich, S., Sartoretti, P., Soubiran, C., Walton, N. A., Arenou, F., Bailer-Jones, C. A. L., Bastian, U., Cropper, M., Drimmel, R., Katz, D., Lattanzi, M. G., van Leeuwen, F., Bakker, J., Cacciari, C., Castañeda, J., De Angeli, F., Ducourant, C., Fabricius, C., Fouesneau, M., Frémat, Y., Guerra, R., Guerrier, A., Guiraud, J., Jean-Antoine Piccolo, A., Masana, E., Messineo, R., Mowlavi, N., Nicolas, C., Nienartowicz, K., Pailler, F., Panuzzo, P., Riclet, F., Roux, W., Seabroke, G. M., Sordo, R., Tanga, P., Thévenin, F., Gracia-Abril, G., Portell, J., Teyssier, D., Altmann, M., Andrae, R., Bellas-Velidis, I., Benson, K., Berthier, J., Blomme, R., Brugaletta, E., Burgess, P. W., Busso, G., Carry, B., Cellino, A., Cheek, N., Clementini, G., Damerdji, Y., Davidson, M., Delchambre, L., Dell'Oro, A., Fernández-Hernández, J., Galluccio, L., García-Lario, P., Garcia-Reinaldos, M., González-Núñez, J., Gosset, E., Haigron, R., Halbwachs, J.-L., Hambly, N. C., Harrison, D. L., Hatzidimitriou, D., Heiter, U., Hernández, J., Hestroffer, D., Hodgkin, S. T., Holl, B., Janßen, K., Jevardat de Fombelle, G., Jordan, S., Krone-Martins, A., Lanzafame, A. C., Löffler, W., Lorca, A., Manteiga, M., Marchal, O., Marrese, P. M., Moitinho, A., Mora, A., Muinonen, K., Osborne, P., Pancino, E., Pauwels, T., Petit, J.-M., Recio-Blanco, A., Richards, P. J., Riello, M., Rimoldini, L., Robin, A. C., Roegiers, T., Rybizki, J., Sarro, L. M., Siopis, C., Smith, M., Sozzetti, A., Ulla, A., Utrilla, E., van Leeuwen, M., van Reeven, W., Abbas, U., Abreu Aramburu, A., Accart, S., Aerts, C., Aguado, J. J., Ajaj, M., Altavilla, G., Álvarez, M. A., Álvarez Cid-Fuentes, J., Alves, J., Anderson, R. I., Anglada Varela, E., Antoja, T., Audard, M., Baines, D., Baker, S. G., Balaguer-Núñez, L., Balbinot, E., Balog, Z., Barache, C., Barbato, D., Barros, M., Barstow, M. A., Bartolomé, S., Bassilana, J.-L., Bauchet, N., Baudesson-Stella, A., Becciani, U., Bellazzini, M., Bernet, M., Bertone, S., Bianchi, L., Blanco-Cuaresma, S., Boch, T., Bombrun, A., Bossini, D., Bouquillon, S., Bragaglia, A., Bramante, L., Breedt, E., Bressan, A., Brouillet, N.,

Bucciarelli, B., Burlacu, A., Busonero, D., Butkevich, A. G., Buzzi, R., Caffau, E., Cancelliere, R., Cánovas, H., Cantat-Gaudin, T., Carballo, R., Carlucci, T., Carnerero, M. I, Carrasco, J. M., Casamiquela, L., Castellani, M., Castro-Ginard, A., Castro Sampol, P., Chaoul, L., Charlot, P., Chemin, L., Chiavassa, A., Cioni, M.-R. L., Comoretto, G., Cooper, W. J., Cornez, T., Cowell, S., Crifo, F., Crosta, M., Crowley, C., Dafonte, C., Dapergolas, A., David, M., David, P., de Laverny, P., De Luise, F., De March, R., De Ridder, J., de Souza, R., de Teodoro, P., de Torres, A., del Peloso, E. F., del Pozo, E., Delbo, M., Delgado, A., Delgado, H. E., Delisle, J.-B., Di Matteo, P., Diakite, S., Diener, C., Distefano, E., Dolding, C., Eappachen, D., Edvardsson, B., Enke, H., Esquej, P., Fabre, C., Fabrizio, M., Faigler, S., Fedorets, G., Fernique, P., Fienga, A., Figueras, F., Fouron, C., Fragkoudi, F., Fraile, E., Franke, F., Gai, M., Garabato, D., Garcia-Gutierrez, A., García-Torres, M., Garofalo, A., Gavras, P., Gerlach, E., Geyer, R., Giacobbe, P., Gilmore, G., Girona, S., Giuffrida, G., Gomel, R., Gomez, A., Gonzalez-Santamaria, I., González-Vidal, J. J., Granvik, M., Gutiérrez-Sánchez, R., Guy, L. P., Hauser, M., Haywood, M., Helmi, A., Hidalgo, S. L., Hilger, T., Hladczuk, N., Hobbs, D., Holland, G., Huckle, H. E., Jasniewicz, G., Jonker, P. G., Juaristi Campillo, J., Julbe, F., Karbevska, L., Kervella, P., Khanna, S., Kochoska, A., Kontizas, M., Kordopatis, G., Korn, A. J., Kostrzewa-Rutkowska, Z., Kruszy´nska, K., Lambert, S., Lanza, A. F., Lasne, Y., Le Campion, J.-F., Le Fustec, Y., Lebreton, Y., Lebzelter, T., Leccia, S., Leclerc, N., Lecoeur-Taibi, I., Liao, S., Licata, E., Lindstrøm, E. P., Lister, T. A., Livanou, E., Lobel, A., Madrero Pardo, P., Managau, S., Mann, R. G., Marchant, J. M., Marconi, M., Marcos Santos, M. M. S., Marinoni, S., Marocco, F., Marshall, D. J., Martin Polo, L., Martín-Fleitas, J. M., Masip, A., Massari, D., Mastrobuono-Battisti, A., Mazeh, T., McMillan, P. J., Messina, S., Michalik, D., Millar, N. R., Mints, A., Molina, D., Molinaro, R., Molnár, L., Montegriffo, P., Mor, R., Morbidelli, R., Morel, T., Morris, D., Mulone, A. F., Munoz, D., Muraveva, T., Murphy, C. P., Musella, I., Noval, L., Ordénovic, C., Orrù, G., Osinde, J., Pagani, C., Pagano, I., Palaversa, L., Palicio, P. A., Panahi, A., Pawlak, M., Peñalosa Esteller, X., Penttilä, A., Piersimoni, A. M., Pineau, F.-X., Plachy, E., Plum, G., Poggio, E., Poretti, E., Poujoulet, E., Prsa, A., Pulone, L., Racero, E., Ragaini, S., Rainer, M., Raiteri, C. M., Rambaux, N., Ramos, P., Ramos-Lerate, M., Re Fiorentin, P., Regibo, S., Reylé, C., Ripepi, V., Riva, A., Rixon, G., Robichon, N., Robin, C., Roelens, M., Rohrbasser, L., Romero-Gómez, M., Rowell, N., Royer, F., Rybicki, K. A., Sadowski, G., Sagristà Sellés, A., Sahlmann, J., Salgado, J., Salguero, E., Samaras, N., Sanchez Gimenez, V.,

Sanna, N., Santoveña, R., Sarasso, M., Schultheis, M., Sciacca, E., Segol, M., Segovia, J. C., Ségransan, D., Semeux, D., Shahaf, S., Siddiqui, H. I., Siebert, A., Siltala, L., Slezak, E., Smart, R. L., Solano, E., Solitro, F., Souami, D., Souchay, J., Spagna, A., Spoto, F., Steele, I. A., Steidelmüller, H., Stephenson, C. A., Süveges, M., Szabados, L., Szegedi-Elek, E., Taris, F., Tauran, G., Taylor, M. B., Teixeira, R., Thuillot, W., Tonello, N., Torra, F., Torra, J., Turon, C., Unger, N., Vaillant, M., van Dillen, E., Vanel, O., Vecchiato, A., Viala, Y., Vicente, D., Voutsinas, S., Weiler, M., Wevers, T., Wyrzykowski, L., Yoldas, A., Yvard, P., Zhao, H., Zorec, J., Zucker, S., Zurbach, C., and Zwitter, T., "Gaia early data release 3 - summary of the contents and survey properties," *A&A*, vol. 649, p. A1, 2021. [Online]. Available: https://doi.org/10.1051/0004-6361/202039657

[106] P. Hoyer, E. Hog, I. Poder, and L. Lindegren, "Derivation of positions and parallaxes from simulated observations with a scanning astrometry satellite," , vol. 101, no. 2, pp. 228–237, Aug. 1981.

[107] L. Lindegren and U. Bastian, "Basic principles of scanning space astrometry," in *EAS Publications Series*, ser. EAS Publications Series, vol. 45, Jan. 2010, pp. 109–114.

[108] Gaia Collaboration, Brown, A. G. A., Vallenari, A., Prusti, T., de Bruijne, J. H. J., Babusiaux, C., Bailer-Jones, C. A. L., Biermann, M., Evans, D. W., Eyer, L., Jansen, F., Jordi, C., Klioner, S. A., Lammers, U., Lindegren, L., Luri, X., Mignard, F., Panem, C., Pourbaix, D., Randich, S., Sartoretti, P., Siddiqui, H. I., Soubiran, C., van Leeuwen, F., Walton, N. A., Arenou, F., Bastian, U., Cropper, M., Drimmel, R., Katz, D., Lattanzi, M. G., Bakker, J., Cacciari, C., Castañeda, J., Chaoul, L., Cheek, N., De Angeli, F., Fabricius, C., Guerra, R., Holl, B., Masana, E., Messineo, R., Mowlavi, N., Nienartowicz, K., Panuzzo, P., Portell, J., Riello, M., Seabroke, G. M., Tanga, P., Thévenin, F., Gracia-Abril, G., Comoretto, G., Garcia-Reinaldos, M., Teyssier, D., Altmann, M., Andrae, R., Audard, M., Bellas-Velidis, I., Benson, K., Berthier, J., Blomme, R., Burgess, P., Busso, G., Carry, B., Cellino, A., Clementini, G., Clotet, M., Creevey, O., Davidson, M., De Ridder, J., Delchambre, L., Dell'Oro, A., Ducourant, C., Fernández-Hernández, J., Fouesneau, M., Frémat, Y., Galluccio, L., García-Torres, M., González-Núñez, J., González-Vidal, J. J., Gosset, E., Guy, L. P., Halbwachs, J.-L., Hambly, N. C., Harrison, D. L., Hernández, J., Hestroffer, D., Hodgkin, S. T., Hutton, A., Jasniewicz, G., Jean-Antoine-Piccolo, A., Jordan, S., Korn, A. J., Krone-Martins, A., Lanzafame, A. C., Lebzelter, T., Löffler, W., Manteiga, M.,

Marrese, P. M., Martín-Fleitas, J. M., Moitinho, A., Mora, A., Muinonen, K., Osinde, J., Pancino, E., Pauwels, T., Petit, J.-M., Recio-Blanco, A., Richards, P. J., Rimoldini, L., Robin, A. C., Sarro, L. M., Siopis, C., Smith, M., Sozzetti, A., Süveges, M., Torra, J., van Reeven, W., Abbas, U., Abreu Aramburu, A., Accart, S., Aerts, C., Altavilla, G., Álvarez, M. A., Alvarez, R., Alves, J., Anderson, R. I., Andrei, A. H., Anglada Varela, E., Antiche, E., Antoja, T., Arcay, B., Astraatmadja, T. L., Bach, N., Baker, S. G., Balaguer-Núñez, L., Balm, P., Barache, C., Barata, C., Barbato, D., Barblan, F., Barklem, P. S., Barrado, D., Barros, M., Barstow, M. A., Bartholomé Muñoz, S., Bassilana, J.-L., Becciani, U., Bellazzini, M., Berihuete, A., Bertone, S., Bianchi, L., Bienaymé, O., Blanco-Cuaresma, S., Boch, T., Boeche, C., Bombrun, A., Borrachero, R., Bossini, D., Bouquillon, S., Bourda, G., Bragaglia, A., Bramante, L., Breddels, M. A., Bressan, A., Brouillet, N., Brüsemeister, T., Brugaletta, E., Bucciarelli, B., Burlacu, A., Busonero, D., Butkevich, A. G., Buzzi, R., Caffau, E., Cancelliere, R., Cannizzaro, G., Cantat-Gaudin, T., Carballo, R., Carlucci, T., Carrasco, J. M., Casamiquela, L., Castellani, M., Castro-Ginard, A., Charlot, P., Chemin, L., Chiavassa, A., Cocozza, G., Costigan, G., Cowell, S., Crifo, F., Crosta, M., Crowley, C., Cuypers+, J., Dafonte, C., Damerdji, Y., Dapergolas, A., David, P., David, M., de Laverny, P., De Luise, F., De March, R., de Martino, D., de Souza, R., de Torres, A., Debosscher, J., del Pozo, E., Delbo, M., Delgado, A., Delgado, H. E., Di Matteo, P., Diakite, S., Diener, C., Distefano, E., Dolding, C., Drazinos, P., Durán, J., Edvardsson, B., Enke, H., Eriksson, K., Esquej, P., Eynard Bontemps, G., Fabre, C., Fabrizio, M., Faigler, S., Falcão, A. J., Farràs Casas, M., Federici, L., Fedorets, G., Fernique, P., Figueras, F., Filippi, F., Findeisen, K., Fonti, A., Fraile, E., Fraser, M., Frézouls, B., Gai, M., Galleti, S., Garabato, D., García-Sedano, F., Garofalo, A., Garralda, N., Gavel, A., Gavras, P., Gerssen, J., Geyer, R., Giacobbe, P., Gilmore, G., Girona, S., Giuffrida, G., Glass, F., Gomes, M., Granvik, M., Gueguen, A., Guerrier, A., Guiraud, J., Gutiérrez-Sánchez, R., Haigron, R., Hatzidimitriou, D., Hauser, M., Haywood, M., Heiter, U., Helmi, A., Heu, J., Hilger, T., Hobbs, D., Hofmann, W., Holland, G., Huckle, H. E., Hypki, A., Icardi, V., Janßen, K., Jevardat de Fombelle, G., Jonker, P. G., Juhász, Á. L., Julbe, F., Karampelas, A., Kewley, A., Klar, J., Kochoska, A., Kohley, R., Kolenberg, K., Kontizas, M., Kontizas, E., Koposov, S. E., Kordopatis, G., Kostrzewa-Rutkowska, Z., Koubsky, P., Lambert, S., Lanza, A. F., Lasne, Y., Lavigne, J.-B., Le Fustec, Y., Le Poncin-Lafitte, C., Lebreton, Y., Leccia, S., Leclerc, N., Lecoeur-Taibi, I., Lenhardt, H., Leroux, F., Liao, S., Licata, E., Lindstrøm, H. E. P., Lister, T. A., Livanou, E., Lobel, A., López,

M., Managau, S., Mann, R. G., Mantelet, G., Marchal, O., Marchant, J. M., Marconi, M., Marinoni, S., Marschalkó, G., Marshall, D. J., Martino, M., Marton, G., Mary, N., Massari, D., Matijevic, G., Mazeh, T., McMillan, P. J., Messina, S., Michalik, D., Millar, N. R., Molina, D., Molinaro, R., Molnár, L., Montegriffo, P., Mor, R., Morbidelli, R., Morel, T., Morris, D., Mulone, A. F., Muraveva, T., Musella, I., Nelemans, G., Nicastro, L., Noval, L., O'Mullane, W., Ordénovic, C., Ordóñez-Blanco, D., Osborne, P., Pagani, C., Pagano, I., Pailler, F., Palacin, H., Palaversa, L., Panahi, A., Pawlak, M., Piersimoni, A. M., Pineau, F.-X., Plachy, E., Plum, G., Poggio, E., Poujoulet, E., Prsa, A., Pulone, L., Racero, E., Ragaini, S., Rambaux, N., Ramos-Lerate, M., Regibo, S., Reylé, C., Riclet, F., Ripepi, V., Riva, A., Rivard, A., Rixon, G., Roegiers, T., Roelens, M., Romero-Gómez, M., Rowell, N., Royer, F., Ruiz-Dern, L., Sadowski, G., Sagristà Sellés, T., Sahlmann, J., Salgado, J., Salguero, E., Sanna, N., Santana-Ros, T., Sarasso, M., Savietto, H., Schultheis, M., Sciacca, E., Segol, M., Segovia, J. C., Ségransan, D., Shih, I-C., Siltala, L., Silva, A. F., Smart, R. L., Smith, K. W., Solano, E., Solitro, F., Sordo, R., Soria Nieto, S., Souchay, J., Spagna, A., Spoto, F., Stampa, U., Steele, I. A., Steidelmüller, H., Stephenson, C. A., Stoev, H., Suess, F. F., Surdej, J., Szabados, L., Szegedi-Elek, E., Tapiador, D., Taris, F., Tauran, G., Taylor, M. B., Teixeira, R., Terrett, D., Teyssandier, P., Thuillot, W., Titarenko, A., Torra Clotet, F., Turon, C., Ulla, A., Utrilla, E., Uzzi, S., Vaillant, M., Valentini, G., Valette, V., van Elteren, A., Van Hemelryck, E., van Leeuwen, M., Vaschetto, M., Vecchiato, A., Veljanoski, J., Viala, Y., Vicente, D., Vogt, S., von Essen, C., Voss, H., Votruba, V., Voutsinas, S., Walmsley, G., Weiler, M., Wertz, O., Wevers, T., Wyrzykowski, L., Yoldas, A., Zerjal, M., Ziaeepour, H., Zorec, J., Zschocke, S., Zucker, S., Zurbach, C., and Zwitter, T., "Gaia data release 2 - summary of the contents and survey properties," *A&A*, vol. 616, p. A1, 2018. [Online]. Available: https://doi.org/10.1051/0004-6361/201833051

[109] M. Riello, F. De Angeli, D. W. Evans, P. Montegriffo, J. M. Carrasco, G. Busso, L. Palaversa, P. W. Burgess, C. Diener, M. Davidson, N. Rowell, C. Fabricius, C. Jordi, M. Bellazzini, E. Pancino, D. L. Harrison, C. Cacciari, F. van Leeuwen, N. C. Hambly, S. T. Hodgkin, P. J. Osborne, G. Altavilla, M. A. Barstow, A. G. A. Brown, M. Castellani, S. Cowell, F. De Luise, G. Gilmore, G. Giuffrida, S. Hidalgo, G. Holland, S. Marinoni, C. Pagani, A. M. Piersimoni, L. Pulone, S. Ragaini, M. Rainer, P. J. Richards, N. Sanna, N. A. Walton, M. Weiler, and A. Yoldas, "Gaia Early Data Release 3. Photometric content and validation," , vol. 649, p. A3, May 2021.

[110] Lindegren, L., Klioner, S. A., Hernández, J., Bombrun, A., Ramos-Lerate, M., Steidelmüller, H., Bastian, U., Biermann, M., de Torres, A., Gerlach, E., Geyer, R., Hilger, T., Hobbs, D., Lammers, U., McMillan, P. J., Stephenson, C. A., Castañeda, J., Davidson, M., Fabricius, C., Gracia-Abril, G., Portell, J., Rowell, N., Teyssier, D., Torra, F., Bartolomé, S., Clotet, M., Garralda, N., González-Vidal, J. J., Torra, J., Abbas, U., Altmann, M., Anglada Varela, E., Balaguer-Núñez, L., Balog, Z., Barache, C., Becciani, U., Bernet, M., Bertone, S., Bianchi, L., Bouquillon, S., Brown, A. G. A., Bucciarelli, B., Busonero, D., Butkevich, A. G., Buzzi, R., Cancelliere, R., Carlucci, T., Charlot, P., Cioni, M.-R. L., Crosta, M., Crowley, C., del Peloso, E. F., del Pozo, E., Drimmel, R., Esquej, P., Fienga, A., Fraile, E., Gai, M., Garcia-Reinaldos, M., Guerra, R., Hambly, N. C., Hauser, M., Janßen, K., Jordan, S., Kostrzewa-Rutkowska, Z., Lattanzi, M. G., Liao, S., Licata, E., Lister, T. A., Löffler, W., Marchant, J. M., Masip, A., Mignard, F., Mints, A., Molina, D., Mora, A., Morbidelli, R., Murphy, C. P., Pagani, C., Panuzzo, P., Peñalosa Esteller, X., Poggio, E., Re Fiorentin, P., Riva, A., Sagristà Sellés, A., Sanchez Gimenez, V., Sarasso, M., Sciacca, E., Siddiqui, H. I., Smart, R. L., Souami, D., Spagna, A., Steele, I. A., Taris, F., Utrilla, E., van Reeven, W., and Vecchiato, A., "Gaia early data release 3 - the astrometric solution," *A&A*, vol. 649, p. A2, 2021. [Online]. Available: https://doi.org/10.1051/0004-6361/202039709

[111] Lindegren, L., Bastian, U., Biermann, M., Bombrun, A., de Torres, A., Gerlach, E., Geyer, R., Hernández, J., Hilger, T., Hobbs, D., Klioner, S. A., Lammers, U., McMillan, P. J., Ramos-Lerate, M., Steidelmüller, H., Stephenson, C. A., and van Leeuwen, F., "Gaia early data release 3 - parallax bias versus magnitude, colour, and position," *A&A*, vol. 649, p. A4, 2021. [Online]. Available: https://doi.org/10.1051/0004-6361/202039653

[112] M. B. Taylor, "TOPCAT & STIL: Starlink Table/VOTable Processing Software," in *Astronomical Data Analysis Software and Systems XIV*, ser. Astronomical Society of the Pacific Conference Series, P. Shopbell, M. Britton, and R. Ebert, Eds., vol. 347, Dec. 2005, p. 29.

[113] R. Schönrich, J. Binney, and W. Dehnen, "Local kinematics and the local standard of rest," , vol. 403, no. 4, pp. 1829–1833, Apr. 2010.

[114] J. G. Fernández-Trincado, T. C. Beers, and D. Minniti, "Jurassic: A chemically anomalous structure in the Galactic halo," , vol. 644, p. A83, Dec. 2020.

[115] M. Steinmetz, T. Zwitter, G. Matijevic, A. Siviero, and U. Munari, "A comparison between rave dr5 and gaia dr2 radial velocities," *Research Notes of the AAS*, vol. 2, no. 4, p. 194, oct 2018. [Online]. Available: https://dx.doi.org/10.3847/2515-5172/aaead0

[116] D. Kawata and C. Chiappini, "Milky way's thick and thin disk: Is there a distinct thick disk?" *Astronomische Nachrichten*, vol. 337, no. 8-9, pp. 976–981, sep 2016. [Online]. Available: https://doi.org/10.1002%2Fasna.201612421

[117] K. Vieira, G. Carraro, V. Korchagin, A. Lutsenko, T. M. Girard, and W. van Altena, "Milky way thin and thick disk kinematics with gaia edr3 and rave dr5," *The Astrophysical Journal*, vol. 932, no. 1, p. 28, jun 2022. [Online]. Available: https://dx.doi.org/10.3847/1538-4357/ac6b9b

[118] Cantat-Gaudin, Tristan and Brandt, Timothy D., "Characterizing and correcting the proper motion bias of the bright gaia edr3 sources," *A&A*, vol. 649, p. A124, 2021. [Online]. Available: https://doi.org/10.1051/0004-6361/202140807

# Acknowledgments

I want express my gratitude to my professor Giovanni Carraro and my referee Dr. Sara Lucatello for invaluable patience, useful questions and feedback. I also could not have undertaken this journey without my defense committee, who generously provided knowledge and expertise. Additionally, this endeavor would not have been possible without the generous support from the University of Padova.

I am also grateful to my classmates and cohort members for their editing help and moral support.

Lastly, I would be remiss in not mentioning my family. Their belief in me has kept my spirits and motivation high during this process.